RECEIVED BY TIC MAY 29 1979

LBL-8510

MASTER

NOISE AND OPTIMIZATION OF THE dc SQUID

Claudia Denke Tesche
(Ph. D. thesis)

November 1978

Prepared for the U. S. Department of Energy
under Contract W-7405-ENG-48

LAWRENCE BERKELEY LABORATORY
UNIVERSITY OF CALIFORNIA
BERKELEY

LBL-8510

NOTICE

This report was prepared as an account of work sponsored by the United States Government. Neither the United States nor the United States Department of Energy, nor any of their employees, nor any of their contractors, subcontractors, or their employees, makes any warranty, express or implied, or assumes any legal liability or responsibility for the accuracy, completeness or usefulness of any information, apparatus, product or process disclosed, or represents that its use would not infringe privately owned rights.

NOISE AND OPTIMIZATION OF THE dc SQUID

by

Claudia Denke Tesche

Materials and Molecular Research Division
Lawrence Berkeley Laboratory
and
Department of Physics
University of California
Berkeley, California 94720

TABLE OF CONTENTS

I. Introduction

II. Lumped Circuit Model for the dc SQUID

A. The Resistively Shunted Junction Model

B. The Thermal Activation Model

C. Equations for the dc SQUID

III. SQUID Characteristics in the Absence of Noise

A. Case I: $v = 0$

B. Case II: $v > 0$

C. Discussion

IV. SQUID Characteristics in the Presence of Noise

A. Numerical Techniques

B. Single Junction with Noise

C. SQUID Characteristics in the Pres nce of Noise

V. SQUID Optimization

A. Determination of the Optimal SQUID Parameters

B. Ultimate Performance of the dc SQUID

VI. Applications

A. The Low Noise dc SQUID Preamplifier

B. Magnetometers

References

Acknowledgments

First I would like to acknowledge the support, guidance and patience of my research advisor, Professor John Clarke. Many useful and illuminating conversations also occurred with Dr. Wolfgang Goubau and my other colleagues in the Clarke group I would especially like to thank my family for their continuing support under what developed into rather trying circumstances. Finally, I would like to thank Professor Evind Wichmann. His honesty and dedication to physics will always be an inspiration to me.

This work was performed under the auspices of the U.S. Energy Research and Development Administration.

LIST OF SYMBOLS

Dimensioned Quantities*

I_o	critical current of single Josephson junction.
R	shunt resistance of single Josephson junction.
C	capacitance of single Josephson junction.
Φ_o	flux quantum, $\Phi_o = h/2e$.
L	SQUID ring inductance.
T	SQUID temperature.

Dimensionless Quantities

β_C	reduced capacitance or hysterysis parameter, $\beta_C = 2\pi I_o R^2 C/\Phi_o$.
β	intrinsic flux ratio, $\beta = 2LI_o/\Phi_o$.
α	critical current asymmetry parameter.
η	inductance asymmetry parameter.
ρ	shunt resistance asymmetry parameter.
Γ	Johnson noise figure, $\Gamma = 2\pi k_B T/I_o\Phi_o$.
θ	dimensionless time, $\theta = t/(\Phi_o/2\pi I_o R)$.
i	dc bias current, $i = I/I_o$.
j	time dependent circulating current, $j = J/I_o$.
$\bar{j}$	time-averaged circulating current.
v	time dependent voltage across the SQUID, $v = V/I_oR$.
$\bar{v}$	time-averaged voltage.

---

*Dimensioned quantities appear in upper case, undimensioned quantities in lower case, with the exception of Γ which has been previously defined.[34]

$\delta, \delta_1, \delta_2$	time dependent quantum mechanical phase differences across the junctions.
ϕ_a	externally applied quasistatic flux, $\phi_a = \Phi_a/\Phi_o$.
i_s	externally applied quasistatic signal current, $i_s = I_s/I_o$.
v_{N1}, v_{N2}	noise voltages, $v_{N1} = V_{N1}/I_oR$, $v_{N2} = V_{N2}/I_oR$.
u	potential energy, $u = U/(I_o\Phi_o/2\pi)$.
i_c	critical current, $i_c = I_c/I_o$.
Δi_c	modulation depth, $\Delta i_c = i_{cmax} - i_{cmin}$.
f_J	fundamental Josephson frequency, $f_J = \bar{v}/2\pi = F_J/(\Phi_o/2\pi I_oR)$.
$(\partial\bar{v}/\partial i)\phi_a$	differential resistance at constant applied flux, $(\partial\bar{v}/\partial i)\phi_a = (\partial\bar{V}/\partial I)_{\phi_a}/R$.
$(\partial\bar{v}/\partial\phi_a)_i$	forward transfer function at constant bias current, $(\partial\bar{v}/\partial\phi_a)_i = (\partial V/\partial\Phi_a)_I/(I_oR/\Phi_o)$.
$S_v(f)$	voltage noise power spectral density, $S_v(f) = S_V(F)/(I_oR\Phi_o/2\pi)$, where $S_V(F) = 2\int_{-\infty}^{\infty} A_V(\tau)e^{-2\pi\tau F}\,d\tau$, $A_V = \lim_{T\to\infty} \frac{1}{T}\int_0^T \langle V(t)V(t+\tau)\rangle\,dt$, and $\langle\rangle$ is the ensemble average.
S_v^o	low frequency voltage noise power spectral density, $S_v^o = S_v(f)$ for $0 < f \ll f_J$.
$S_j(f)$	circulating current noise power spectral density, $S_j(f) = S_J(F)/(I_o\Phi_o/2\pi R)$.
S_j^o	low frequency circulating current noise power spectral density, $S_j^o = S_j(f)$ for $0 < f \ll f_J$.

$S_{vj}(f)$ correlation noise power spectral density $S_{vj}(f) = S_{VJ}(F)/(I_o\Phi_o/2\pi)$.

S^o_{vj} low frequency correlation noise power spectral density, $S^o_{vj} = S_{vj}(f)$ for $0 < f \ll f_J$.

$S_\phi(f)$ equivalent input flux noise power spectral density, $S_\phi(f) = S_v/(\partial\bar{v}/\partial\phi_a)^2 = S_\phi/(\Phi_0{}^3/2\pi I_o R)$.

S^o_ϕ low frequency flux noise spectral density, $S^o_\phi = S_\phi(f)$ for $0 < f \ll f_J$.

ζ_ϕ normalized low frequency flux noise spectral density, $\zeta_\phi = S^o_\phi/(2\Gamma)$.

Noise and Optimization of the dc SQUID

Claudia Denke Tesche

Materials and Molecular Research Division
Lawrence Berkeley Laboratory
and
Department of Physics
University of California
Berkeley, California 94720

ABSTRACT

A lumped circuit model is described for the dc SQUID. The junctions are non-hysteretic, resistively shunted Josephson tunnel junctions. Current-voltage ($I-\bar{V}$) characteristics are obtained for the noise-free case as functions of the applied flux, Φ_a, SQUID inductance, L, junction critical current, I_o, shunt resistance, R, and temperature, T. The effects of asymmetry in L, I_o, and R are discussed. ($I-\bar{V}$) characteristics, forward transfer functions, $(\partial\bar{V}/\partial\Phi_a)$, and low frequency spectral densities for the voltage noise, S_V^o, circulating current noise, S_J^o, and correlation noise, S_{VJ}^o, are obtained at experimentally interesting values of the SQUID parameters in the presence of Johnson noise in the resistive shunts. The flux spectral density, $S_\Phi^o = S_V^o/(\partial\bar{V}/\partial\Phi_a)^2$, and energy spectral density, $S_\Phi^o/2L$, are determined from the computed values of S_V^o and $(\partial\bar{V}/\partial\Phi_a)$. The resolution of the SQUID with ac flux modulation is discussed. The flux resolution calculated for the dc SQUID of Clarke, Goubau, and Ketchen is $1.6 \times 10^{-5}\ \Phi_o\ Hz^{-\frac{1}{2}}$, approximately one half the experimental value.

Optimization of the isolated SQUID energy resolution is discussed.

The optimal resolution is obtained for $\beta = 2LI_o/\Phi_o = 1$ and $\beta_C = 2\pi I_o R^2 C/\Phi_o \lesssim 1$. The energy spectral density for $\beta = 1$, $\beta_C = 1$ is $S_\Phi^o/2L = 4k_B T(\pi LC)^{\frac{1}{2}}$. Thus the energy spectral density is proportional to the junction area. In the limit of small L, C, and/or T (i.e. $2k_B T(\pi LC)^{\frac{1}{2}} \lesssim h$ with $\beta = 1$, $\beta_C = 1$) the dominant noise source is the shot noise in the Josephson junctions, and $S_\Phi^o/2L \approx h/2$, where h is Planck's constant.

A model is developed for the SQUID coupled to an input L_i-R_i-C_i circuit through a mutual inductance, $M_i = \alpha_i^2 L L_i$. The SQUID voltage noise at the output in the presence of the input circuit is computed as a function of the circuit and SQUID parameters, and the noise figures S_V^o, S_J^o and S_{VJ}^o. The model is used to compute the noise temperature of the dc SQUID voltage preamplifier and the energy resolution of the dc SQUID magnetometer in the tuned and untuned case.

The untuned noise temperature optimized at frequency ω_o for a Johnson noise limited SQUID with $\beta = 1$, $\Gamma = 2\pi k_B T/I_o\Phi_o = 0.05$ is $T_N^{opt}(\omega_o) = 8(R_i^{opt}/L_i)(L/R)T/\alpha^2$, where $R_i^{opt} = \omega_o L_i(1+1.5\alpha^2+0.7\alpha^4)^{\frac{1}{2}}$ In the shot noise limited SQUID with $\alpha^2 = 1/2$, $T_N^{opt}(\omega_o) \approx 17\ \hbar\ \omega_o/k_B$. For the Johnson noise limited tuned preamplifier, $T_N^{opt}(\omega_o) \approx 2.8(\omega_o L/R)T$ for $R_i^{opt} \approx 0.35\alpha^2\ \omega_o L_i$ and $(1/\omega_o C_i^{opt}) \approx (1+3\alpha^2/4)\omega_o L_i$. In the shot noise limit, $T_N^{opt}(\omega_o) \approx 2.2\hbar\omega_o/k_B$. Both the tuned and untuned shot noise limited optimal noise temperatures are consistent with the uncertainty principle limit for the noise temperature of a linear amplifier, $T_N(\omega_o) \gtrsim \hbar\omega_o/k_B$.

The minimum resolvable energy density, u_o, in the input coil of a tuned and untuned magnetometer is computed as a function of the SQUID

noise figures and input circuit parameters. For the tuned magnetometer, the mean squared voltage signal developed across the coil inductance L_p satisfies $\langle E_i^2 \rangle = 2\omega_o^2 u_o L_p \gtrsim 4k_B R_i B(T_i + T_N^*)$, where R_i is the input circuit resistance at temperature T_i, T_N^* is the noise temperature of the SQUID preamplifier, and B is the bandwidth. For most applications, $T_N^* \sim (\omega_o L/R)T \ll T_i$ over a wide range of values of the input circuit parameters. The SQUID noise temperature approaches the input circuit temperature in the high Q, high frequency limit. For $Q = 1000$, $\omega_o = 2 \times 10^6$ rad s^{-1}, $L_i = L_p$ and $T_i = T$, $T_N^*(\omega_o) = T_i$. In the low temperature limit, $T_i \to 0$ and $T \to 0$, the energy resolution is limited by the shot noise sources in the SQUID, $2\omega_o^2 u_o L_p > (4k_B R_i B)\hbar\omega_o/k_B$.

For the untuned magnetometer with $R_i = 0$, the optimal energy resolution for the Johnson noise limited SQUID with $\beta = 1.0$, $\Gamma = 0.05$, and $\alpha^2 = 1/2$ is $u_o^{opt} \approx 9k_B T(B/F_J) \approx 5 \times 10^{-30}(B/1\text{Hz})\text{J}$, where the Josephson frequency $F_J \approx R/10L$. The optimal value of the input coil to the SQUID for this case is $L_i^{opt} \approx 0.72\ L_p$. In the shot noise limit, $u_o^{opt} \approx 11hB$.

I INTRODUCTION

The dc SQUID[1] (Superconducting QUantum Interference Device) consists of a superconducting ring of inductance L interrupted by two Josephson junctions[2] each with critical current I_o. The SQUID is biased at a constant current I and develops a voltage $\overline{V}$ which is a periodic function of the applied flux Φ_a threading the ring. Thus the dc SQUID is a device which transforms an input signal in the form of a change in magnetic flux, $\Delta\Phi_a$, into an output signal in the form of a change in voltage, $\Delta\overline{V}$.

The performance of the Josephson tunnel junction SQUIDs presently used[3,4] is limited by the Johnson noise generated in the resistive shunts used to eliminate hysteresis in the I-$\overline{V}$ characteristics. For the case of the isolated dc SQUID used directly as a magnetometer, the voltage noise produced at the output by the Johnson noise sources can be expressed as an equivalent flux noise spectral density, S_Φ, at the input. Approximate expressions[3,5] for S_Φ have been obtained in the limit $\beta = 2LI_o/\Phi_o \gg I$ and $\beta \ll 1$. However, most dc SQUID's are operated with $\beta \sim 1$, for which value no detailed calculation of S_Φ has been made.

In addition, the dc SQUID can be coupled to various input circuits and used as a magnetometer, gradiometer or voltage amplifier. In many applications the SQUID is coupled to the input circuit via a mutual inductance M_i to an input coil of inductance L_i. If the effect of the input circuit on the voltage noise at the SQUID output is ignored, the performance of the SQUID is characterized by the effective flux noise spectral density, the SQUID inductance, L, and the coupling efficiency α^2 between the SQUID and the input coil. The appropriate figure of

merit in this case is the equivalent energy spectral density referred to the input coil,[6] $S_E = L_i(S_\Phi/M_i^2)/2 = S_\Phi/2\alpha^2 L$, where $M_i^2 = \alpha^2 L L_i$.

In other applications, the SQUID can be coupled via M_i to an input L_i-R_i or L_i-R_i-C_i circuit containing a voltage source. In the small signal limit ($\Delta\Phi_a \ll \Phi_o$), the output voltage change is linearly related to the applied flux change, and thus to the input voltage change. In addition, the SQUID preserves the phase of the input signal. As a result, the dc SQUID plus input circuit can be characterized as a linear amplifier.[7] The appropriate figure of merit is the noise temperature $T_N(\omega)$, which is a function of the SQUID parameters, the input circuit parameters, and the signal frequency ω. In this case, the input circuit affects the SQUID voltage noise at the output. Thus both the effective flux noise spectral density, S_Φ, and the circulating current noise spectral density, S_J, which is coupled back into the input circuit via M_i, must be known.

Finally, the SQUID can be operated as a magnetometer. In this case, the input circuit can be a superconducting transformer or a tuned L_i-R_i-C_i circuit. The volume of the pick-up coil is considered to be fixed by experimental limitations (dewar size, etc.). The quantity to be optimized is the smallest detectable mean square signal energy in the volume of the coil. Again, the voltage spectral density at the output is a function of the input parameters, and a model for the SQUID plus input circuit must be developed which involves both S_Φ and S_J.

Previous calculations of the behavior of the isolated dc SQUID have been concerned mostly with the noise-free properties of the isolated

SQUID in the zero voltage state. For example, the dependence of the critical current on applied external flux has been investigated by Jaklevic, Lambe, Silver, and Mercereau,[1] Zimmerman and Silver,[8] Schulz-DuBois,[9] and by De Waele and De Bruyn Ouboter[10,11] for the symmetric SQUID, by Fulton,[12] Clarke and Paterson,[13] and Tsang and Van Duzer[14] for the asymmetric SQUID, and by Fulton, Dunkleburger and Dynes,[15] and Tsang and Van Duzer[16] for the SQUID with non-sinusoidal current-phase relationships. A qualitative discussion of the noise-free current-voltage characteristic for the SQUID in the small inductance limit has been given by DeWaele and DeBruyn Ouboter,[10] and by Tinkham.[5] However, no quantitative calculation of the flux dependence of the current-voltage characteristics, the effective flux noise spectral density S_Φ, and the circulating current noise spectral density S_J as a function of the SQUID parameters has previously been made.

Several authors have discussed the characterization of SQUIDs used as low noise galvanometers, preamplifiers and magnetometers. Clarke, Tennant, and Woody[17] discuss the effective noise temperature of superconducting galvanometers based on the SLUG.[18,19] Radhakrishnan and Newhouse[20] generalize the definition of noise figure and noise temperature to include amplifiers with superconducting inputs. Davidson, Newbower, and Beasley[21] characterize the use of SQUIDs as narrow-band, low-impedance, low noise temperature voltage amplifiers. They derive an expression for the noise temperature of the SQUID amplifier in terms of the equivalent energy spectral density, $S_\Phi/2\alpha^2L$, and the time constant of the input circuit determined by the source resistance and input inductance. In general, they find low noise temperatures ($T_N \sim \mu K$) can

be obtained only for source resistances $R_s \ll 1\Omega$. Claussen[6] discusses the sensitivity of the SQUID used as a magnetometer, ammeter and voltmeter. He finds the effective energy resolution, $S_\Phi/2\alpha^2 L$, to be the appropriate figure of merit for the SQUID in all three cases. In all of the above treatments, however, the effect of the circulating current noise, S_J, on the device performance was ignored.

The natural bandwidth of the dc SQUID preamplifier is determined by the input circuit parameters and SQUID impedance. The useful bandwidth can be extended if the SQUID is used as a null detector in a negative feedback circuit. The effect of feedback on bandwidth has been discussed by McWane, Neighbor, and Newbower,[22] by Newbower,[23] by Gifford, Webb and Wheatly,[24] by Davidson, Newbower, and Beasley,[21] and by Claussen.[6] The authors find that, although feedback can improve the frequency response and can enromously increase the dynamic range of changes in applied flux over which a linear response in output voltage change can be obtained, the bandwidth for which the optimal noise temperature is obtained is still determined by the intrinsic input circuit bandwidth.

The low noise temperatures computed for the SQUID voltage amplifier are obtained only for source resistances considerably less than 1Ω.[17,21,6] This is because the SQUID responds to the flux applied through the SQUID loop, and thus to the current flowing through the input circuit. Small input voltages will produce the required input currents only for the case of small source resistances. For source resistances on the order of 1Ω, low noise temperatures may still be obtained provided a superconducting transformer is used to match the source resistance to the optimal input resistance. Clarke, Tennant, and Woody[17] describe the operation

of a superconducting transformer used with a SLUG galvanometer. Davidson, Newbower, and Beasley[21] calculate noise temperatures < 4K for source impedances on the order of a few ohms for a SQUID amplifier used with a superconducting transformer. Claussen[6] discusses the effect of a superconducting transformer on the effective flux noise spectral density of the SQUID. Again, a complete treatment would also involve the effect of the flux transformer on the contribution of the circulating current noise spectral density to the device sensitivity.

Davidson, Newbower and Beasley[21] compare a typical SQUID preamplifier to the commercially available Princeton Applied Research (PAR) model 185. They find the PAR 185 to be a broadband, high-impedance amplifier with noise temperature $\sim$ 0.6K when ideally coupled through a transformer to a 1Ω source, while the SQUID amplifier is a narrower-band low impedance device with noise temperature on the order of 10^{-6}K when ideally coupled to a 1Ω source.

Heffner[7] derives the minimum noise temperature of arbitrary linear amplifiers which is consistent with the uncertainty principle. Giffard[25] has developed a model for the rf SQUID preamplifier which predicts a minimum noise temperature in agreement with Heffner's results. A similar restriction on the dc SQUID preamplifier noise temperature must also be derived.

In this thesis, we develop a lumped circuit model for the isolated dc SQUID. We derive a set of coupled non-linear differential equations for the output voltage and circulating current as functions of time. Next, we develop a computer algorithm to compute the time-averaged SQUID I-V characteristics and noise spectral densities. The noise source

explicitly included in the SQUID equations is the Johnson noise in the shunt resistances. For certain values of the SQUID parameters, the Johnson noise sources are dominated by the shot noise in the Josephson junctions.[26,27] We approximate the noise figures for the SQUID in this case. At low frequencies ($F \lesssim 10^{-2}$ Hz), 1/F noise is also generated in the SQUID junctions.[29] We do not include this noise source explicitly in the calculation. Finally, we develop a model for the dc SQUID voltage preamplifier and magnetometer and compute the corresponding noise temperature and energy resolution as functions of the SQUID and input circuit parameters.

In section II we develop the lumped circuit model for the isolated dc SQUID. The resistively shunted junction model[30,31] is used to describe the two non-hysteretic Josephson tunnel junctions. The basic SQUID equations are derived for the general case of the completely asymmetric SQUID and cast into a convenient dimensionless form.

In section III the SQUID characteristics in the absence of noise are discussed. After briefly reviewing the relationship between critical current and applied flux as a function of the SQUID parameters, the noise-free current-voltage characteristics for the symmetric and asymmetric SQUID are calculated numerically.

In section IV the calculation is extended to include explicitly the voltage noise sources associated with the shunt resistances. The numerical techniques used to compute the noise-rounded current-voltage characteristics and the noise power spectral densities are described in detail. The algorithm is checked by computing I-$\bar{V}$ characteristics as a function of the noise parameter $\Gamma = 2\pi k_B T/I_o \Phi_o$ for the single junction,

and compared with the results obtained by Auracher[32] using a similar method, and by Ambegaokar and Halperin[33] using a Fokker-Planck calculation. The agreement is excellent. In addition, low frequency voltage power spectral densities S_V° are computed for the single junction and agree well with those computed by Vystavkin et al[34] by another method. A thermal activation model for the single junction noise rounded I-$\overline{V}$ characteristics and voltage noise spectral densities at values of the bias current below the critical current, I_c, is developed following a treatment suggested by Kurkijarvi,[35] Kurkijarvi and Webb,[36] and Fulton.[37] The voltage noise spectral density predicted by the model agrees well with the calculated results of Vystavkin et al[34] and with Fulton's activation model.[37]

The computer algorithm is extended to the dc SQUID equations. We compute noise-rounded current-voltage characteristics, voltage, circulating current, and correlation noise spectral densities, and effective flux noise spectral densities for experimentally interesting values of the SQUID parameters. A thermal activation model is developed for the dc SQUID by analogy to the single junction model for $I < I_c$, $\Phi_a = 0.5\ \Phi_o$. The values of S_V° predicted by the thermal activation model are in good agreement with the values calculated from the computor algorithm. The model is then used to compute S_J° for $I < I_c$, $\phi_a = 0.5$. A large increase in S_J° below I_c is observed.

The equivalent energy spectral density, $S_\Phi^\circ/2L$, is computed as a function of the SQUID parameters. The values obtained in the limits $\beta \gg 1$ and $\beta \ll 1$ are compared with values obtained from approximate expressions valid in those limits. The agreement is excellent. The

measured value of $S_\Phi^\circ/2L$ for the dc SQUID developed by Clarke, Goubau and Ketchen,[3] approximately 4×10^{-30} J Hz^{-1} for $\beta \sim 2.5$, is greater by a factor of four than the calculated value.

In section V the optimization of the SQUID equivalent energy resolution for fixed coupling efficiency, α^2, is discussed for the case in which the SQUID is operated in a flux-locked loop at $\Phi_a = 0.25\ \Phi_0$. We show that, if the values of the SQUID inductance and capacitance are fixed by the geometry of the SQUID, then the shunt resistance and junction critical current are determined by the two constraints $\beta_c = 2\pi I_o R^2 C/\Phi_o \lesssim 1$ and $\beta = 2LI_o/\Phi_o \sim 1$. As an example of optimization, we consider possible improvements in the tunnel junction dc SQUID of Clarke, Goubau, and Ketchen.[3] If the inductance were lowered by a factor of 3 to 0.35 nH, and if the junction capacitance were lowered by a factor of 200, the predicted energy resolution would be $S_\Phi^\circ/2\alpha^2 L \sim 4 \times 10^{-32}$ JHz^{-1} for $\alpha^2 \sim 1/2$. This is a factor of 25 smaller than the predicted energy resolution for the SQUID with $L = 10^{-9}$ H and C = 200 pF. In general, the optimal energy spectral density is fixed by the inductance and capacitance, $S_\Phi^\circ/2L = 4k_B T(\pi LC)^{1/2}$, for the SQUID limited by Johnson noise in the shunts. The ultimate resolution is obtained when the SQUID noise is dominated, not by the Johnson noise in the shunts, but rather by the shot noise in the junctions. In this case, $S_\Phi^\circ/2L \approx h/2$.

In section VI a model is developed for the dc SQUID preamplifier and dc SQUID magnetometer. The noise temperature of the preamplifier is computed as a function of the frequency, SQUID parameters L and R, SQUID noise figures S_V°, S_J°, and S_{VJ}°, and the imput circuit parameters. The model used is compared to the model developed by Davidson, Newbower

and Beasley[21] involving the single noise figure S_V^o. The optimal noise temperature at frequency ω_o for the untuned preamplifier with a Johnson noise limited SQUID with $\beta = 1$, $\Gamma = 0.05$ is $T_N^{opt} \approx 8(R_i^{opt}/L/RL_i)T/\alpha^2$ where the optimal source resistance is $R_i^{opt} \approx \omega_o L_i(1 + 1.5\alpha^2 + 0.7\alpha^4)^{\frac{1}{2}}$. The optimal noise temperature for the tuned input circuit for $\beta = 1.0$, $\Gamma = 0.05$ is $T_N^{(opt\ R_i, C_i)} \approx 2.8\ (\omega_o\ L/R)T$ where $R_i^{opt} \approx 0.35\ \alpha^2\omega_o L_i$ and $1/\omega_o C_i^{opt} \approx \omega_o L_i(1 + 3\alpha^2/4)$. In the shot noise limit, $T_N \gtrsim 17\hbar\omega_o/k_B$ for $\alpha^2 = 1/2$ in the untuned case, and $T_N \gtrsim 2.2\hbar\omega_o/k_B$ in the tuned case. Both relationships are consistent with the minimum noise temperature consistent with the uncertainty principle as determined by Heffner,[7] $T_N \gtrsim \hbar\omega_o/k_B$.

The minimum resolvable input energy density, u_o, in the input coil, L_p, of a dc SQUID magnetometer is computed from the model in the untuned and tuned case. In the untuned case, the optimal Johnson noise limited value is $u_o^{opt} \approx 9k_BT(B/F_J)$, and the optimal shot noise limited value is $u_o^{opt} \sim 11hB$ for $\alpha^2 = 1/2$. In the tuned case, the mean square signal voltage $\langle E_i^2 \rangle$ satisfies $\langle E_i^2 \rangle = 2\omega_o^2 u_o L_p \gtrsim 4k_BR_iB(T_i+T_N^*)$ where R_i is the resistance, T_i is the temperature of the input circuit, and T_N^* is the noise temperature of the SQUID. In the low temperature limit, $T_i \to 0$ and $T \to 0$, the SQUID noise temperature $T_N^* \sim 2.8\ (\omega_o L/R)T \to \hbar\omega_o/k_B$. Thus the minimum value of $\langle E_i^2 \rangle$ is determined by the SQUID shot noise sources, $\langle E_i^2 \rangle \gtrsim 4k_BT_N^*R_iB$.

Many of the results reported in this thesis have been published previously in the literature. The isolated SQUID results appear in references 38-40. The SQUID preamplifier and magnetometer results are discussed in reference 41.

II. LUMPED CIRCUIT MODEL FOR THE DC SQUID

A. The Resistively Shunted Junction Model

The dc SQUID[1] consists of a superconducting loop interrupted by two Josephson junctions (see Fig. 1a). The dc SQUIDs presently used are thin film devices. The behavior of the Josephson tunnel junctions used is adequately described by the resistively shunted junction model developed by Stewart[30] and McCumber[31]. Many of the features of the single junction behavior appear in the behavior of the SQUID. Thus we discuss this model in some detail.

The tunnel junction is modeled by an ideal Josephson junction with critical current I_o in parallel with a resistance R and capacitance C (see Fig. 1b). The total current through the combination depends on the quantum mechanical phase δ across the junction according to

$$I_J = I_o \sin\delta. \tag{2.1}$$

The voltage across the junction, V, is given by

$$V = \frac{\hbar}{2e}\frac{d\delta}{dt} = (\Phi_o/2\pi)\frac{d\delta}{dt} \tag{2.2}$$

The total current through the combination satisfies

$$I = I_o \sin\delta + (\Phi_o/2\pi R)\frac{d\delta}{dt} + (C\Phi_o/2\pi)\frac{d^2\delta}{dt^2} \tag{2.3}$$

It is convenient to use the following dimensionless units: voltage in units of I_oR, current in units of I_o, flux in units of Φ_o, and time θ in units of $\Phi_o/2\pi I_oR$. The dimensionless quantities are expressed in lower case letters. The reduced capacitance is $\beta_c = (2\pi I_oR^2/\Phi_o)C$. Eq. (2.3) then becomes

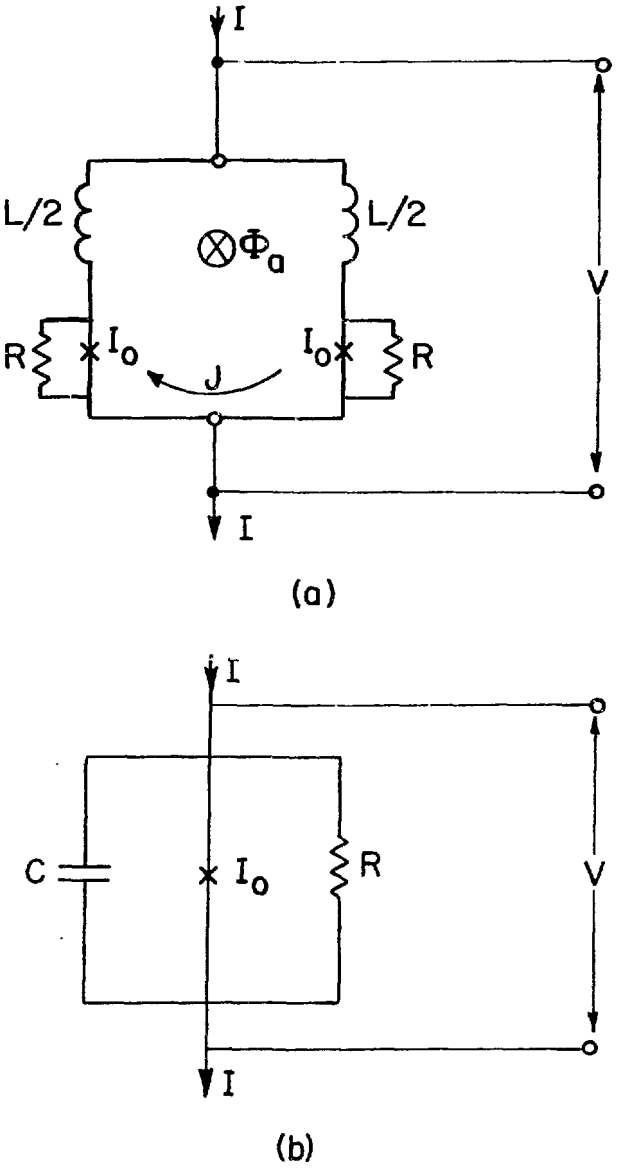

XBL 7811-6190

Fig. 1: (a) Lumped circuit model for the symmetric dc SQUID, and (b) resistively shunted junction model for the Josephson junction.

$$\beta_c \frac{d^2\delta}{d\theta^2} + \frac{d\delta}{d\theta} = \frac{-\partial u}{\partial \delta}, \tag{2.4}$$

where

$$u = U/(I_o\Phi_o/2\pi) = -\cos\delta - i\delta \tag{2.5}$$

corresponds to a potential energy for the junction.

Eq. (2.4) has the same form as the equation of motion of a particle moving in a viscous medium under the influence of gravity down a washboard surface (see J. R. Waldram's review of the Josephson effects in weakly coupled superconductors[42]). The mass of the particle corresponds to the reduced capacitance β_c, and the velocity of the particle to the voltage across the junction. For the case $i = 0$, the washboard tilt is zero. The particle velocity then damps to zero and the particle settles into a minimum at $\delta = n\pi$ ($n = 0, \pm 1, \pm 2 \ldots$). This corresponds to zero voltage across the junction. As the bias current increases, the corresponding tilt of the washboard increases until, at some critical tilt angle corresponding to a critical current i_c, the particle is no longer stationary, but moves freely down the washboard. The periodic particle velocity corresponds to an oscillating voltage developed across the junction. For the case $\beta_c = 0$, the instantaneous voltage $v(\theta)$ is given by

$$v(\theta) = \bar{v}^2/(i + \cos(\bar{v}\theta)), \tag{2.6}$$

where $\bar{v}$ is the time-averaged voltage[43]

$$\bar{v} = (i^2 - 1)^{\frac{1}{2}}. \tag{2.7}$$

For the case $\beta_c \neq 0$, the particle has inertia. If the particle is initially at rest, then it remains at rest for all values of tilt cor-

responding to $i < i_c$. If the particle is given an initial velocity, then it can sustain motion down the board over a range of tilt angles ($i < i_c$) depending on the value of β_c. Thus the corresponding $i - \bar{v}$ characteristics are hysteretic. For most applications of the dc SQUID hysteresis in the junctions results in a loss of sensitivity and is undesirable. This places a constraint on the parameter β_c. For $\beta_c \leq 1$, the effects of hystersis on the junctions are negligible[30,31]. In the equations which follow, we will take $\beta_c = 0$.

B. The Thermal Activation Model

The main sources of noise in the tunnel junctions are the Johnson noise generated in the resistive shunt and the shot noise generated by the interaction of the current through the junction and the electromagnetic field in the junction cavity. The Johnson noise is the dominant noise source for the junctions used in the dc SQUIDs fabricated at this time. The Johnson noise is modeled by a voltage noise source v_N in series with the shunt resistor. Eq. (2.4) then becomes

$$\beta_c \frac{d^2\delta}{d\theta^2} + \frac{d\delta}{d\theta} = \frac{-\partial u}{\partial \delta} + v_N, \tag{2.7}$$

where the potential $u = -\cos\delta - i\delta$. The noise voltage v_N is a function of the temperature T. In the analogous problem of a particle on a washboard surface, v_N corresponds to a random force acting on the particle. The particle undergoes Brownian motion in the force field, $-(\partial u/\partial\delta)$, oscillating within the washboard valleys and also making transitions between valleys. The average particle velocity, $\overline{\langle d\delta/d\theta \rangle}$, corresponds to the time-average voltage $\bar{v}$ developed across the junc-

tion.

Kurkijarvi[35], Kurkijarvi and Webb[36], and Fulton[37] have developed a thermal activation model to describe the behavior of the junction for bias currents $i < i_c$. In terms of the analogy to a particle on a washboard, the transition between wells is modeled by the thermally activated classical escape of a swarm of particles from a potential valley over a potential barrier. In so doing, they ignore the contribution of the motion of the particle within the well to the time-averaged velocity. Chandrasekhar[44] following a discussion by Kramers[45], has given an expression for the escape probability in terms of the curvature of the potential well and barrier, $(\partial^2 u/\partial\delta^2)_{min}$ and $(\partial^2 u/\partial\delta^2)_{max}$, the barrier height, Δu, the dimensionless thermal energy, $\Gamma = 2\pi k_B T/I_o\Phi_o$, and the inertia, which corresponds to the reduced capacitance β_c. In the limit $\beta_c < 1$ and $\Delta u >> \Gamma$, the frequency with which a particle switches from one well to the next is given by[44]

$$f_s = \frac{1}{2\pi}\left(\left|\frac{\partial^2 u}{\partial\delta^2}\right|\right)^{\frac{1}{2}}_{min}\left(\left|\frac{\partial^2 u}{\partial\delta^2}\right|\right)^{\frac{1}{2}}_{max} \exp(-\Delta u/\Gamma). \tag{2.8}$$

At the potential minimum and maximum for the single junction, we have $\partial u/\partial\delta = \sin\delta - i = 0$, $|\partial^2 u/\partial\delta^2| = \sqrt{1 - i^2}$, and $\Delta u = 2\sqrt{1 - i^2} - 2i \arccos i$, where the bias current $i < 1$.

The escape of the particle from one well to the next corresponds to the generation of a voltage pulse across the junction. The area of the pulse, a, is

$$a = \int_{well_1}^{well_2} v d\theta = 2\pi, \tag{2.9}$$

(in dimensioned units $A = \Phi_o$). The time averaged voltage for $i < 1$ is

$$\bar{v} = af_s = (1 - i^2)^{\frac{1}{2}}\exp((2/\Gamma)(-\sqrt{1 - i^2} + i \arccos i)). \qquad (2.10)$$

This approximation ignores the possibility that the voltage pulses overlap, and thus is accurate provided the pulse duration $\tau \sim 2\pi << 1/f_s$. The low frequency voltage noise spectral density, S_v^o, can be approximated as follows[37]. The average number of pulses in unit time is f_s. The root mean square fluctuation in the number of pulses in unit time is $\sqrt{f_s}$. The area of each pulse is $a = 2\pi$. Thus the mean square voltage in a unit bandwidth is $\langle v^2 \rangle = a^2 f$ and the voltage noise spectral density at frequencies f satisfying $0 < f \ll f_s$

$$S_v^o(f) = a^2 f_s = 2\pi\bar{v} . \qquad (2.10)$$

Fulton[37], following the model described by Kirkijarvi[35] uses a slightly different expression for the switching frequency f_s. He takes $\Delta u = 1.88(1 - i)^{3/2}$ and thus

$$\bar{v}_f = \exp(-1.88(1 - i)^{3/2}/\Gamma). \qquad (2.11)$$

The voltage noise power spectral density is again given by $S_v^o = 2\pi\bar{v}$.

Ivanchenko and Zil'berman[46] and Ambegaokar and Halperin[47] have calculated the $i - \bar{v}$ characteristics directly for all values of bias current using a Fokker-Planck technique. Their results are compared with Fulton's thermal activation results and our thermal activation results in Fig. 2a. In addition, voltage noise power spectral densities have been computed by Vystavkin, et al.[34] Their results are compared with the thermal activation models in Fig. 2b. Notice that both thermal activation models give $S_v^o \propto \bar{v}$. The agreement is adequate in both cases. We shall generalize our thermal activation model to the dc SQUID in section IV.5.

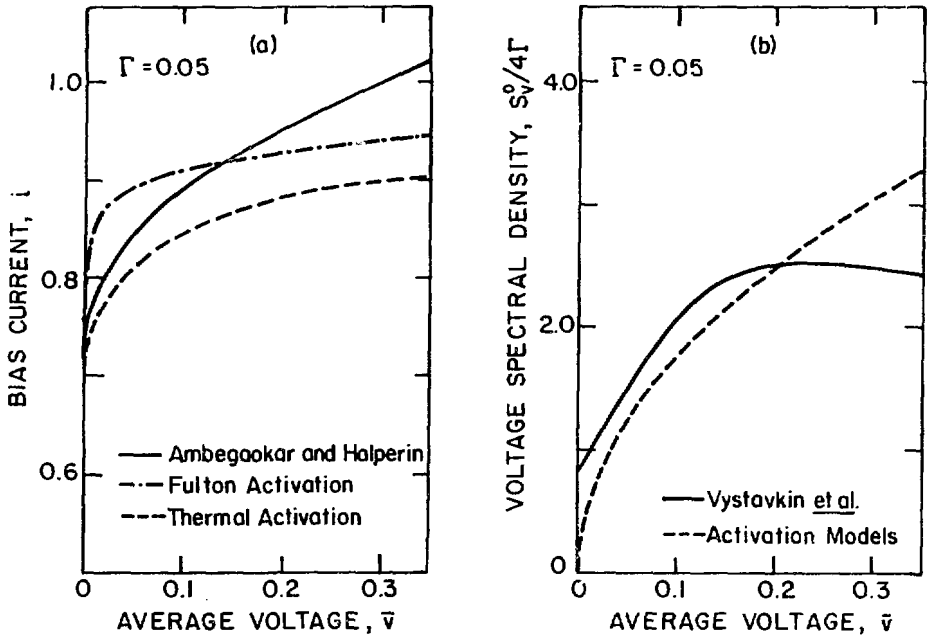

XBL 7811-6193

Fig. 2: (a) Current-voltage characteristic for the single junction with $\Gamma = 0.05$. The solid curve is from Ambegaokar and Halperin,[47] the dotted and dashed curve is from Fulton's activation model,[37] and the dotted curve is from the activation model developed here. (b) Voltage spectral density vs. average voltage. The smooth curve is from Vystavkin, et al,[34] the dotted curve is from the activation models.

C. Equations for the dc SQUID

We now derive the equations for the lumped circuit model of the dc SQUID. We consider the general case of a completely asymmetric SQUID (see Fig. 3a). The critical currents of the two junctions are $(1 - \alpha)I_o$ and $(1 + \alpha)I_o$ $(|\alpha| \leqslant 1)$. The shunt resistances are $R/(1 - \rho)$ and $R/(1 + \rho)$ $(|\rho| < 1)$. The self inductances of the two arms are L_1 and L_2, the mutual inductance between the arms is M, and the ring inductance is L. The constant bias current is I, and the time-dependent currents in each are $I_1(t)$ and $I_2(t)$. Thus

$$I = I_1 + I_2. \tag{2.12}$$

We define the circulating current J(t) to be

$$J = (I_2 - I_1)/2. \tag{2.13}$$

We assume that the flux threading each junction is always much less than a flux quantum, Φ_o, and that the currents flowing through the junctions obey the Josephson current-phase relation. The currents $I_1(t)$ and $I_2(t)$ are related to the voltages $V_1(t)$ and $V_2(t)$ and phase differences $\delta_1(t)$ and $\delta_2(t)$ across the junctions by

$$I_1 = (1 - \alpha)I_o \sin\delta_1 + (1 - \rho)(V_1 - V_{N1})/R, \tag{2.14}$$

and

$$I_2 = (1 + \alpha)I_o \sin\delta_2 + (1 + \rho)(V_2 - V_{N2})/R. \tag{2.15}$$

Here, V_{N1} and V_{N2} are the time-dependent Johnson noise voltages in series with the shunt resistors. The phase differences develop in time according to the voltage-frequency relations

$$d\delta_1/dt = (2e/\hbar)V_1, \tag{2.16}$$

and

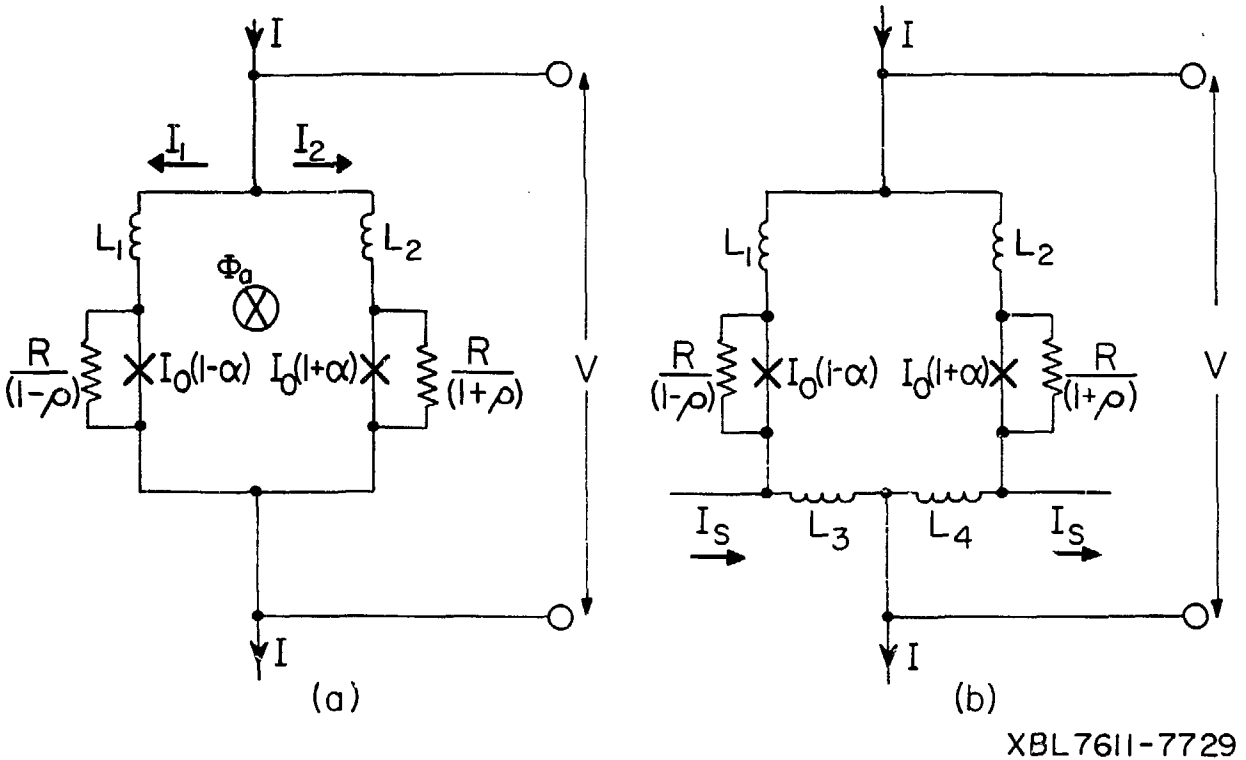

XBL7611-7729

Fig. 3: Model for the dc SQUID with (a) externally applied flux Φ_a, and (b) flux generated by a current, I_s.

$$d\delta_2/dt = (2e/\hbar)V_2, \tag{2.17}$$

The total voltage V developed across the SQUID is

$$V = V_1 + L_1 dI_1/dt + M dI_2/dt \tag{2.18}$$

and

$$V = V_2 + L_2 dI_2/dt + M dI_1/dt. \tag{2.19}$$

The phase differences δ_1 and δ_2 are related by[8]

$$\delta_1 - \delta_2 = 2\pi\Phi_T/\Phi_o, \tag{2.20}$$

where Φ_T is the total flux threading the superconducting ring. The total flux is the sum of the individual fluxes Φ_1 and Φ_2 produced by the currents I_1 and I_2 and the externally applied quasistatic flux, Φ_a. We can restrict Φ_a to the range $0 \leqslant \Phi_a \leqslant \Phi_o$ without loss of generality since all SQUID responses are periodic in Φ_a with period Φ_o. The fluxes Φ_1 and Φ_2 are proportional to the currents I_1 and I_2. Defining $\mathcal{L}_1 = -\Phi_1/I_1$ and $\mathcal{L}_2 = +\Phi_2/I_2$ we can easily show that $\mathcal{L}_1 + \mathcal{L}_2 = L$; we take $\mathcal{L}_1 = (1 - \eta)L/2$ and $\mathcal{L}_2 = (1 + \eta)L/2$ $(|\eta| \leqslant 1)$. The total flux thus becomes

$$\Phi_T = \Phi_a + LJ + \eta LI/2, \tag{2.21}$$

where we have used Eqs. (2.12) and (2.13). The geometric quantities L, L_1, L_2, $\mathcal{L}_1$, $\mathcal{L}_2$, and M are related in the following way. Suppose that in some time-dependent mode $dI_1/dt \neq 0$ and $dI_2/dt = 0$. The inductive voltage drop around the entire loop (neglecting any contributions from the junctions or shunts) is $V = L_1 dI_1/dT - M dI_1/dT$. The rate of change of flux in the ring yields $V = \mathcal{L}_1 dI_1/dt$ (again ignoring any flux contributions from the junctions or shunts). Hence $\mathcal{L}_1 = L_1 - M$, and, similarly, $\mathcal{L}_2 = L_2 - M$. Using these expressions for

M and the fact that $dJ/dt = - dI_1/dt = dI_2/dt$ (since I is constant), we can reduce Eqs. (2.18) and (2.19) to

$$V = V_1 - (1 - \eta) \frac{L}{2} \frac{dJ}{dt}, \tag{2.22}$$

and

$$V = V_2 + (1 + \eta) \frac{L}{2} \frac{dJ}{dt}. \tag{2.23}$$

These equations include the effect of the mutual inductance even though M does not appear explicitly.

The final set of equations for J and V in terms of the bias current I, the applied flux Φ_a, the noise voltages V_{N1} and V_{N2}, and the SQUID parameters I_o, R, L, α, ρ, and η are obtained from Eqs. (2.12) - (2.23) by eliminating I_1, I_2, V_1, and V_2. As in the single junction model, we use the following dimensionless units: voltage in units of I_oR, current in units of I_o, flux in units of Φ_o, and time θ in units of $\Phi_o/2\pi I_oR$. The dimensionless quantities are expressed in lower case letters. We define $\beta = 2LI_o/\Phi_o$. Hence from Eqs. (2.20) and (2.21):

$$j = (\delta_1 - \delta_2 - 2\pi\Phi_a)/\pi\beta - \eta i/2; \tag{2.24}$$

from Eqs. (2.16) - (2.23):

$$v = \frac{(1 + \eta)}{2} \frac{d\delta_1}{d\theta} + \frac{(1 - \eta)}{2} \frac{d\delta_2}{d\theta}; \tag{2.25}$$

and from Eqs. (2.12) to (2.17):

$$\frac{d\delta_1}{d\theta} = \frac{i/2 - j - (1 - \alpha) \sin\delta_1}{1 - \rho} + v_{N1}, \tag{2.26}$$

and

$$\frac{d\delta_2}{d\theta} = \frac{i/2 + j - (1 + \alpha) \sin\delta_2}{1 + \rho} + v_{N2}. \tag{2.27}$$

Equations (2.24)-(2.27) can also be used to describe the behavior of the SQUID shown in Fig. 3(b). This configuration is used in the SLUG[48], and the thin film gradiometer[4]. In this case, the applied flux is coupled to the SQUID by means of a signal current, I_s. The current I_s generates a current $I_s/2$ in the inductances L_1 and L_2 and in L_3 and L_4, together with a circulating current J_s. These currents are superimposed on the currents I/2 and J produced by the bias current, I. Hence the currents through L_1, L_2, L_3, and L_4 are

$$I_1 = I/2 - J - I_s/2 - J_s, \tag{2.28}$$

$$I_2 = I/2 + J + I_s/2 + J_s, \tag{2.29}$$

$$I_3 = I/2 - J + I_s/2 - J_s, \tag{2.30}$$

and

$$I_4 = I/2 + J - I_s/2 + J_s. \tag{2.31}$$

The bias current I is constant in time; we assume that I_s is quasi-static. Thus $dI_1/dt = dI_3/dt = - dI_4/dt = -dI_2/dt = - dJ_T/dt$, where $J_T = J + J_s$.

Since only the time dependent circulating currents J and J_s determine the voltages across the inductances, Eqs. (2.22) and (2.23) become

$$V = V_1 - (1 - \eta)(L/2)(dJ_T/dt), \tag{2.32}$$

and

$$V = V_2 + (1 + \eta)(L/2)(dJ_T/dt). \tag{2.33}$$

The parameter η describes the imbalance between the inductance of the arm containing L_1 and L_3, and the arm containing L_2 and L_4. Equations (2.14)-(2.17) for V_1, V_2, δ_1, and δ_2 are unchanged. Equation (2.21)

for the total flux Φ_T is modified by I_s. We define a parameter ξ analogous to η that describes the imbalance between the inductance of the arm containing L_1 and L_2, and the arm containing L_3 and L_4; the signal flux is then $\Phi_s = LJ_s + \xi LI_s/2$. Hence

$$\Phi_T = LJ_T + \eta LI/2 + \xi LI_s/2. \tag{2.34}$$

From Eqs. (2.28)-(2.34) with Eqs. (2.14)-(2.17), the basic equations in dimensionless parameters are:

$$j_T = (\delta_1 - \delta_2)/\pi\beta - \eta i/2 - \xi i_s/2, \tag{2.35}$$

$$v = \frac{(1 + \eta)}{2}\frac{d\delta_1}{d\theta} + \frac{(1 - \eta)}{2}\frac{d\delta_2}{d\theta}, \tag{2.36}$$

$$\frac{d\delta_1}{d\theta} = \frac{i/2 - (i_s/2 + j_T) - (1 - \alpha)\sin\delta_1}{(1 - \rho)} + v_{N1}, \tag{2.37}$$

$$\frac{d\delta_2}{d\theta} = \frac{i/2 + (i_s/2 + j_T) - (1 + \alpha)\sin\delta_2}{(1 + \rho)} + v_{N2}. \tag{2.38}$$

Equations (2.35)-(2.38) have the same form as Eqs. (2.24)-(2.27) if we identify j with $(j_T + i_s/2)$ and Φ_a with $-(1 - \xi)\beta\, i_s/4$. With these substitutions, all of the enusing results can be applied to SQUIDs in this configuration. In particular, the critical current and voltage across the SQUID are periodic in the signal current with period $(1 - \xi)LI_s/2$.

III. SQUID CHARACTERISTICS IN THE ABSENCE OF NOISE

In this section we discuss the behavior of the SQUID in the absence of noise. We thus set $v_{N1} = v_{N2} = 0$ in Eqs. (2.26) and (2.27).

A. Case I: $v = 0$

Consider first the case in which the bias current i is sufficiently low that no voltage is produced across the SQUID. The largest such current, i_c, is a function of α, β, η, and ϕ_a. Although curves of $i_c(\phi_a)$ have appeared previously in the literature,[9-16] for future reference, we include here plots of i_c vs. ϕ_a for various values of α, β, and η. For $v = 0$, we can set the time derivatives in Eqs. (2.24)-(2.27) equal to zero to obtain

$$i = (1 - \alpha)\ \sin\delta_1 + (1 + \alpha)\ \sin\delta_2\ , \tag{3.1}$$

$$2j = -(1 - \alpha)\ \sin\delta_1 + (1 + \alpha)\ \sin\delta_2\ , \tag{3.2}$$

and

$$\delta_2 = \delta_1 - 2\pi\phi_a - \pi\beta j - \pi\beta\eta i/2\ . \tag{3.3}$$

Eqs. (3.1) to (3.3) are independent of the shunt imbalance, ρ, as we expect for $v = 0$. We compute the variation of i_c with ϕ_a by numerically solving these equations.*

The procedure used to calculate $i_c(\phi_a)$ is as follows. By combining Eqs. (3.1)-(3.3) we eliminate j, and express δ_2 as a function of δ_1 and i:

$$\delta_2 = \delta_1 - 2\pi\phi_a - \pi\beta i(1 + \eta)/2 + \pi\beta(1 - \eta)\ \sin\delta_1\ . \tag{3.4}$$

We define a function of i and δ_1 to be

$$F(i,\delta_1) = i - (1 - \alpha)\ \sin\delta_1 - (1 + \alpha)\ \sin\delta_2\ . \tag{3.5}$$

---

*An elegant alternative method of solution has been given by Tsang and Van Duzer.[16]

Eq. (3.1) is satisfied when $F(i,\delta_1) = 0$. Plots of $F(i,\delta_1)$ vs. δ_1 for fixed i generate a family of continuous curves each labeled by the value of i. Since F is also continuous in i, the curve corresponding to the greatest value of i that still has a zero (i.e. $F(i,\delta_1) = 0$ for some δ_1) will necessarily satisfy $\partial F/\partial\delta_1 = 0$ at that point. Hence,

$$\partial F/\partial\delta_1 = -(1 - \alpha)\cos\delta_1 - (1 + \alpha)[1 + \pi\beta(1 - \alpha)\cos\delta_1]\cos\delta_2 \ . \quad (3.6)$$

Equation (3.5) with F = 0 and Eq. (3.6) with $\partial F/\partial\delta_1 = 0$ allow us to express δ_1 in terms of i:

$$i = (1 - \alpha)\sin\delta_1 + \left\{(1 + \alpha)^2 - \left[\frac{(1 - \alpha)\cos\delta_1}{1 + \pi\beta(1 - \alpha)\cos\delta_1}\right]^2\right\}^{1/2} \ . \quad (3.7)$$

Now both F and $\partial F/\partial\delta_1$ can be expressed as function of a single variable δ_1. We search for the simultaneous zeros of F and $\partial F/\partial\delta_1$ with respect to δ_1 using a Newton-Raphson search routine in one variable only, and thus determine the maximum supercurrent, i_c, as a function of α, β, η, and ϕ_a.

Curves of i_c vs. ϕ_a for variable α and η with $\beta = 1.0$ appear in Figs. 4(a) and 4(b) respectively. Equations (3.1)-(3.3) imply that i_c attains the maximum value, 2.0, for some ϕ_a whatever the values of α, η, and β. With $\delta_1 = \delta_2 = \pi/2$, we have $j = \alpha$ and $\phi_a = -\beta(\alpha + \eta)/2$ at that point. The values of i_c at other values of ϕ_a depend on η and α in the following manner. When $\eta = 0$, the modulation depth $\Delta i_c = i_{cmax} - i_{cmin}$, falls to zero as α is increased from 0 to 1. In addition, the value of ϕ_a at which i_{cmin} occurs shifts away from 0.5 as the SQUID asymmetry increases. In the limit $|\alpha| = 1$, $i_c = 2$ for all ϕ_a. It

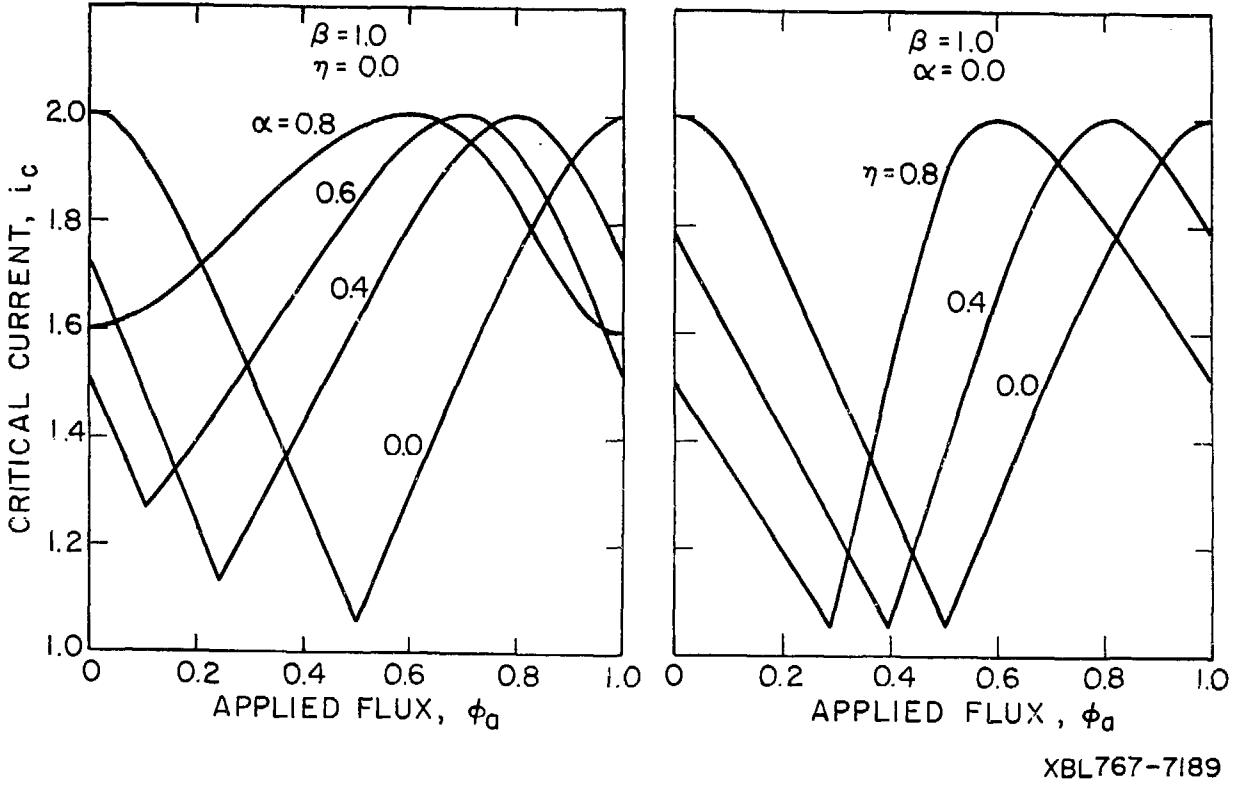

Fig. 4: Critical current of SQUID vs. applied flux as a function of (a) α, and (b) η.

should be noted that in the large β limit, Δi_c is much less sensitive to the value of α: Zimmerman and Silver[8] demonstrated experimentally that Δi_c becomes significantly reduced only when the critical current of one of the junctions fall below $\Delta i_c(\alpha = 0)$.

The modulation Δi_c is independent of the value of η, as can be seen from Fig. 4(b). For $\alpha = 0$, the value of ϕ_a at i_{cmin} is shifted from $\phi_a = 0.5$ for $\eta = 0$ to $\phi_a = 0.5 - \beta\eta i_{cmin}/4$ for $\eta \neq 0$. In fact, the entire i_c vs. ϕ_a curve for arbitrary η can be readily generated from the corresponding $\eta = 0$ curve. A particular value of i_c at ϕ_a^o for $\eta = 0$ will occur at $\phi_a^\eta = \phi_a^o - \beta\eta i_c/4$ for $\eta \neq 0$. Since the amount by which ϕ_a^η is shifted increases with i_c, the $\eta \neq 0$ curves appear skewed. To see this, suppose the set of values (v^o, j^o, ϕ_a^o) satisfy Eqs. (2.24)-(2.27) for arbitrary α, ρ, β, and i with $\eta = 0$. We want to show that the set $(v^\eta, j^\eta, \phi_a^\eta)$ for $\eta \neq 0$ can be shifted so that the shifted values satisfy the $\eta = 0$ equations, and hence have the $\eta = 0$ time-averaged values. Now the set $(v^\eta, j^\eta, \phi_a^\eta)$ satisfy Eqs. (2.24)-(2.27) with $\eta \neq 0$. Rewriting these equations, we have

$$j^\eta = (\delta_1 - \delta_2)/\pi\beta - (\phi_a^\eta - \pi\beta i/4)2/\beta \ , \tag{3.8}$$

$$\text{and } v^\eta - (d\delta_1/d\theta - d\delta_2/d\theta)\eta/2 = (d\delta_1/d\theta + d\delta_2/d\theta)/2 \ . \tag{3.9}$$

Since both ϕ_a and i are independent of time, we have

$$\eta\beta dj^\eta/d\theta = d\delta_1/d\theta - d\delta_2/d\theta \ . \tag{3.10}$$

Hence

$$v^\eta - (\pi\eta\beta/2)dj^\eta/d\theta = (d\delta_1/d\theta + d\delta_2/d\theta)/2 \ . \tag{3.11}$$

If we take $v^s = v^\eta - (\pi\eta\beta/2)dj^\eta/d\theta$, $j^s = j^\eta$, and $\phi_a^s = \phi_a^\eta - \pi\beta i/4$ we see

that the shifted set (v^s, j^s, ϕ_a^s) satisfy Eqs. (2.24)-(2.27) for $\eta = 0$. Hence the time-averaged values $\overline{v^s}$ and $\overline{j^s}$ evaluated at ϕ_a^s will equal the original average values $\overline{v^o}$ and $\overline{j^o}$ at $\phi_a^o = \phi_a^s$. But $\overline{j^s} = \overline{j^\eta}$, and $\overline{v^s} = \overline{v^\eta} - (\pi\eta\beta/2)dj^\eta/dt = \overline{v^\eta}$. Hence the values $\overline{v^\eta}$ and $\overline{j^\eta}$ at some ϕ_a^η are just the values of $\overline{v^o}$ and $\overline{j^o}$ at $\phi_a^\eta - \eta\beta i/4$. Consequently, an imbalance η in the SQUID inductance appears as an effective external flux $-\eta\beta i/4$ for fixed bias current i.

Curves of i_c vs. ϕ_a for various values of β with $\alpha = \eta = 0$ are plotted in Fig. 5. Similar curves have been published elsewhere.[49] Notice the cusp in the curve at $\phi_a = 0.5$. Let $\Delta I_c = 2I_o - I_c(\Phi_o/2)$ be the modulation depth in dimensioned units. We display the dependence of ΔI_c on the parameters L and I_o in Fig. 6. For variable L and fixed I_o, the modulation depth is expressed in dimensionless units as $(\Delta I_c/2I_o)$, and plotted vs. $\beta = L(2I_o/\Phi_o)$ in Fig. 6(a). As L is reduced below a value corresponding to $\beta \approx 0.1$, ΔI_c approaches the limit $2I_o$ independent of L. Hence decreasing the SQUID inductance below 0.1 $\Phi_o/2I_c$ has little effect on ΔI_c.

The dependence of ΔI_c on I_o for fixed SQUID inductance L is plotted in Fig. 6(b). Here, the modulation depth is plotted as the dimensionless parameter $\Delta I_c/(\Phi_o/L)$ vs. $\beta = I_o(2L/\Phi_o)$. For $\beta \gtrsim 40$, $\Delta I_c \approx \Phi_o/L$. Thus the modulation depth approaches a limit independent of I_o for sufficiently large values of I_o. The experimental points shown were obtained by Clarke and Paterson using a SQUID with SNS junctions.[50] The agreement is excellent.

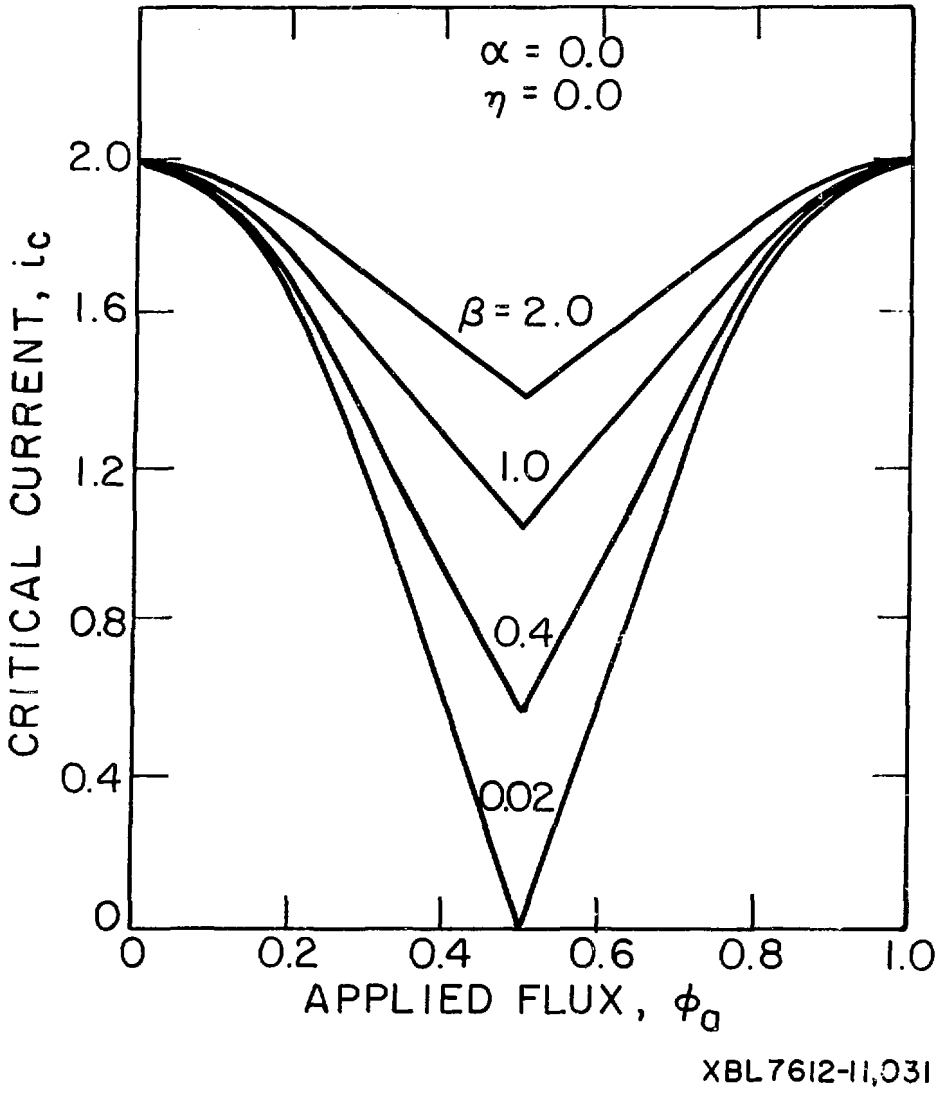

Fig. 5: Critical current of SQUID vs. applied flux as a function of β.

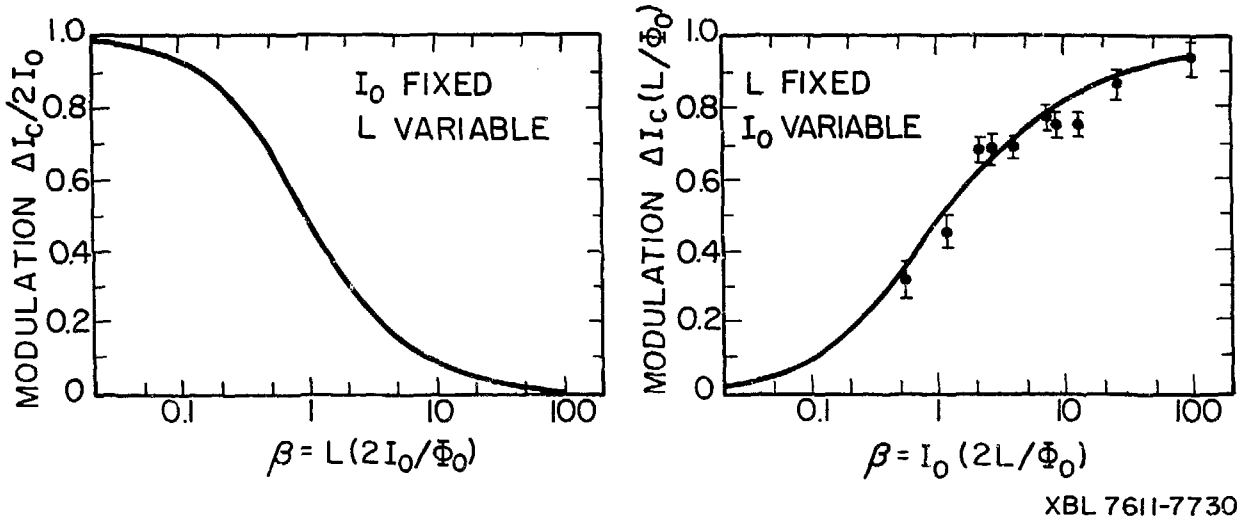

Fig. 6: Critical current modulation vs. β as a function of (a) L, and (b) I_0.

B. Case II: $v > 0$

When the SQUID is biased at a constant current $i > i_c$, the circulating current j and voltage v oscillate in time. We integrate Eqs. (2.24) to (2.27) stepwise in time to determine the dependence of $v(\theta)$ and $j(\theta)$ on α, β, η, ρ, and ϕ_a. The initial conditions are chosen to minimize the transient response of the SQUID. The results shown for $v(\theta)$ and $j(\theta)$ are taken after several oscillations, and thus reflect the steady state behavior corresponding to the state of least energy of the SQUID. Fig. 7 shows $v(\theta)$ and $j(\theta)$ vs. time for several values of the SQUID parameters. The period of oscillation for $v(\theta)$ is $\tau = 2\pi/\bar{v}$ in all cases, where $\bar{v}$ is the time-averaged voltage. For the special case of a completely symmetric SQUID ($\alpha = \eta = \rho = 0$) at $\phi_a = 0$, $j(\theta) \equiv 0$. For the symmetric SQUID at $\phi_a = 0.5$, $j(\theta)$ oscillates symmetrically about zero with period $\tau/2$. For all other cases, the current $j(\theta)$ also oscillates with the period τ of the voltage oscillations. For bias currents very near i_c, $v(\theta)$ and $j(\theta)$ exhibit sharp spikes, indicating the presence of many higher harmonics of the fundamental frequency. As i is increased, $v(\theta)$ and $j(\theta)$ become progressively more sinusoidal. This behavior is very similar to that observed in single junctions.[43]

The curves of voltage vs. time can be averaged over a complete cycle to yield i-$\bar{v}$ characteristics as functions of the various SQUID parameters. In Fig. 8(a) we plot i-$\bar{v}$ characteristics for the symmetric SQUID with $\beta = 1.0$ for several values of ϕ_a. The effect of changing β on the i-$\bar{v}$ characteristics for $\phi_a = 0.5$ is seen in Fig. 8(b). As i increases, the characteristics approach the equivalent single junction curve (represented in Fig. 8(a) as $\phi_a = 0$, and in Fig. 8(b) as $\beta \sim \infty$).

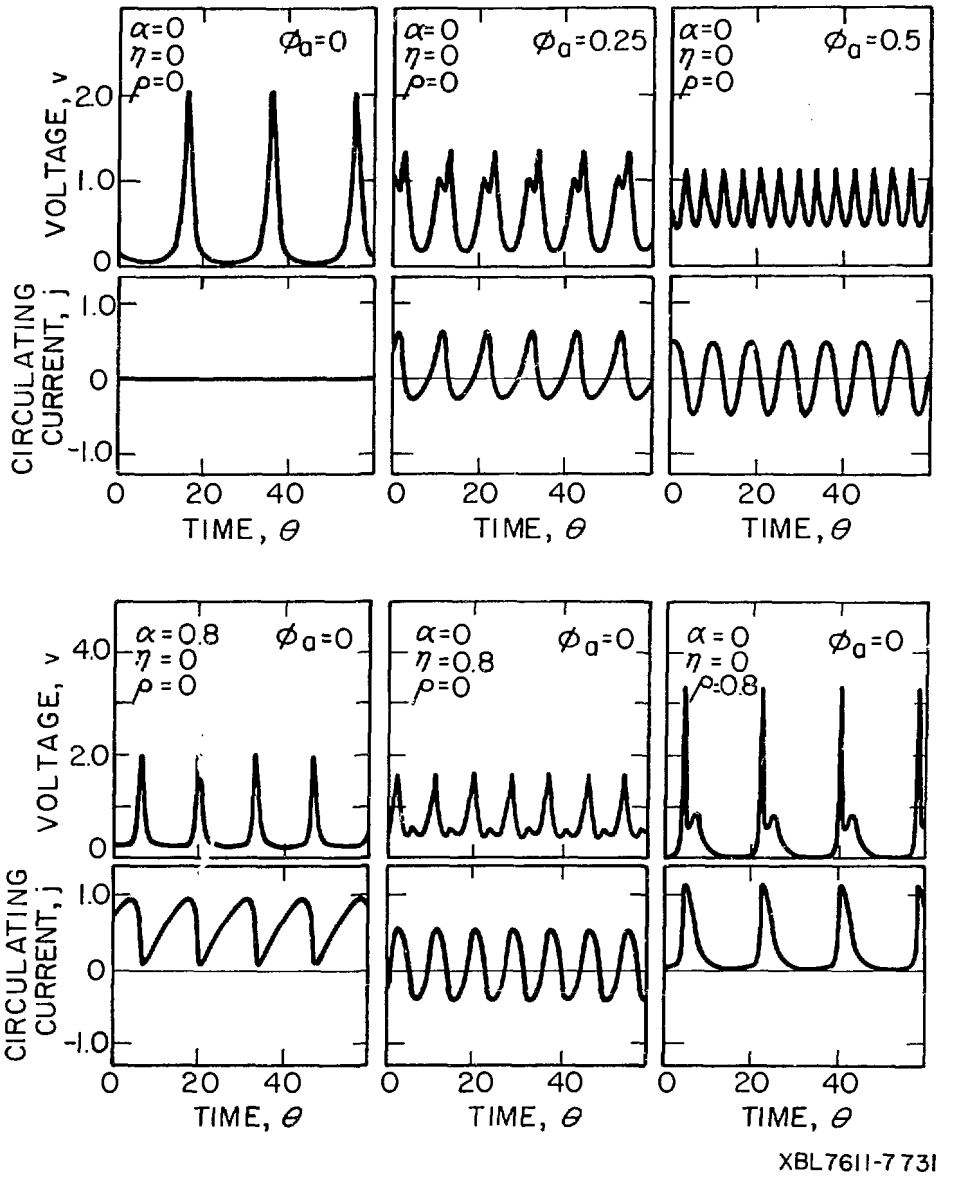

Fig. 7: Voltage and circulating current vs. time as functions of applied flux, α, η, and ρ.

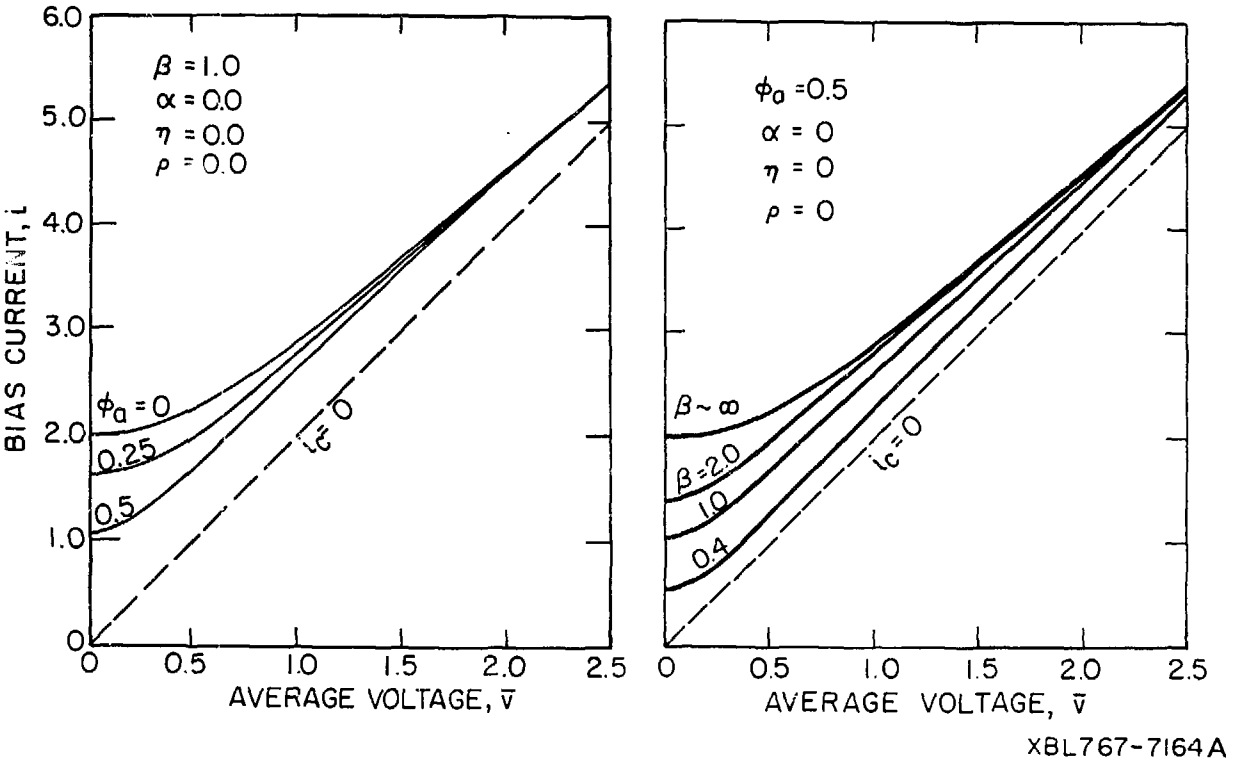

Fig. 8: Current-voltage characteristics of the symmetric SQUID as a function of (a) applied flux, and (b) β.

Hence the SQUID voltage becomes essentially independent of the applied flux, ϕ_a, for large values of i ($i \gtrsim 4.0$). At lower values of i, the presence of instantaneous circulating currents through the junctions for $\phi_a \neq 0$ produces an increase in $\bar{v}$ over the single junction value.

The dependence of the average $\bar{v}$ and average circulating current $\bar{j}$ on ϕ_a for the symmetric SQUID for various values of β at $i = 2.1$ is shown in Fig. 9. We see that $\bar{j} = 0$ for $\phi_a = 0$ and 0.5 only.

The dependence of the i-$\bar{v}$ characteristics and the curves of $\bar{j}$ vs. ϕ_a and $\bar{v}$ vs. ϕ_a on the degree of SQUID asymmetry is shown in Fig. 10 for $\beta = 1$. Notice that the discontinuity in slope in the i_c vs. ϕ_a curves is not present in the $\bar{v}$ vs. ϕ_a curves. Consider first the family of curves [Figs. 10(a)-(c)] for $\eta \neq 0$. The curves of $\bar{j}$ and $\bar{v}$ vs. ϕ_a with $\eta \neq 0$ are found by shifting the curves for $\eta = 0$ by flux $- \eta\beta i/4$ as discussed in section 3A. However, since the shift is proportional to i, the i-$\bar{v}$ characteristics for $\eta \neq 0$ cannot be generated by a simple shift of the $\eta = 0$ characteristics.

The i-$\bar{v}$ characteristics for $\phi_a = 0.5$, and curves of $\bar{j}$ and $\bar{v}$ vs. ϕ_a for $i = 2.1$ are plotted in Fig. 10(d)-(f) for several values of α, the critical current imbalance. As $|\alpha| \to 1$, the i-$\bar{v}$ characteristic becomes independent of ϕ_a, and approaches the single junction characteristic. This behavior can also be seen in $\bar{v}$ vs. ϕ_a [Fig. 10(f)]. In addition, as $|\alpha| \to 1$, $\bar{j}$ increases for all values of ϕ_a.

The curves in Fig. 10(g)-(i) for various values of ρ show the effects of an imbalance in the shunt resistances. For $\phi_a = 0.5$, the i-$\bar{v}$ characteristics are relatively independent of ρ. This insensitivity to ρ is reflected in the $\bar{v}$ vs. ϕ_a curves. However, the curves of $\bar{j}$ vs. ϕ_a

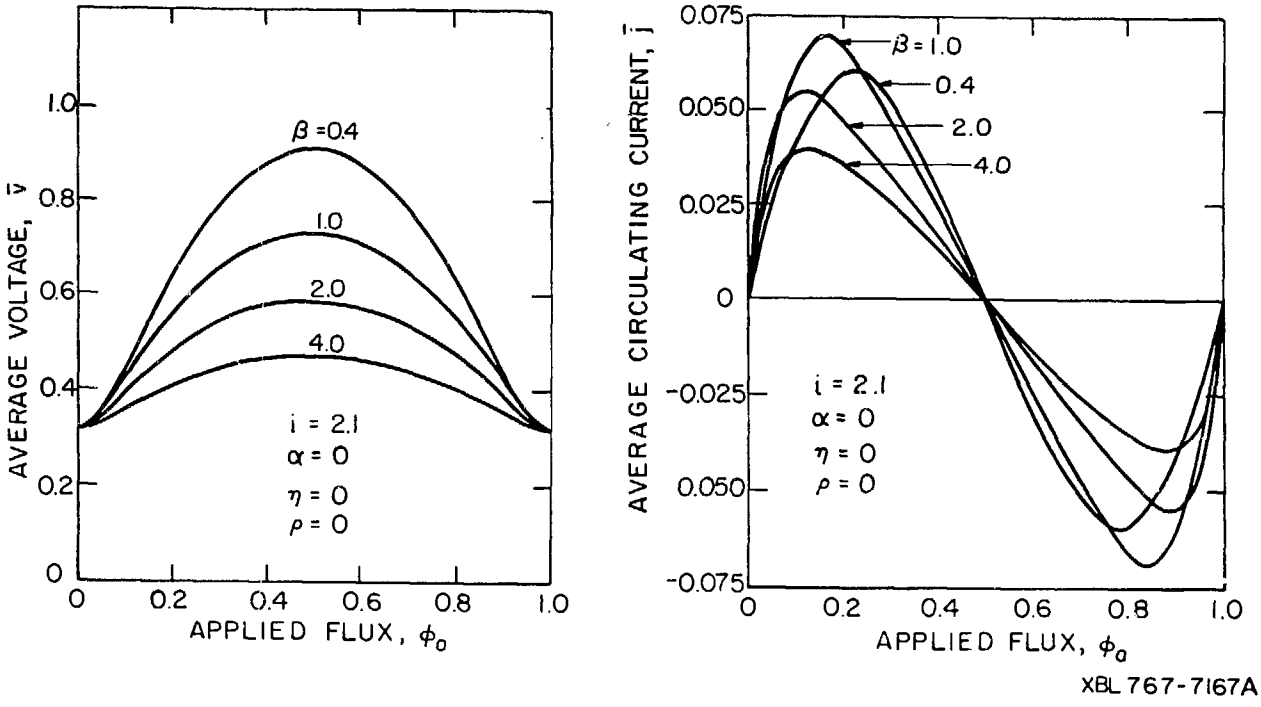

Fig. 9: (a) Average voltage and (b) average circulating current vs. applied flux as a function of β.

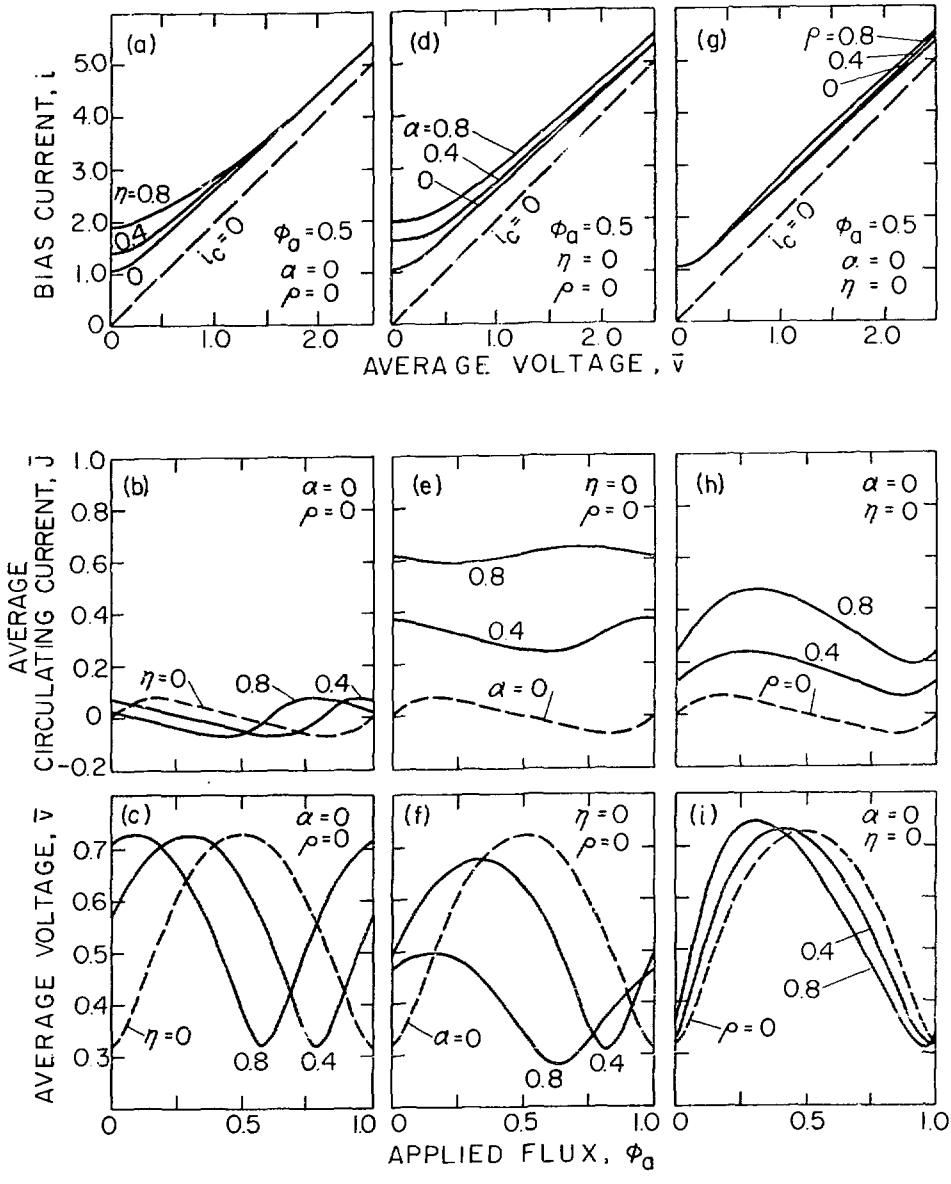

XBL 7612-11,036

Fig. 10: (a), (d), (g) Current-voltage characteristics; (b), (e), (h) average circulating current vs. applied flux; and (c), (f), (i) average voltage vs. applied flux, for the SQUID as functions of η, α, and ρ. In all cases $\beta = 1$.

are relatively sensitive to the value of ρ; in the limit of large i, $\bar{j}$ approaches $i\rho/2$.

C. Discussion

We conclude that the behavior of the dc SQUID is relatively insensitive to quite large asymmetries in the inductance of the two arms, in the critical currents, or in shunt resistances of the two junctions, provided that neither critical current falls below $\Delta i_c(\alpha = 0)$. Consequantly, it appears that near-optimum performance can be achieved with a wide range of values of η, α, and ρ. In the remainder of the thesis we will be concerned only with the symmetric case $\eta = \alpha = \rho = 0$.

IV. SQUID CHARACTERISTICS IN THE PRESENCE OF NOISE

In this section we discuss the behavior of the SQUID in the presence of Johnson noise generated in the resistive shunts. We first discuss our numerical techniques. As a check on these techniques, we show that our results for the noise-rounded i-$\bar{v}$ characteristics and voltage noise spectral densities for a single shunted junction are in good agreement with work previously published[32,33,34,37]. We then compute the i-$\bar{v}$ characteristics, voltage noise spectral density, current noise spectral density, correlation noise spectral density, and flux resolution of the SQUID as functions of the relevant parameters.

A. Numerical Techniques

We assume that the Johnson noise voltages across the external shunt resistances dominate any other source of noise in the SQUID, for example, shot noise in the junctions[26,27], or thermal fluctuations in the critical current[29]. The voltage noise sources v_{N1} and v_{N2} in Eqs. (2.24)-(2.27) are then uncorrelated, each having a white voltage spectral density, $S_V^N = 4k_BTR$, or, in dimensionless units, $S_v^N = 4\Gamma$, where[34] $\Gamma = 2\pi k_BT/I_o\Phi_o$. We approximate the random voltages $v_N(\theta)$ by trains of voltage pulses each of duration $\Delta\theta$ and random amplitude v_k. We have used two different techniques to generate the v_k. In Method I we generate a pseudo-random set of Gaussian distributed v_k. We then integrate Eqs. (2.24)-(2.27) using a simple integration routine. The resultant $v(\theta)$ is used to calculate noise-rounded i-$\bar{v}$ characteristics. Unfortunately, as we shall discuss, the calculation of spectral densities from these $v(\theta)$ requires large amounts of computer time. In

Method II we use an approximation for the v_k that reduces significantly the computation time for the spectral densities.

Method I. We use a pseudo-random number generator to generate a Gaussian-distributed set v_k of zero mean with $\langle v_k^2 \rangle = 2\Gamma/\Delta\theta$. The computed power spectrum of the voltage pulses averaged over many sets v_k is white and tends to a constant, 4Γ, as required. Two independent trains of voltage pulses are used to approximate v_{N1} and v_{N2} in Eqs. (2.24)-(2.27). We integrate the phases $\delta_1(\theta)$ and $\delta_2(\theta)$ using an iterative scheme $\delta(\theta + \Delta\theta) = \delta(\theta) + \Delta\theta\, d\delta/d\theta$. The value of $\Delta\theta$ is chosen so that $\Delta\theta\, d\delta/d\theta \ll 2\pi$. The noise-rounded i-$\bar{v}$ characteristics labeled Method I in Figs. 13(a) and 14(a) and the transfer functions in Fig. 15 were generated by time-averaging $v(\theta)$ computed in this way. We estimate that the results are accurate to ± 5%.

Spectral densities, S_v, S_j, and S_{vj}, can be calculated directly from the $v(\theta)$ and $j(\theta)$ generated by Method I. For example, N values of $v(\theta)$ at equal time steps $\Delta\theta$ can be used to calculate S_v at frequency intervals of $\delta f = 1/N\Delta\theta$. For the case of a single shunt resistance ($i_c = 0$), the values of $v(\theta)$ are just the v_k, and the spectral density (averaged over many sets of v_k) tends to 4Γ as required. We shall be interested in computing spectral densities for the single junction and the SQUID from values of $v(\theta)$ sampled at time intervals corresponding to $n\Delta\theta$ (n is an integer). In those cases, the averaged spectral density for a single shunt resistance is white with a magnitude $n4\Gamma$. The additional factor n is a result of the normalization of the v_k. For v_k defined over time steps $\Delta\theta$, $\langle v_k^2 \rangle = 2\Gamma/\Delta\theta$, while for v_k defined over $n\Delta\theta$, $\langle v_k^2 \rangle = 2\Gamma/n\Delta\theta$. Hence generating v_k over time steps $\Delta\theta$ and sampling

the resultant $v(\theta)$ over time steps $n\Delta\theta$ increases the spectral density by a factor n. It is important to notice that this simple relationship will <u>not</u> hold in general for the case of the single shunted junction or SQUID, since in the limit $\Gamma \to 0$ those spectral densities must be independent of n. Hence to obtain results for S_v that are consistent in both the noise-dominated and noise-free limits, we must take $n = 1$.

The restriction $n = 1$ limits our ability to calculate spectral densities efficiently from $v(\theta)$ and $j(\theta)$ generated by Method I. To see this, we briefly discuss the general behavior of the spectral densities for $i \neq 0$, $\Gamma \neq 0$. The spectral densities contain noise-broadened peaks at the fundamental Josephson frequency $f_J = \bar{v}/2\pi$ and its harmonics. We are interested in computing the low frequency spectral densities, S_v°, S_j°, and S_{vj}°, at frequencies well below f_J, where the spectral densities are white. As the bias current, i, is lowered towards i_c the harmonics become more important, and, as $\Gamma(T)$ is increased from zero, the broadening increases. Thus, for $i \sim i_c$, and for experimentally interesting values of Γ, S_v, S_J and S_{VJ} must be computed for frequencies well above and well below f_J. However, the lowest frequency is $\delta f = 1/N\Delta\theta$, where $\Delta\theta \sim 10^{-4}/f_J$. Thus $N \gg 10^4$ (for example, for $i \sim i_c$ and $\Gamma \sim 0.05$, $N \sim 10^6$), and the computation of a single spectral density is very time consuming. In addition, many spectral densities (typically 40) must be averaged together to obtain accurate results. We thus use an alternative method to generate v_k; this method significantly reduces the computation time for spectral densities at experimentally relevant values of i and Γ.

Method II. We generate values of the Fourier transform, $\tilde{v}_k$, of the Johnson noise voltages at N equal frequency intervals δf. The interval δf is fixed by the requirement $\delta f \ll f_J$, and N is fixed by the requirement $N\delta f \gg f_J$. The actual values of N and δf are determined empirically by computing low frequency spectral densities S_v° for the SQUID for variable N and δf. N is increased and δf is decreased until S_v° becomes independent of N and δf. Typically, N = 512 and $\delta f = 0.01$ f_J. Our values $\tilde{v}_k$ approximate the Johnson noise in the following way. The Fourier transform of a set of Gaussian distributed noise voltages, v_k, is a set of complex numbers with Gaussian distributed amplitudes and uniformly distributed phases.[51] We approximate the Fourier transform of the noise pulses by a set of complex numbers with constant amplitude and uniformly distributed phases. The amplitude of $\tilde{v}_k$ is fixed by the requirement $\langle v_k^2 \rangle = 2\Gamma N\delta f$, and the random phases are generated by a pseudo-random number generator with uniform distribution over $[0, 2\pi]$. We find that the voltage pulse amplitudes, v_k, generated in this way are Gaussian distributed. Figure 11 shows a histogram of the v_k obtained from 30 sets of $\tilde{v}_k$ in this way, together with the exact Gaussian distribution with $\langle v^2 \rangle = 2\Gamma N\delta f$. The agreement between the two curves is good. This approximation enables us to compute smooth average spectral densities for a single junction using only one set of $\tilde{v}_k$, and for the SQUID using only a small number of sets of $\tilde{v}_k$.

The Fourier transforms of the $\tilde{v}_k$ were taken as representative values of the Johnson noise over pulse times $\delta\theta = 1/2N\delta f$. Since $\delta\theta$ was considerably larger than the value of $\Delta\theta$ used in Method I, we interpolated between adjacent noise values. We found our results for S_v° were

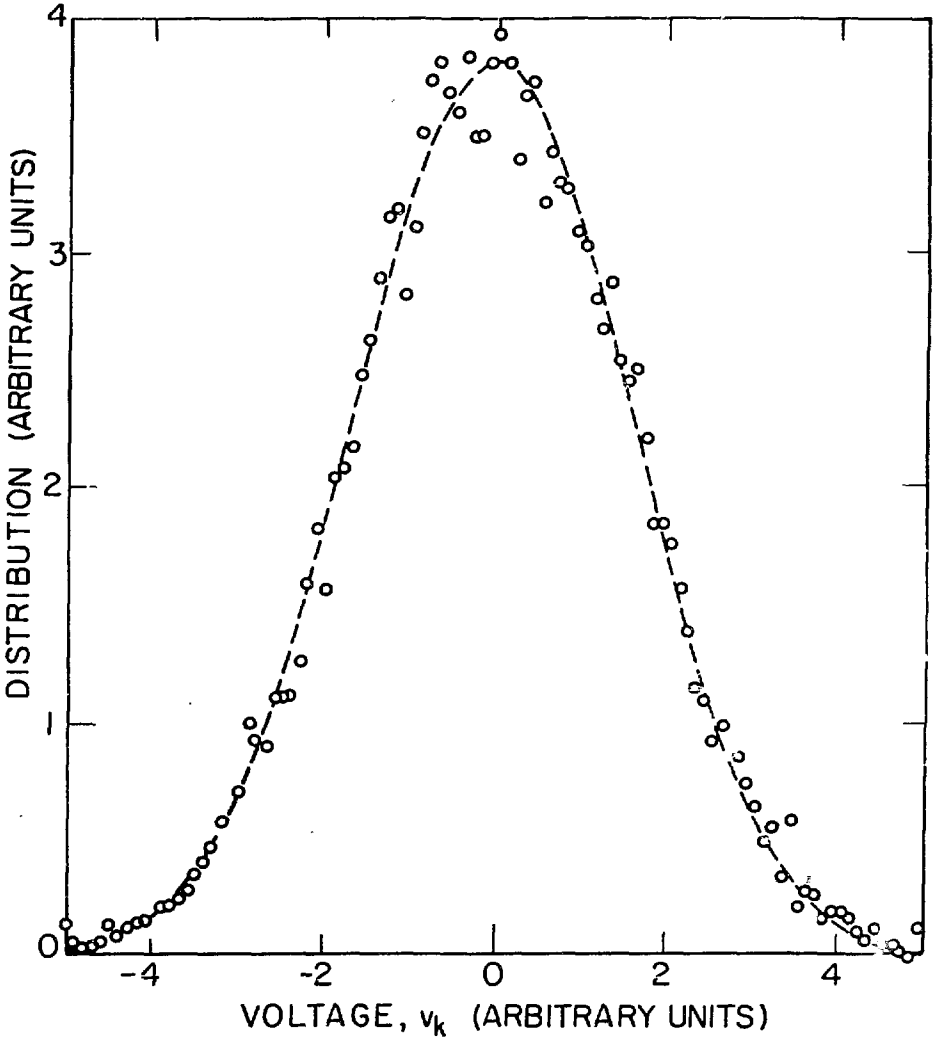

XBL 773-5170

Fig. 11: Histogram of random voltages v_k generated by Method II for 30 trials. Dotted curve is Gaussian with the same normalization.

independent of the details of the interpolation scheme used. Hence we use a linear interpolation for convenience.

We found Methods I and II yielded identical noise-rounded i-$\bar{v}$ characteristics for a single junction (section IV.B). We also computed spectral densities of the voltage noise across a single junction for $i \gg i_c$ from $v(\theta)$ generated by Methods I and II. The two methods yielded spectral densities that were in good agreement. However, whereas we needed to average the spectral density typically 40 times using Method I, only a single set of v_k was required using Method II. We also computed spectral densities using $\tilde{v}_k$ with Gaussian distributed amplitudes. The values for S_v^o averaged over many trials were in agreement with those obtained with constant amplitude v_k. We conclude that our approximation scheme adequately represents the Johnson noise for our purposes.

Method II was used to compute the voltage noise spectral densities [Fig. 16], the current noise spectral densities [Fig. 17], and the correlation spectral densities [Fig. 18]. Equations (2.24)-(2.27) were integrated with interpolated noise values determined by the v_k as in the single junction case. We checked the values of the average voltage computed from $v(\theta)$ at time intervals $\delta\theta$ with those obtained by Method I, and found good agreement. Because the SQUID involves two independent random noise sources, we found it necessary to average the spectral densities over typically 8 sets of v_k to achieve a satisfactory result. We estimate that our values are accurate to ± 5%.

B. Single Junction with Noise

In order to test our numerical techniques, we first applied Methods I and II of section IV.A to the case of a single resistively shunted

Josephson junction. For a junction biased at a constant current i, the voltage v and phase δ across the junction satisfy[33]

$$v = i - \sin\delta + v_N \quad , \tag{4.1}$$

and

$$d\delta/d\theta = v \ , \tag{4.2}$$

where v_N is the Johnson noise voltage across the shunt resistance. We have eliminated the junction capacitance, β_c, as discussed in section II. We integrated these equations stepwise in time for various values of i and Γ. Representative plots of $\delta(\theta)$ and $v(\theta)$ for $i = 0.9$ and $\Gamma = 0.05$ appear in Fig. 12. The phase $\delta(\theta)$ undergoes random excursions of considerably less than 2π about an equilibrium position for a period of time, then makes a fairly sharp transition of $+ 2\pi$ to an equivalent equilibrium position. These transitions are randomly timed and, according to Eq. (4.2), give rise to voltage pulses during the transitions. These voltage pulses are somewhat obscured in the plot of v vs. θ in Fig. 12(b). The v vs. θ curve appears to be dominated by the random noise source v_N shifted by a constant voltage. This behavior is consistent with Eq. (4.1) since the term $(i - \sin\delta)$ is approximately constant between the transitions $\delta \to \delta + 2\pi$. Notice that, although the excursions of δ around the equilibrium positions are small compared with 2π, the time derivative, $d\delta/d\theta = v$, is not small compared with the amplitude of the voltage pulses associated with the transitions in δ. In fact, as we decrease $\Delta\theta$ to improve our approximation for the Johnson noise source, $v \sim v_N \propto 1/\Delta\theta$ increases. Since the voltage pulses associated with the 2π transitions of δ have fixed area and duration, they become buried in the Johnson noise voltage pulses as $\Delta\theta$ decreases.

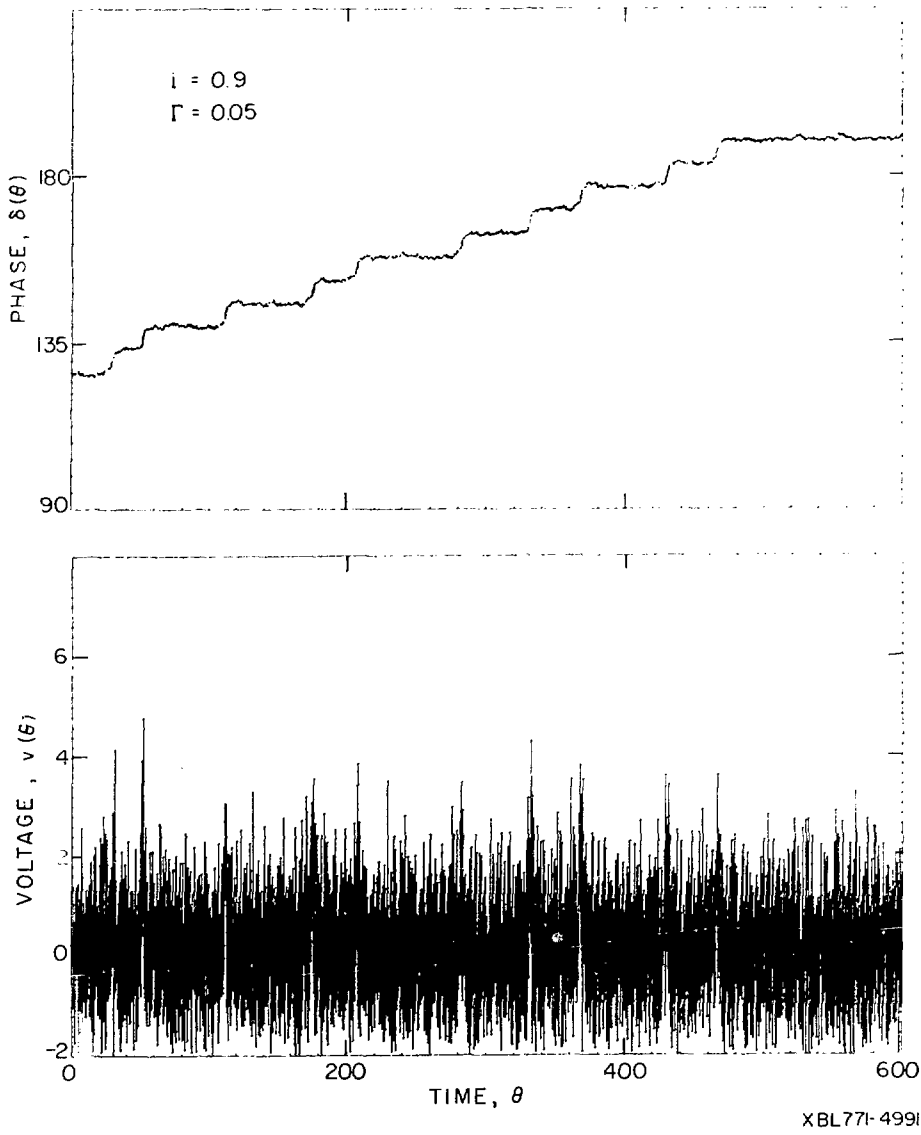

Fig. 12: Representative plots of (a) phase, and (b) associated voltage vs. time for single junction with $\Gamma = 0.05$, and $i = 0.9$.

This behavior is consistent with the thermal activation model described in section II.A. The oscillation of the phase about the equilibrium value corresponds to the Brownian motion of the particle within the well. Since the well is not symmetric for $i > 0$ but skewed slightly downward for increasing values of δ, the average velocity (corresponding to the average voltage) due to the motion within the well is slightly positive. The jumps of 2π between equilibrium values of the phase correspond to the transitions of the particle between wells. Note that in the thermal activation model, the contribution to $\bar{v}$ and S_v from the oscillations within the wells is neglected, and the calculation restricted to bias currents $i \ll 1$.

We obtained i-$\bar{v}$ characteristics by time-averaging $v(\theta)$ at fixed i. The i-$\bar{v}$ characteristics obtained using both Methods I and II to generate $v(\theta)$ are shown in Fig. 13(a). The smooth curves are from the Fokker-Planck calculation of Ambegaokar and Halperin.[33] The results of the two numerical techniques are in excellent agreement with each other, with the Fokker-Planck calculation,[33] and with other numerical calculations.[32,52]

We also computed voltage power spectral densities, S_v, from curves of v vs. θ using Method II. We observed that the peaks in S_v corresponding to the noise-free Josephson frequency, f_J, and its harmonics become broadened in the presence of thermal noise. As i is reduced, the noise broadening increases in a manner that is consistent with the results of Vystavkin et al.[34] At frequencies well below f_J the power spectrum is white. We take the value of S_v in this region to be the low frequency spectral density S_v°. In Fig. 13(b) we plot the square

Fig. 13: (a) Current-voltage characteristics of single resistively shunted junction in presence of noise computed with Method I (•), and Method II (Δ, □, o). Solid curves are from Ambegaokar and Halperin.[47] Dotted line is noise-free characteristic. (b) Low frequency voltage spectral density vs. average voltage for single resistively shunted junction computed with Method II (Δ, □, o). Solid curves are from Vystavkin et al.[34]

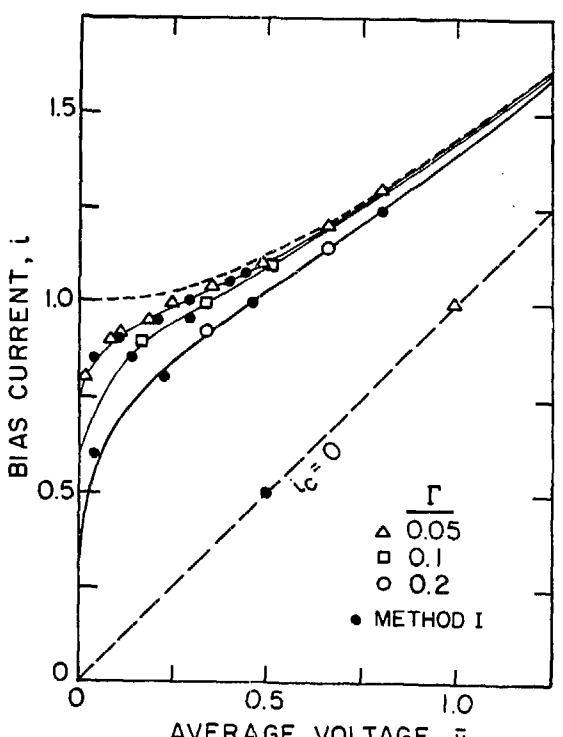

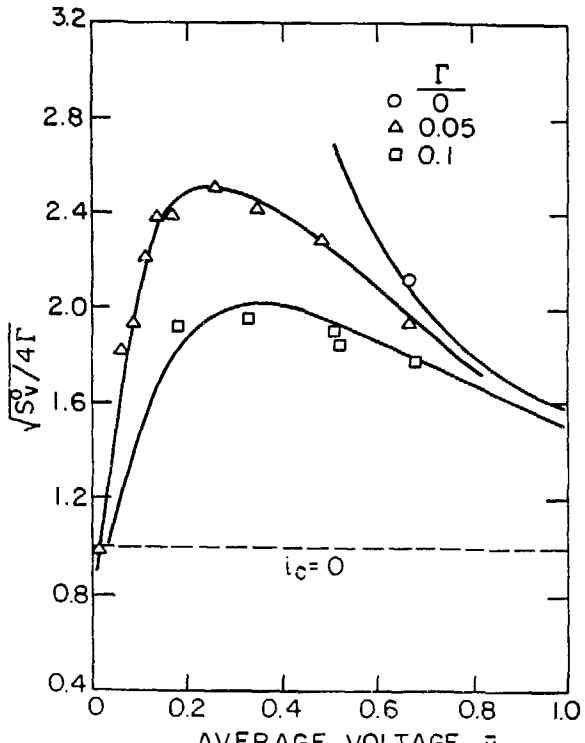

XBL 767-7192A

root of the normalized low frequency voltage spectral density $(S_v^\circ/4\Gamma)^{\frac{1}{2}}$ vs. the noise-rounded voltage $\bar{v}$ for two values of Γ. These values are in excellent agreement with the results of Vystavkin et al[34] (obtained by another method) that are plotted as smooth curves in Fig. 13(b). By comparing Figs. 13(a) and (b), we observe that the maxima in $(\partial\bar{v}/\partial i)$ and in S_v° occur at the same value of current, $i \approx i_c$. In addition, a decrease in the maximum of $(\partial\bar{v}/\partial i)$ (for example, as a result of increasing Γ) is accompanied by a decrease in the maximum of S_v°.

C. SQUID Characteristics in the Presence of Noise

1. SQUID Transfer Function

We now use the methods of section IV.A to compute from Eqs. (2.24)-(2.27) the voltage $v(\theta)$ and circulating current $j(\theta)$ for the SQUID in the presence of noise. As in section III.B, we frequently select the value $\beta = 1.0$ in calculating results, since, as we shall see later, this value is optimum for practical SQUIDs. If we choose $\beta = 1.0$ and $L = 1$ nH, we find $I_o \approx 1$ μA and for $T \lesssim 4.2$ K, $\Gamma \lesssim 0.2$. Noise-rounded i-$\bar{v}$ characteristics for the symmetric SQUID are plotted in Fig. 14(a) with $\Gamma = 0.05$ and $\beta = 1.0$ for several values of ϕ_a. The noise-free i-$\bar{v}$ characteristics are also shown. We observe that the differential resistance, $(\partial\bar{v}/\partial i)_{\phi_a}$, is a function of both i and ϕ_a. In particular, the maximum differential resistance decreases as ϕ_a increases from 0 to 0.5. From these i-$\bar{v}$ characteristics we obtain the variation of $\bar{v}$ with ϕ_a [Fig. 14(b)] for several values of i with $\Gamma = 0.05$ and $\beta = 1.0$. The corresponding noise-free curves are also shown. For bias currents $i \gtrsim 3$, $\bar{v}$ becomes relatively independent of ϕ_a, while for $i \lesssim 1$, $\bar{v}$ is zero for most values of ϕ_a. At intermediate values of i, the SQUID

Fig. 14: (a) Current-voltage characteristics of the SQUID in presence of noise as functions of applied flux computed with Method I (●), and Method II (Δ, □, o). Dotted lines are noise-free characteristics. (b) Average voltage vs. applied flux for the SQUID as function of bias current, i, in presence of noise with $\Gamma = 0.05$ (solid lines). Dotted lines are noise-free values.

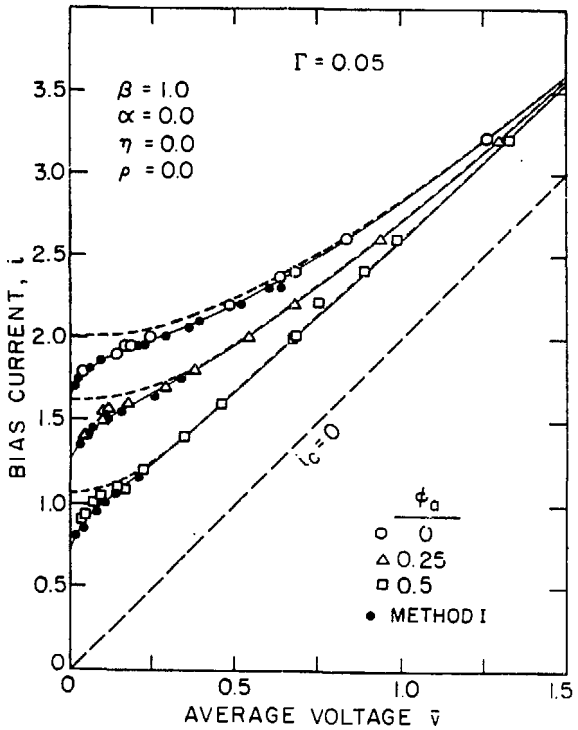

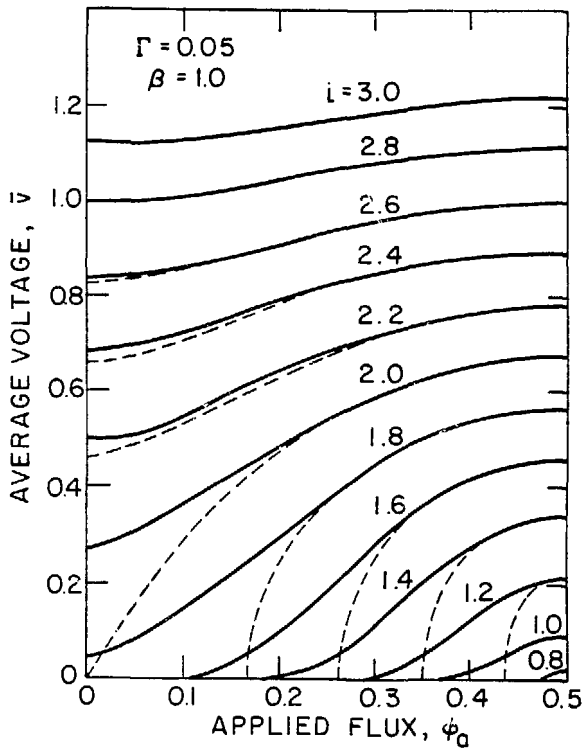

XBL 768-7265A

transfer function, $(\partial\bar{v}/\partial\phi_a)_i$, depends on ϕ_a and the parameters $\beta(L, I_o)$ and $\Gamma(I_o, T)$.

We plot $(\partial\bar{v}/\partial\phi_a)_i$ vs. i for variable ϕ_a, L, T, and I_o in Figs. 15(a)-(d). All the curves show a peak in $(\partial\bar{v}/\partial\phi_a)_i$ at a bias current corresponding roughly to the noise-free critical current determined by ϕ_a and β. The height and width of the curves are a function of ϕ_a, β, and Γ. For example, the family of curves in Fig. 15(a) for variable ϕ_a ($\Gamma = 0.05$ and $\beta = 1.0$) shows maxima which decrease as $\phi_a \to 0$ and $\phi_a \to 0.5$. At $\phi_a = 0$ and 0.5, $(\partial\bar{v}/\partial\phi_a)_i = 0$ for all values of i. Thus, changes in ϕ_a can produce substantial changes in $(\partial\bar{v}/\partial\phi_a)_i$. The curves of $(\partial\bar{v}/\partial\phi_a)_i$ vs. i for fixed I_o and T, and for variable $L(\propto \beta)$ are plotted in Fig. 15(b) for $\Gamma = 0.05$ and $\phi_a = 0.25$. For $\beta \lesssim 0.1$, the curves approach a limit independent of L. This result reflects the fact that for $\beta \lesssim 0.1$, $\Delta I_c \to 2I_o$ independent of L. For large L ($\beta \gg 1$) $(\partial\bar{v}/\partial\phi_a)_i \to 0$.

The temperature dependence of $(\partial\bar{v}/\partial\phi_a)_i$ is plotted in Fig. 15(c) for $\phi_a = 0.25$ and $\beta = 1.0$. As T ($\propto \Gamma$) increases, the SQUID i-$\bar{v}$ characteristics approach the i-$\bar{v}$ characteristics of the shunts, and hence $(\partial\bar{v}/\partial\phi_a)_i \to 0$. For $T \to 0$ ($\Gamma \lesssim 0.001$), the SQUID i-$\bar{v}$ characteristics approach the noise-free curves. Thus $(\partial\bar{v}/\partial\phi_a)_i$ approaches a noise-free limit that diverges at $i = i_c(\beta, \phi_a)$.

The critical current I_o appears in both the parameters β ($\propto I_o$) and Γ ($\propto 1/I_o$). Thus, in Fig. 15(d), the curves of $(\partial\bar{v}/\partial\phi_a)_i$ vs. i for variable I_o reflect a combination of Figs. 15(b) and (c). Since the dependences of $(\partial\bar{v}/\partial\phi_a)_i$ on β and Γ tend to cancel as I_o is varied,

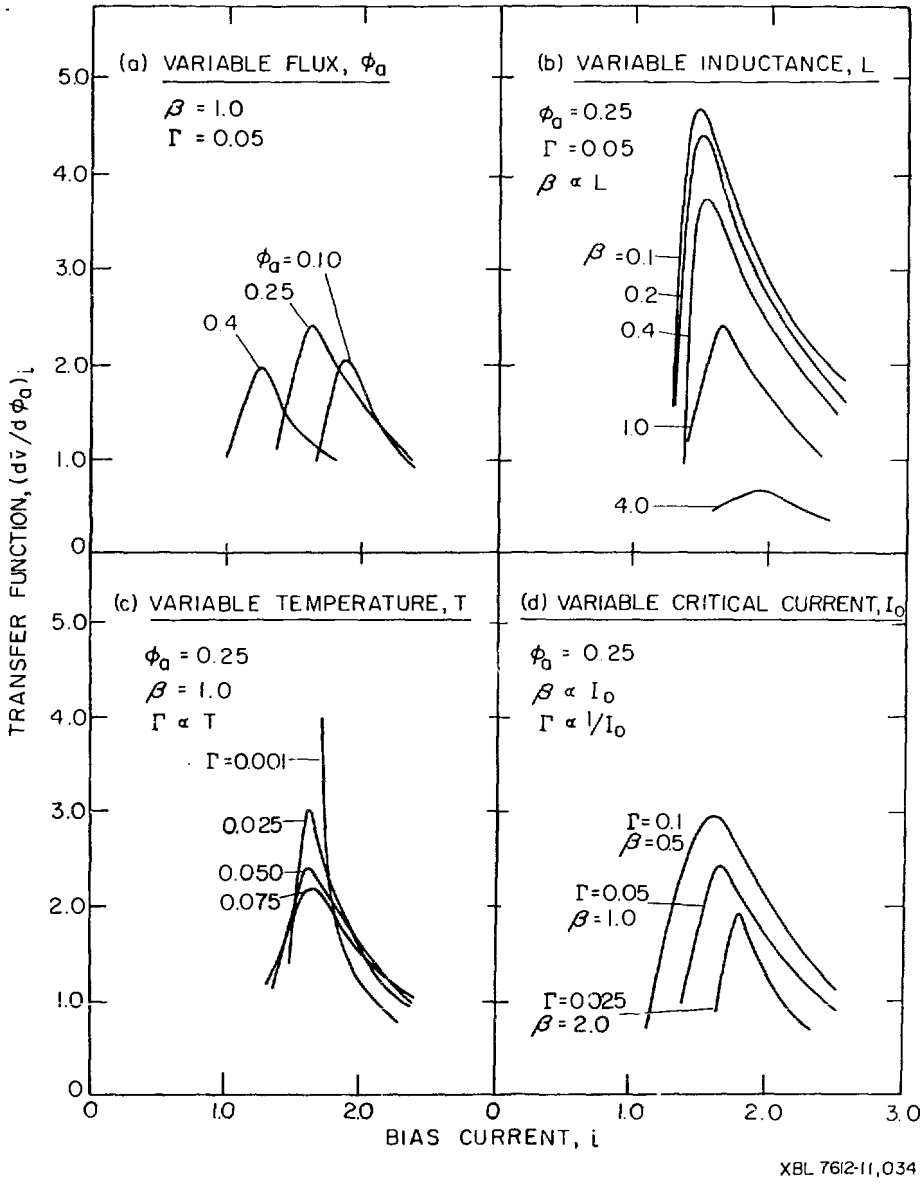

Fig. 15: SQUID transfer function vs. bias current as a function of (a) applied flux, (b) SQUID inductance, (c) temperature, and (d) critical current per junction.

$(\partial\bar{v}/\partial\phi_a)$ is less strongly dependent on I_o than on β or Γ separately.* In the limit of large I_o ($\Gamma \ll 0.1$, $\beta \gg 10$) the values of $(\partial\bar{v}/\partial\phi_a)_i$ approach the noise-free large β limit, and $(\partial\bar{v}/\partial\phi_a)_i \to 0$ for all i. This result is consistent with the fact that as $\beta \to \infty$, $\Delta I_c \to \Phi_o/L$ [Fig. 6(b)], or $\Delta i_c = \Delta I_c/I_o \to \Phi_o/LI_o = 2/\beta$. Hence the i-$\bar{v}$ curves for all i and ϕ_a collapse into the $\phi_a = 0$ curve as $\beta \to \infty$, and $(\partial\bar{v}/\partial\phi_a)_i \to 0$. Although in the range displayed in Fig. 15(d) $(\partial\bar{v}/\partial\phi_a)_i$ increases as I_o decreases, in fact, for very low values of I_o, $(\partial\bar{v}/\partial\phi_a)_i$ must fall off, and tend to zero as $I_o \to 0$. This behavior is a result of the fact that when $\beta \to 0$, $(\partial\bar{v}/\partial\phi_a)_i \to$ constant [Fig. 15(b)], whereas when $\Gamma \to \infty$, $(\partial\bar{v}/\partial\phi_a)_i \to 0$ [Fig. 15(c)].

2. *SQUID Voltage Noise Power Spectral Density*

We compute voltage spectral densities for the SQUID as a function of the various parameters using Method II of section IV.A. The spectral densities have the same general characteristics as the spectral densities of the single junction. There are a series of noise broadened peaks at the Josephson frequency, f_J, and harmonics. Well below f_J the spectral density is white; we are interested in S_v^o, the average value of the spectral density in this low frequency range.

In Fig. 16(a), we plot the normalized frequency voltage spectral density $S_v^o/2\Gamma$ vs. i for $\beta = 1.0$ and $\Gamma = 0.05$ for four values of ϕ_a. For $i \gg i_c(\phi_a)$ the spectral densities approach the Johnson noise limit of 1.0 (for two shunts in parallel, the shunt spectral density is 2Γ). Near $i_c(\phi_a)$, the spectral density is a maximum, as in the case of the

*Notice that $(\partial\bar{v}/\partial\phi_a)_i$ is a dimensionless quantity. The corresponding dimensional variable $(I_oR/\phi_o)(\partial\bar{v}/\partial\phi_a)_i$ is roughly proportional to I_o for the range of parameters in Fig. 15(d).

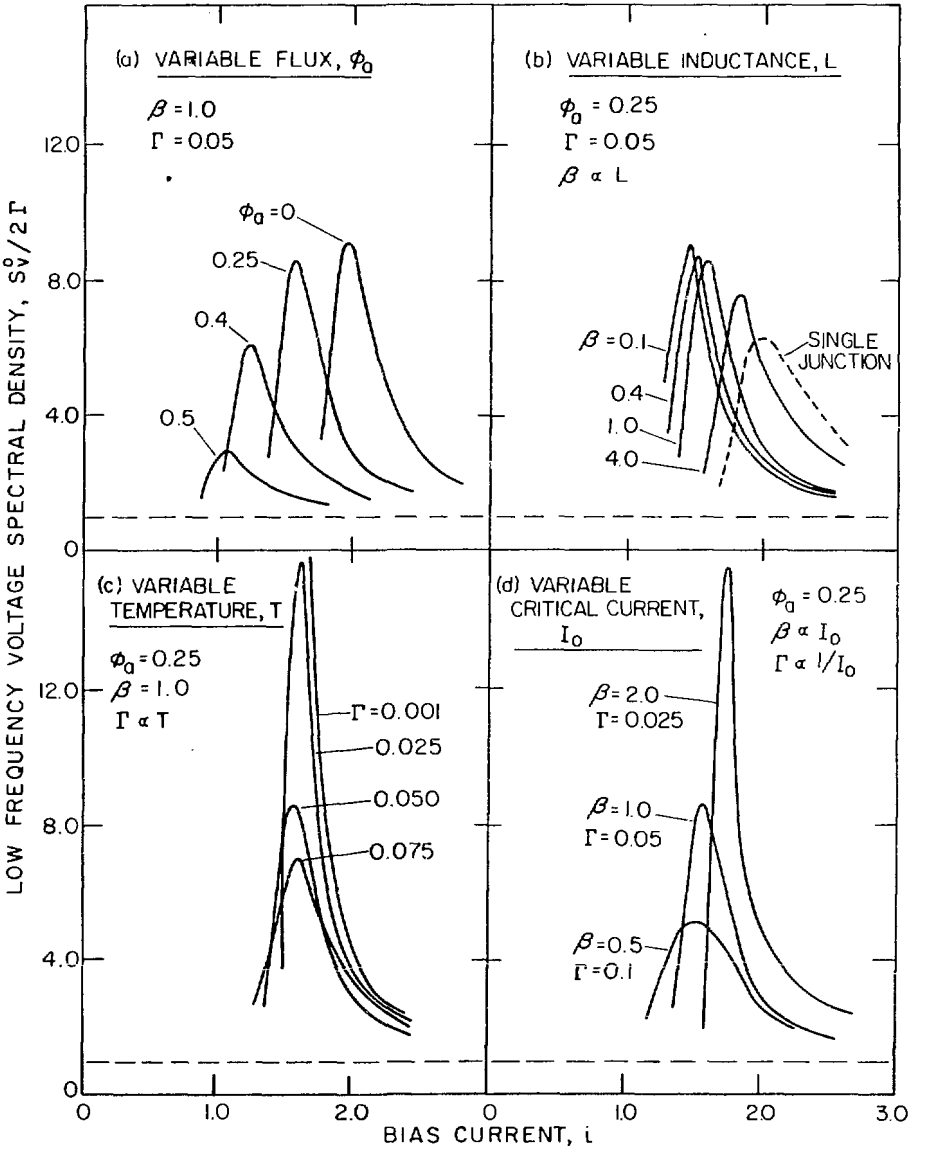

XBL7612-11,035

Fig. 16: Low frequency voltage spectral density vs. bias current as a function of (a) applied flux, (b) SQUID inductance, (c) temperature, and (d) critical current per junction. Dashed lines represent Johnson noise limit.

single junction. The value of the maximum decreases as ϕ_a increases from 0 to 0.5. This effect is consistent with the decrease in the maximum differential resistance, $(\partial\bar{v}/\partial i)_{\phi_a}$, with increasing flux that is observed in the noise rounded i-$\bar{v}$ characteristics (sec. IV.C.1).

The dependence of $S_v^\circ/2\Gamma$ on the variables L, T, and I_o for ϕ_a = 0.25 is plotted in Figs. 16(b)-(d). As the inductance L ($\propto \beta$) increases [Fig. 16(b)], $S_v^\circ/2\Gamma$ approaches the limit of a single junction with critical current $2I_o$. In the low inductance limit ($\beta \lesssim 0.1$), the spectral densities approach a limiting form. This result is consistent with the independence of ΔI_c [Fig. 6(a)] and $(\partial\bar{v}/\partial\phi_a)_i$ [Fig. 15(b)] on L in the low β limit.

The dependence of $S_v^\circ/2\Gamma$ on temperature [Fig. 16(c)] is similar to that of the single junction. As $T \to 0$ ($\Gamma \lesssim 0.01$), the spectral density approaches a limit determined by the noise-free differential resistance; as $i \to i_c$, $(\partial\bar{v}/\partial i)_{\phi_a} \to \infty$, and $S_v^\circ/2\Gamma$ diverges. In the large temperature limit ($\Gamma \gtrsim 1$) the noise tends to the Johnson noise of the shunts, and $S_v^\circ/2\Gamma \to 1$ for all i.

The dependence of $S_v^\circ/2\Gamma$ on I_o [Fig. 16(d)] is a combination of the effects in Figs. 16(b) and (c). In the limit $I_o \to \infty (\beta \to \infty, \Gamma \to 0)$, the curves approach the corresponding single junction noise-free limit. As $I_o \to 0$ ($\beta \to 0$, $\Gamma \to \infty$), the β-dependence drops out for $\beta \lesssim 0.1$, and the curves approach the Johnson noise limit, $S_v^\circ/2\Gamma = 1$.

3. *SQUID Equivalent Flux Noise Power Spectral Density*

We take as a measure of the rms flux noise the square root of the normalized low frequency flux noise power spectral density, $\zeta_\phi^{1/2} = (S_v^\circ/2\Gamma)^{1/2}/(\partial\bar{v}/\partial\phi_a)_i$. Curves of $\zeta_\phi^{1/2}$ vs. i for variable ϕ_a, L, T, and I_o

are plotted in Figs. 17(a)-(d). The family of curves for variable ϕ_a with $\Gamma = 0.05$ and $\beta = 1.0$ [Fig. 17(a)] exhibit minima at $i \sim i_c(\phi_a)$. For $0.1 < \phi_a < 0.4$, the value of $\zeta_{\phi min}^{\frac{1}{2}}$ is relatively independent of ϕ_a for $\beta = 1.0$, $\Gamma = 0.05$. For $\phi_a \to \pm n/2$ ($n = 0, 1, 2, \ldots$), $\zeta_\phi^{\frac{1}{2}} \to \infty$ for all values of $i[(\partial\bar{v}/\partial\phi_a)_i \to 0)]$.

The family of curves of $\zeta_\phi^{\frac{1}{2}}$ vs. i for variable L ($\propto \beta$) [Fig. 17(b)] with $\Gamma = 0.05$ and $\phi_a = 0.25$ also have minima at $i \sim i_c(\beta)$. As $\beta \to 0$ the curves become progressively flatter, and $\zeta_{\phi min}^{\frac{1}{2}}$ approaches a limit ≈ 0.5. As β increases beyond unity, the curves become sharper with $\zeta_{\phi min}^{\frac{1}{2}}$ growing roughly as β.

The dependence of $\zeta_\phi^{\frac{1}{2}}$ on temperature [Fig. 17(c)] is weak for $0.025 < \Gamma < 0.075$, where $\zeta_\phi \approx 1.0$. In the high temperature limit ($T \propto \Gamma \to \infty$), $S_v^\circ/2\Gamma \to 1$ and $(\partial\bar{v}/\partial\phi_a)_i \to 0$; hence we expect $\zeta_\phi^{\frac{1}{2}} \to \infty$. For $\Gamma \propto T \to 0$, both $S_v^\circ/2\Gamma$ and $(\partial\bar{v}/\partial\phi_a)_i$ diverge at $i = i_c(\beta, \phi_a)$; $\zeta_\phi^{\frac{1}{2}}$ becomes a sharp function of i, falling to zero as $i \to i_c$.

A family of curves of $\zeta_\phi^{\frac{1}{2}}$ for variable I_o is plotted in Fig. 17(d) for $\phi_a = 0.25$. As I_o increases, the curves of $\zeta_\phi^{\frac{1}{2}}$ become progressively sharper, and $\zeta_{\phi min}^{\frac{1}{2}}$ increases. As I_o decreases, the curves flatten for intermediate values of β; however, for very small values of I_o, the dependence of $\zeta_\phi^{\frac{1}{2}}$ on β drops out, and $\zeta_\phi^{\frac{1}{2}} \to \infty$ as $\Gamma \to \infty$.

4. *SQUID Current Noise Power Spectral Density and Correlation Power Spectral Density*

Figures 18 and 19 show the circulating current noise power spectral density, S_j°, and the imaginary part of the correlation noise power spectral density, S_{vj}°, as functions of i for several values of ϕ_a. The real part of the correlation power spectral density is computed to be

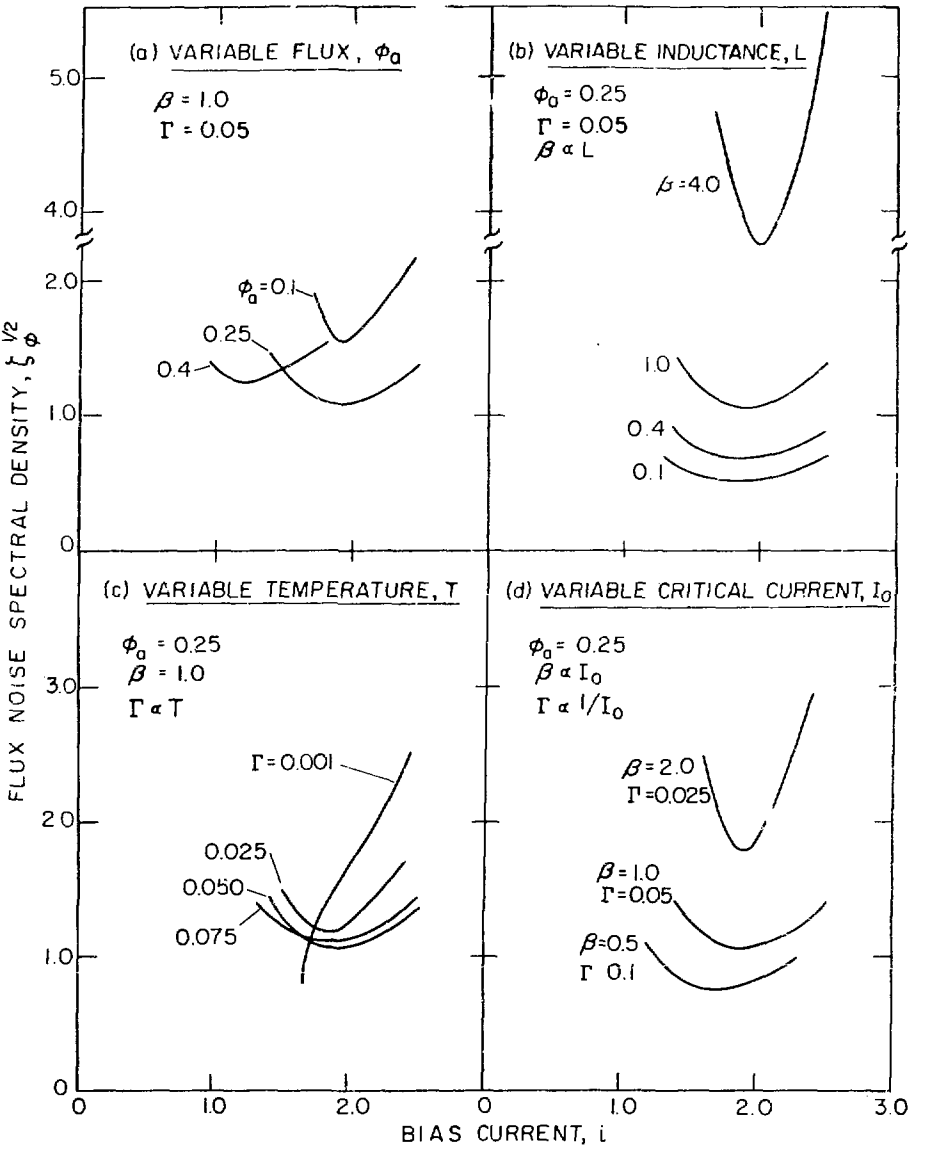

Fig. 17: Flux noise spectral density, $\zeta_\Phi^{\frac{1}{2}}$, vs. bias current i as a function of (a) applied flux, (b) SQUID inductance, (c) temperature, and (d) critical current per junction.

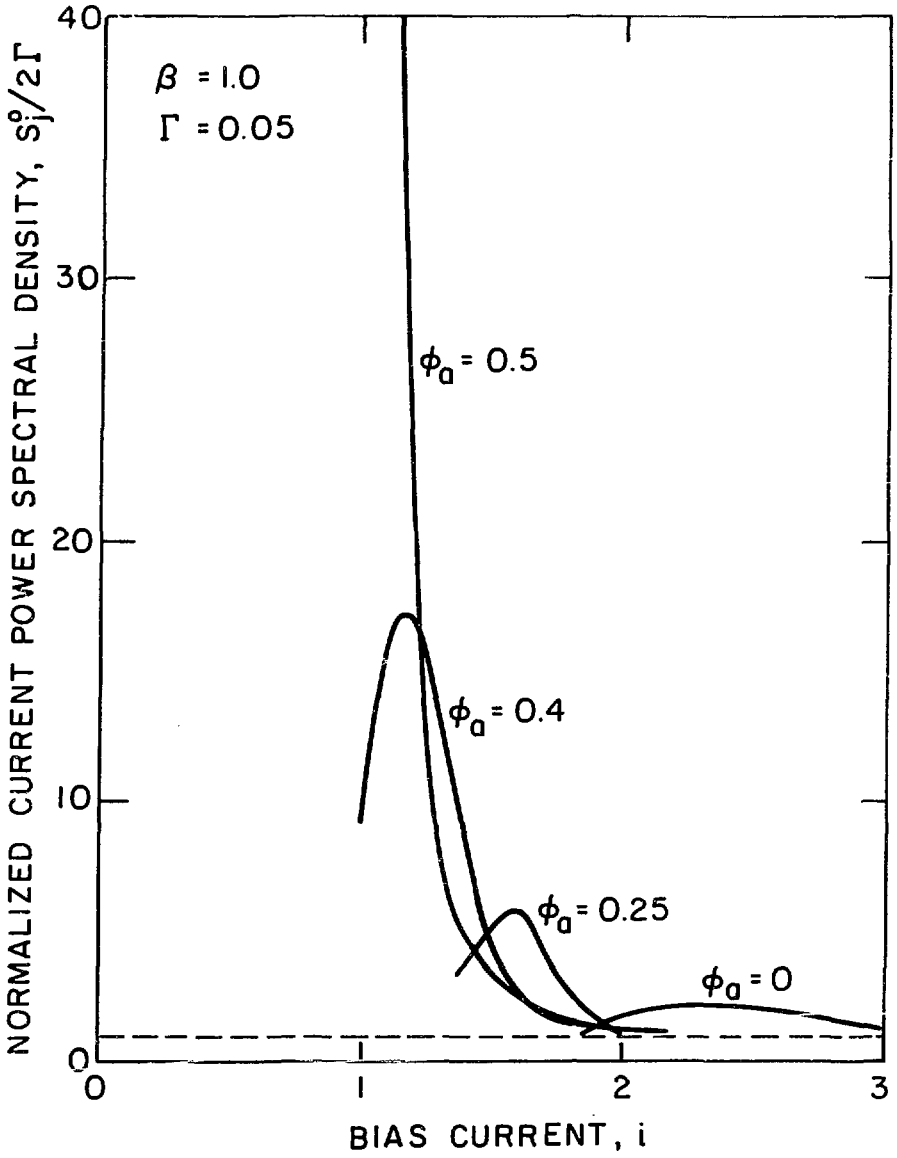

XBL 787-5388

Fig. 18: Low frequency, current power spectral density vs. bias current for β = 1.0, Γ = 0.05 as a function of applied flux.

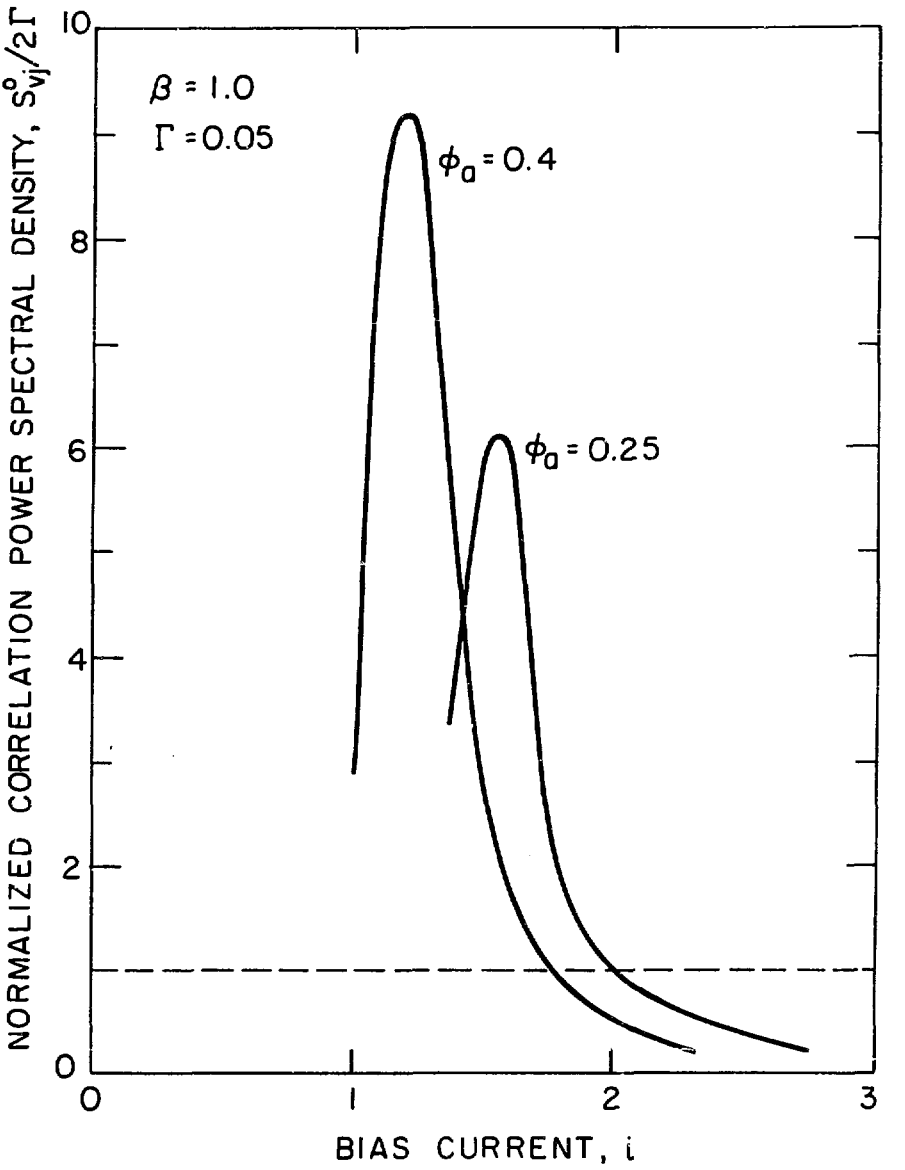

XBL 787-5389

Fig. 19: Low frequency, correlation power spectral density vs. bias current for β = 1.0, Γ = 0.05 as a function of applied flux.

zero for all values of i as expected. For simplicity, we have plotted only the case $\beta = 1$, $\Gamma = 0.05$. These quantities must be known in addition to S_v° and $(\partial\bar{v}/\partial\phi_a)$ to properly optimize the SQUID plus input circuit in the general case. Notice that for bias currents $i \gg 1$, S_j° tends to the circulating Johnson noise value determined by the two shunts in series: $S_j^\circ \to 2\Gamma = (2k_BT/R)/(I_o\phi_o/2\pi R)$. Furthermore, since the voltage and circulating current noises produced by the Johnson noise in the two resistors are uncorrelated, $S_{vj}^\circ \to 0$ for $i \gg i_c$. Near i_c, the effect of the junctions and loop is to increase both S_v° and S_j° above the value for the resistors, 2Γ, and, in addition, to correlate the voltage and current noises. The correlation can be understood qualitatively from the following argument. The total flux through the SQUID is $\phi_T = \phi_a + \beta j/2$. Thus, Johnson noise superimposed on j produces a noise in the total flux that is similar to an externally applied flux noise. The SQUID transfer function, $\partial\bar{v}/\partial\phi_a$, relates changes in the time averaged voltage $\bar{v}$ to changes in ϕ_a, and thus relates the effective flux noise due to noise in j to the total voltage noise. For $i \sim i_c$, $\partial\bar{v}/\partial\phi_a \neq 0$ and the voltage noise is correlated with the current noise. For $i \gg i_c$, $\partial\bar{v}/\partial\phi_a \to 0$ and no correlation is introduced between the voltage and current noises. Note that in the special case $\phi_a = 0, 0.5$, $\partial\bar{v}/\partial\phi_a \approx 0$, and $S_{vj}^\circ = 0$ for all values of bias current.

As ϕ_a is increased from 0 to 0.5, S_v° decreases in a way that is consistent with the corresponding decrease in the dynamic resistance of the SQUID.[5] On the other hand, the maximum value of S_j° increases as ϕ_a is increased from 0 to 0.5. In addition, for $\phi_a = 0.5$, S_j° rises rapidly as i is lowered below i_c. This behavior can be understood by developing

a thermal activation model for the SQUID along the lines of the single junction model.

5. *Thermal Activation Model,* $\phi_a = 0.5$

We first express the equations of motion, Eqs. (2.24)-(2.27), in terms of a potential energy for the phases δ_1 and δ_2. Thus, for the symmetric SQUID,

$$\frac{d\delta_1}{d\theta} = -\frac{\partial u}{\partial \delta_1} + v_{N1} , \tag{4.3}$$

and

$$\frac{d\delta_2}{d\theta} = -\frac{\partial u}{\partial \delta_2} + v_{N2} , \tag{4.4}$$

where

$$u = -\cos\delta_1 - \cos\delta_2 - (\delta_1+\delta_2)i/2+\beta\pi j^2/2 , \tag{4.5}$$

and

$$j = (\delta_1-\delta_2 - 2\pi\phi_a)/\pi\beta . \tag{4.6}$$

A contour plot for u as a function of δ_1 and δ_2 for $i = 0$ and $\phi_a = 0.5$ is shown in Fig. 20. In this case, the first minimum shown at A occurs at $\delta_{1min} = 0.2\pi$ and $\delta_{2min} = -0.2\pi$. The next minimum at B occurs at $\delta_{1min} = 2\pi - 0.2\pi$, $\delta_{2min} = +0.2\pi$. The maximum at C occurs at $\delta_1 = \pi$ and $\delta_2 = 0$. For $i = 0$, $u_{min} = -1.05$ and $u_{max} = 0$ in all cases. Notice that at A, $j = -0.6$ at B, $j = +0.6$, and at C, $j = 0$.

We can understand the time development of the phases under the influence of the noise voltages v_{N1} and v_{N2} by analogy to the single junction case discussed in section II.B. A classical particle with coordinates δ_1 and δ_2 undergoes Brownian motion in the two dimensional potential u. If it is initially within the well centered at A, it will bounce around in the well under the influence of the thermally induced noise voltages v_{N1} and v_{N2}. In addition, at some random time the

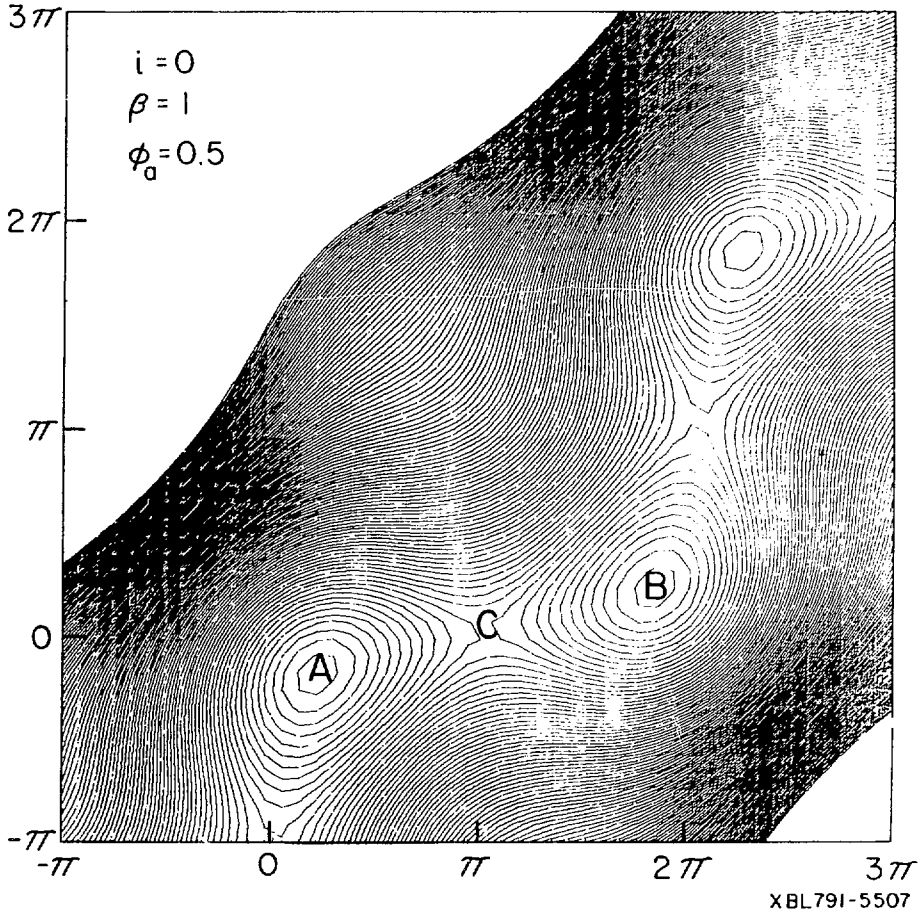

Fig. 20: Contour plot of the dc SQUID potential energy for $\beta = 1.0$, $\Phi_a = 0.5$ and $i = 0$.

particle will be kicked over the barrier at C and settle down into the next well at B. In the process, the current will switch from $j = -0.6$ through zero to $j = +0.6$, and a voltage pulse will be generated. This behavior can be observed in Fig. 21 for $i = 0.9$, $\phi_a = 0.5$, $\beta = 1.0$ and $\Gamma = 0.05$.

The switching frequency, f_s, can be approximated roughly by considering motion only along the line joining the two wells ($\overline{AB}$). Then

$$f_s \sim \frac{1}{2\pi}\left(\frac{\partial^2 u}{\partial\delta^2_{\overline{AB}}}\right)_A^{\frac{1}{2}} \left(\frac{\partial^2 u}{\partial\delta^2_{\overline{AB}}}\right)_C^{\frac{1}{2}} e^{-\Delta u/\Gamma} , \tag{4.7}$$

where

$$\left(\frac{\partial^2 u}{\partial\delta^2_{\overline{AB}}}\right) = \cos^2\theta_A\cos\delta_{1A} + \sin^2\theta_A\cos\delta_{2A}$$

$$+ (1 - 2\sin\theta_A\cos\theta_A)/\pi , \tag{4.8}$$

and

$$\theta_A = \arctan\left(|\delta_{2A}|/\pi - |\delta_{1A}|\right) . \tag{4.9}$$

The circulating current noise spectral density is

$$S_j(f) = 2\int_{-\infty}^{\infty} A(\tau)e^{-i2\pi f\tau}\, d\tau , \tag{4.10}$$

where the autocorrelation function is

$$A(\tau) = \lim_{T\to\infty} \frac{1}{T}\int_0^T \langle j(\theta)j(\theta+\tau)\rangle d\theta . \tag{4.11}$$

Now $j(\theta)j(\theta+\tau) = +j_s^2$ if the number of switches between θ and $\theta+\tau$ is even, and $j(\theta)j(\theta+\tau) = -j_s^2$ if the number of switches is odd. The probability of n switches occurring during τ is given by the Poisson

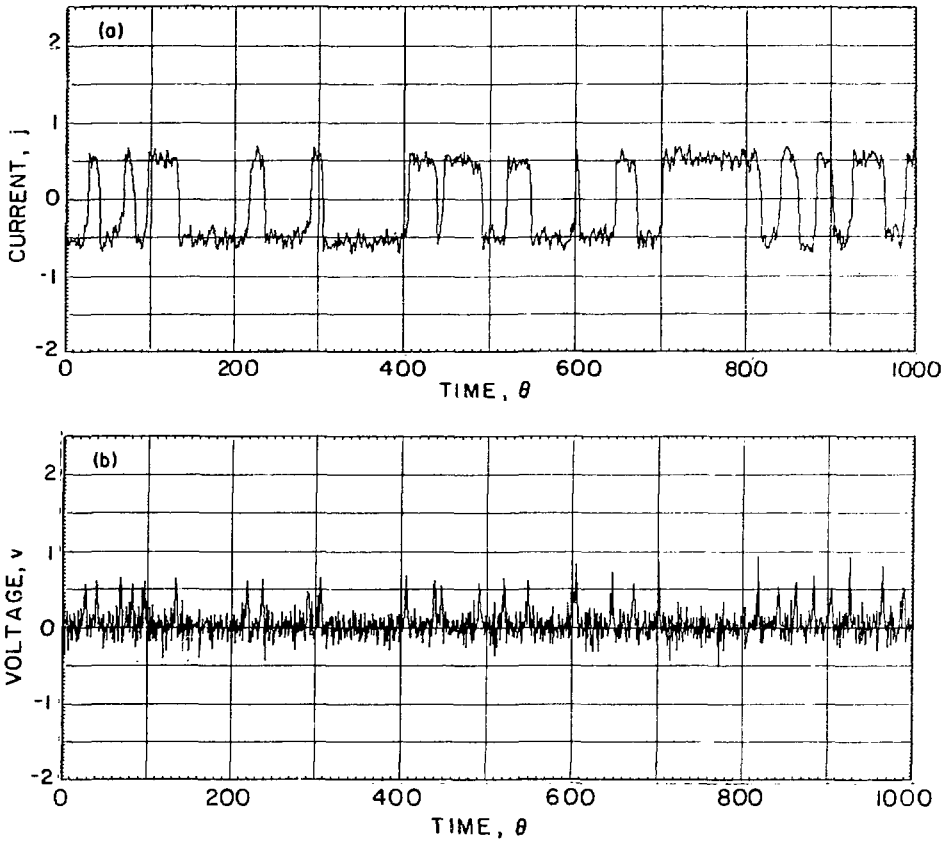

XBL 787-5385

Fig. 21: Voltage and circulating current vs. time for $\beta = 1.0$, $\Gamma = 0.05$, $\phi_a = 0.5$ and $i = 0.9$.

distribution

$$P(n) = \frac{(f_s|\tau|)^n}{n!} \exp(-f_s|\tau|) \ , \tag{4.12}$$

provided the switching time is much shorter than the average time between switches. This will hold for bias currents $i \ll i_c$, the region in which the thermal activation model is expected to hold. The autocorrelation function becomes

$$A(\tau) = j_s^2 e^{-f_s|\tau|} \sum_{n=0}^{\infty} \frac{(-f_s|\tau|)^n}{n!} = j_s^2 e^{-2f_s|\tau|} \tag{4.13}$$

The circulating current noise spectral density is

$$S_j(f) = 2f_s j_s^2/(f_s^2 + \pi^2 f^2) \ , \tag{4.14}$$

and the low frequency value for $f \ll f_s$ is

$$S_j^\circ = 2j_s^2/f_s \ .$$

Notice that $\langle j^2 \rangle = \int_0^\infty S_j(f)df = j_s^2$, independent of f_s, as expected.

The voltage noise power spectral density is approximated as in the single junction case (see section II.B). The area of each voltage pulse is

$$a = \int_A^B v d\theta = \pi \ , \tag{4.15}$$

the average voltage is $\bar{v} = af_s = \pi f_s$, and the voltage noise power spectral density is

$$S_v^\circ = \pi^2 f_s \ . \tag{4.16}$$

The switching frequency, f_s, is dominated by the exponential, $\exp(-\Delta u/\Gamma)$. Since Δu increases as the bias current decreases, as $i \to 0$, S_v° approaches

a maximum, while S_v° approaches zero.

The correlation noise spectral density is identically zero in this case. This is because the current switches are alternating between $+j_s$ to $-j_s$ and $-j_s$ to $+j_s$, while the voltage pulses are always positive. Thus the ensemble average $\langle v(\theta)j(\theta+\tau)\rangle = 0$ and $S_{vj}^\circ = 0$. This is in agreement with the computer model results.

In Fig. 22 we compare the predictions of the thermal activation model with the computer curves of S_v° and S_j° versus i for $\beta = 1$ and $\Gamma = 0.05$. Notice that the thermal activation model is applicable only for values of $i < i_c = 1.04$. Also notice that the computer calculation of S_j° is plotted only for $i \gtrsim i_c$. This is because the low frequency value of $S_j(f)$ must be obtained for $f \ll f_s$. However, for $i \sim i_c$, $f_s \sim f_J$. Thus, as i is reduced below i_c, $f_s \ll f_J$, and values of $S_j(f)$ must be calculated not just for $f \ll f_J$, but for $f \ll f_s \ll f_J$. This is impractical with the present algorithm.

At $i = 0$, $\Gamma = 0.05$ and $\phi_a = 0.5$, the thermal activation model yields $f_s = 10^{-10}$. For $I_o = 1\mu A$ and $R = 1\Omega$, this corresponds to a frequency of $F_s = f_s(2\pi I_o R/\Phi_o) = 0.3$ Hz. Thus well below 0.3 Hz, the current noise spectral density is white and $S_j^\circ = 7.2 \times 10^9$ ($S_J^\circ = S_j^\circ(2k_BT/R) = 1.4 \times 10^{10}\ k_BT/R$). Well above 0.3 Hz, $S_j = 2j_s^2 f_s/\pi^2 f^2 = 7.3 \times 10^{-12}/f^2$ ($S_J(F) \approx 10^9\ k_BT/RF^2$, for frequency F in Hz).

In conclusion, we see that the thermal activation model for $\phi_a = 0.05$ gives good agreement with the computer calculation for S_v°. In addition, the model permits calculation of S_j° for $i < i_c$ and provides an explanation for the large values of S_j° below i_c. Finally, notice that the model has been applied only to the case $\phi_a = 0.5$, where two

Fig. 22: (a) Current-voltage characteristic for $\beta = 1.0$, $\phi_a = 0.05$, and $\Gamma = 0.05$ and (b) low frequency, voltage power spectral density and low frequency, current-power spectral density vs. bias current, i. The smooth curve is from the computer calculation; the dotted curve is from the thermal activation model. The dashed curve is the critical current, i_c.

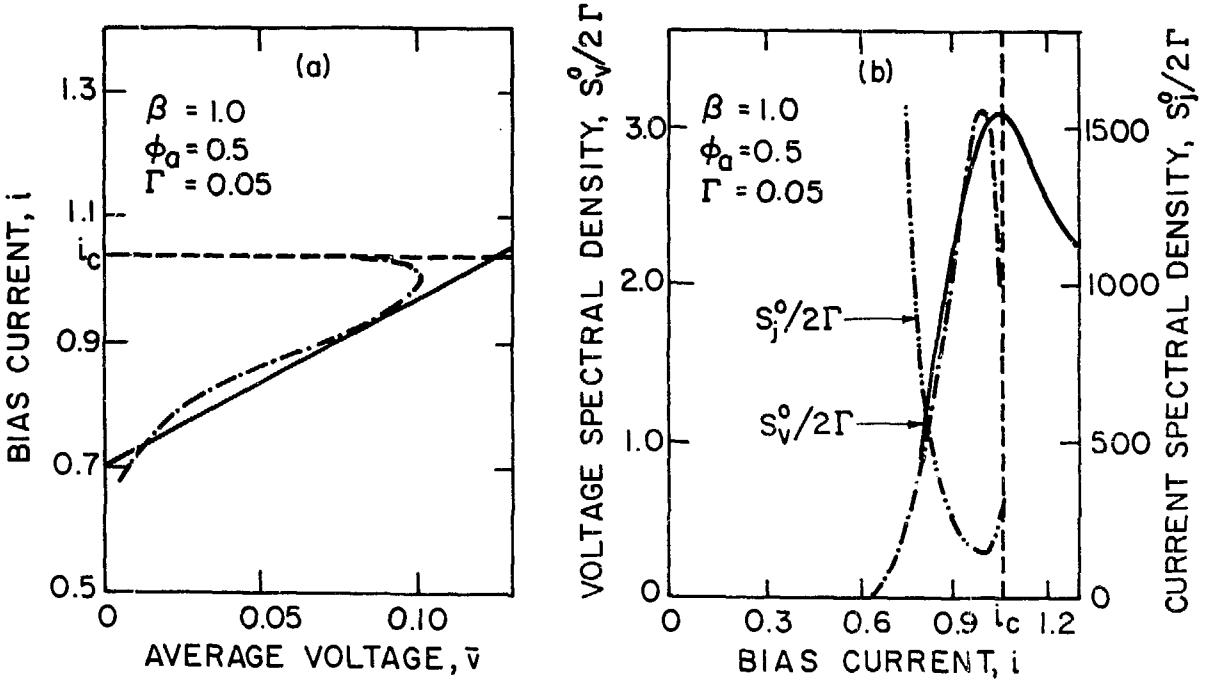

XBL7811-6194

families of equilibrium states with $\pm j_s$ are observed. At values of $\phi_a \neq 0.05$, the two families have unequal magnitudes of j, and unequal switching frequencies. As a result, the circulating current is also pulselike, and thus both $S_v^\circ \propto f_s \to 0$ and $S_j^\circ \propto f_s \to 0$ as $i \to 0$ (see Fig. 16 and Fig. 17). Since no difficulty in computing S_v° and S_j° in the region $i \sim i_c$ (where most practical SQUID devices are used) was encountered, we did not extend the thermal activation model to values $\phi_a \gtrsim 0.5$.

6. *SQUID Energy Resolution*

In most applications,[6,17,20,21] a relevant figure of merit is the energy spectral density, $S_E^\circ = L_i(S_\Phi^\circ/M_i^2)/ = S_\Phi^\circ/2\alpha^2 L$, where $M_i^2 = \alpha^2 L L_i$ is the mutual inductance of the input coil, L_i, coupled to the SQUID. If the effect of the input circuit on the total SQUID noise at the output is ignored, then S_E° becomes the only figure of merit. (Note: S_E° is a function of $(\partial\bar{v}/\partial\phi_a)$, S_v° and $\alpha^2 L$. In the general case, the total SQUID noise at the output also depends on S_j°, S_{vj}° and the input and SQUID circuit parameters. See section I.) Notice that S_E° is only a function of the SQUID parameters and the coupling efficiency, α^2. Practical SQUID devices[3,4] have $\alpha^2 \sim 1/2$. We assume in the following discussion that the SQUID inductance is restricted to values for which $\alpha^2 \sim 1/2$ is obtainable.

In this section, we relate the computed normalized flux noise spectral density, ζ_ϕ, to the effective energy resolution, $S_\Phi^\circ/2L$. We discuss an approximation for $S_\Phi^\circ/2L$ developed previously[3,5] for $\beta \gg 1$, and derive an approximate expression for $S_\Phi^\circ/2L$ for $\beta \ll 1$.

We take the flux noise referred to the input of the SQUID as

$S_\Phi^\circ = S_V^\circ/(\partial\bar{V}/\partial\Phi_a)_I^2$. With $(\partial\bar{V}/\partial\Phi_a)_I = (\partial\bar{v}/\partial\Phi_a)_i I_o R/\Phi_o$, $S_V^\circ = (S_V^\circ/2\Gamma)2k_BTR$, and $2L = \beta\Phi_o/I_o$, we have the following expression for $S_\Phi^\circ/2L$ in terms of ζ_Φ.

$$S_\Phi^\circ/2L = (\Phi_o^2/\pi)\zeta_\Phi(\beta, \Gamma, i, \phi_a)\ \Gamma/R\beta \quad , \tag{4.17}$$

$$\text{or} \quad S_\Phi^\circ/2L = (2k_BTL/R)\ (2/\beta^2)\zeta_\Phi(\beta, \Gamma, i, \phi_a) \quad . \tag{4.18}$$

Equations (4.17) and (4.18) are exact expressions for the energy resolution in terms of the computed flux spectral density, ζ_Φ.

From a different viewpoint, approximate expressions for the energy resolution in the high- and low-β limits can be obtained as follows. For $\Phi \approx (n \pm 1/4)\Phi_o$, we take $(\partial\bar{V}/\partial\Phi_a)_I \approx (\partial\bar{V}/\partial I_c)_I(\partial I_c/\partial\Phi_a) \approx R\Delta I_c/\Phi_o$, where we have set $(\partial\bar{V}/\partial I_c)_I \approx (R/2)$ for $I \approx I_c$, and $\partial I_c/\partial\Phi_a = 2\Delta I_c/\Phi_o$. From Fig. 6(b), we find $\Delta I_c \approx \Phi_o/L$ for $\beta \gtrsim 40$, so that $(\partial V/\partial\Phi_a)_I \approx R/L$ as $\beta \to \infty$. From Fig. 6(a), we find that for $\beta \lesssim 0.1$, $\Delta I_c \approx 2I_o \approx \beta\Phi_o/L$, and $(\partial\bar{V}/\partial\Phi_a)_I \approx \beta R/L$. We make the following approximation[3] for S_V°. For $I_o = 0$ (shunt resistances only), the voltage spectral density is $S_V^R = 4k_BT(R/2)$ and the circulating current spectral density is $S_J^R = 4k_BT/(2R)$, where S_V^R and S_J^R are independent and uncorrelated. For the SQUID ($I_o \neq 0$), the voltage is a function of the currents flowing through the junctions and around the SQUID loop. Hence for $\phi_a \neq 0, 0.5$, S_V and S_J are no longer uncorrelated, as we have found in sec. IV.C.4, and $S_V^\circ > S_V^R$ for $I \sim I_c$. The contribution of the circulating currents to S_V° for $\phi_a = 0.25$ is approximated by $(\partial\bar{V}/\partial\Phi_a)_I^2\ S_\Phi^R$, where $S_\Phi^R = L^2S_J^R$. Thus

$$S_V^\circ \simeq S_V^R + (\partial\bar{V}/\partial\Phi_a)_I^2\ L^2S_J^R \quad . \tag{4.19}$$

In the high β limit, $(\partial\bar{V}/\partial\Phi_a)_I \approx R/L$, and

$$S_\Phi^\circ/2L \approx 2k_BTL/R, \qquad (\beta \gg 1) \quad , \tag{4.20}$$

while in the low β limit, $(\partial\bar{V}/\partial\Phi_a)_I \approx R/\beta L$ and

$$S_\Phi^\circ/2L \approx k_BTL/R\beta^2, \qquad (\beta \ll 1) \quad . \tag{4.21}$$

We now compare the computed expression for S_Φ [Eq. (4.18)] with the approximate expressions [Eqs. (4.20) and (4.21). In the high β-limit, our calculated curves of $\zeta_\Phi^{\frac{1}{2}}$ vs. i become sharp functions of i. We choose the minimum value of $\zeta_\Phi^{\frac{1}{2}}$ corresponding to $i \approx i_c(\Phi_a, \beta)$ for the comparison. Calculations of ζ_Φ for $\Phi_a = 0.25$ and $\beta \gtrsim 10$ yield $\zeta_\Phi \approx \beta^2/2$ at $i \sim i_c(\Phi_o, \beta)$, and hence $S_\Phi^\circ/2L \approx 2k_BTL/R$, in agreement with Eq. (4.20). From Fig. 17(b) for $\Gamma = 0.05$ and $\Phi_a = 0.25$, we see that $\zeta_\Phi^{\frac{1}{2}}$ approaches a limit of about 0.5 for $\beta \lesssim 0.1$ over a wide range of bias currents. Hence, from Eq. (4.18), $S_\Phi^\circ/2L \to k_BTL/R\beta^2$ as $\beta \to 0$, in agreement with Eq. (4.21). We conclude that Eq. (4.18) shows the correct limiting behavior for high and low β.

Finally, we compared our computed results with the measured flux resolution of the tunnel junction dc SQUID of Clarke et al.[3] It should be noted that whereas the model calculation assumes that the junction capacitance is zero, practical junctions have a capacitance and are usually operated with $\beta_c = 2\pi I_o R^2 C/\Phi_o \approx 1$. However, since the I-V characteristics with $\beta_c = 1$ are not very different from those with $\beta_c = 0$,[30] and since we are concerned with frequencies much less than $(RC)^{-1}$, we do not expect the calculated flux noise power spectra with $\beta_c = 1$ to differ substantially from our calculated spectra.

In the tunnel junction SQUID, the inductance was L = 1 nH, the shunt resistance was R = 0.6 Ω, and the critical current of each junction, was about 2.5 μA. Thus $\beta \approx 2.5$ and $\Gamma \approx 0.072$. The SQUID was

biased above the critical current at $i \sim 2$, and a modulating flux of peak amplitude $\Phi_o/4$ was applied. The ac voltage across the SQUID was demodulated with a lock-in amplifier, and the output from the lock-in was fed back to flux-lock the SQUID in the usual manner. The measured flux resolution was $S_\Phi^{\frac{1}{2}} \approx 3.5 \times 10^{-5}\ \Phi_o\ Hz^{-\frac{1}{2}}$. We compute a flux resolution for the SQUID with Φ_a fixed at $\Phi_o/4$ of $S_\Phi^{\frac{1}{2}} = 1.3 \times 10^{-5}\Phi_o Hz^{-\frac{1}{2}}$. This value applies to a SQUID that is not flux modulated, but is used as a small signal amplifier for Φ_a near $\Phi_o/4$. The flux modulation scheme increases $S_\Phi^{\frac{1}{2}}$ as follows. First, the voltage noise S_V° of the SQUID is a function of the modulation flux. For a SQUID biased at $i = 2$ and modulated about $\Phi_a = 0$, we estimate that the effective modulated voltage noise is $S_{V_m}^\circ \lesssim 2\ S_V^\circ\ (\Phi_a = 0.25)$ [see Fig. 17(a)]. Second, the transfer function $(\partial\bar{V}/\partial\Phi_a)_I$ at $\Phi_q = \Phi_o/4$ must be replaced with $(\partial V_m/\partial\Phi_q)_I$ at $\Phi_q = 0$, where V_m is the amplitude of the Fourier component of the SQUID voltage at the modulation frequency, $\omega_o/2\pi$, and Φ_q is the quasistatic applied flux. By plotting $\bar{V}$ vs. t for $\Phi_a = \Phi_q + (\Phi_o/4)\cos\omega_o t$ from the curves of $\bar{V}$ vs. Φ_a [Fig. 14(b)], we find $(\partial V_m/\partial\Phi_q)_I$ at $\Phi_q = 0$ is approximately equal to $1.3(\partial\bar{V}/\partial\Phi_a)_I$ at $\Phi_a = \Phi_o/4$. From these results, we compute a flux resolution for the modulated SQUID of $S_\Phi^{\frac{1}{2}} \approx 1.6 \times 10^{-5}\Phi_o Hz^{-\frac{1}{2}}$. In view of the uncertainty in the measured values of the SQUID parameters and of the neglect of the capacitance in the calculation, we conclude that the computed spectral density of the flux noise is in sensible agreement with the experimentally measured value.

V. SQUID OPTIMIZATION

A. Determination of the Optimal SQUID Parameters

We now consider the choice of the SQUID parameters L, R, I_o, and the bias current i that minimizes the energy spectral density, $S_\Phi^o/2\alpha^2L$, at a given temperature T. Since $S_\Phi^o \propto L^2$ in the high β limit [Eq. (4.20)], $S_\Phi^o/2\alpha^2L$ can be reduced by decreasing L, provided that α^2 is not also correspondingly decreased. In practice, the constraint on α^2 appears to impose a lower limit on L of 10^{-10} to 10^{-9} H. To avoid hysteresis, the junction parameters must also satisfy the constraint $2\pi I_o R^2 C \lesssim \Phi_o$, where C is the junction capacitance. In practice, there is a lower limit on C that is set by the area of the smallest tunnel junction that can be fabricated. Hence, there is an upper limit on R for fixed I_o of $R^2 \lesssim \Phi_o/2\pi I_o C$. Thus for L and C fixed, $S_\Phi^o/2\alpha^2L$ becomes a function only of I_o and T, or of $\beta = I_o(2L/\Phi_o)$ and $\Gamma = 2\pi k_B T/I_o\Phi_o$.

We consider first the simpler case in which the SQUID is not in a flux-locked loop, but is operated as a small signal amplifier with no ac flux modulation. We assume that α is essentially independent of L. From Eqs. (4.20) and (4.21) we find $S_\Phi^o/2L \propto \beta^{\frac{1}{2}}$ ($\beta \gg 1$) and $S_\Phi^o/2L \propto \beta^{-3/2}$ ($\beta \ll 1$). Consequently, there is an intermediate value of β that minimizes $S_\Phi^o/2L$. As an example of a calculation to find the optimal value of β, consider the following parameters for a hypothetical SQUID. Suppose the SQUID is a cylindrical tunnel junction SQUID with the diameter of the cylinder reduced from 3 mm to 2 mm, and the area of the junctions reduced from 10^{-2} mm^2 to $7\mu \times 7\mu = 0.5 \times 10^{-4}$ mm^2. The inductance of the cylinder is reduced from 0.75 nH to 0.35 nH. This is the SQUID inductance provided a geometry is used which reduces the parasitic

inductance of the junction region substantially from the value ~ 0.5 nH estimated for the SQUID of Clarke, Goubau, and Ketchen.[53] The junction capacitance is reduced from 200 pF to 1 pF. With L = 0.35 nH and C = 1 pF, $R^2 I_o = 200\ \Omega^2 \mu A$ ($\beta_c \approx 0.6$). Let T = 4.2 K. Thus the value of $I_o = \beta\Phi_o/2L$ fixes the value of R and Γ. In Fig. 23 we plot computed values of $S_\Phi^\circ/2L$ vs. β for variable I_o. The value of $S_\Phi^\circ/2L$ is taken at the optimal bias current, $i \sim i_c(\phi_a,\beta)$ where $\phi_a = 0.25$. Equations (4.20) and (4.21) are also plotted for all values of β: Notice that the computed value of $S_\Phi^\circ/2L$ agrees well with these equations in the appropriate limits. The computed curve is almost constant for $1 \lesssim \beta \lesssim 10$. A SQUID operated as a small signal amplifier with $\alpha \approx 1$ at $\phi_a = 0.25$ and $i = i_c\ (\phi_a,\ \beta)$ would have $S_\Phi/2L \approx 1.6 \times 10^{-32} \mathrm{JHz}^{-1}$, relatively independent of β in that range.

When the SQUID is flux modulated and operated in the usual flux-locked mode, the energy resolution depends more strongly on β than in the unmodulated case. Since the optimal choice of bias current depends on the applied flux, the SQUID operated at constant bias current cannot be optimally biased over the entire modulation cycle. As a result, as β increases the average value of $S_\Phi^\circ/2L$ at fixed bias current also increases. In addition, from Fig. 17 we see that $S_\Phi^\circ/2L$ becomes a sharp function of $i = I/I_o$ for large β. Thus small variations in the bias current I or the junction critical current I_o can lead to substantial increases in $S_\Phi^\circ/2L$. Hence, for the flux modulated SQUID with L = 0.35 nH, C = 1 pF, $R^2 I_o = 200\ \Omega^2 \mu A$ and T = 4.2 K, the optimal value of β is approximately 1. Similar calculations at other values of the SQUID parameters also lead to $\beta \approx 1$ as the value for optimal energy resolution

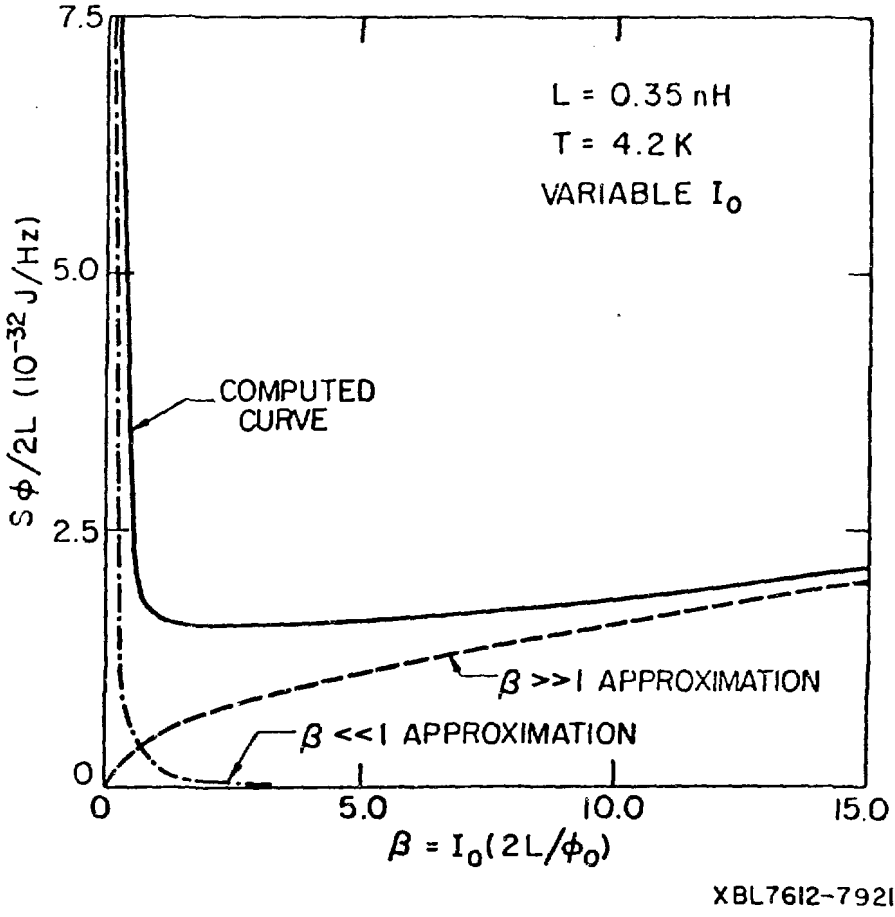

Fig. 23: $S_\phi^\circ/2L$ vs. β for L = 0.35 nH, T = 4.2K and variable critical current I_o.

in the flux-locked mode. We estimate an energy spectral density $S_\Phi^\circ/2\alpha^2 L$, with $\alpha^2 \sim 1/2$, of 4×10^{-32} JHz^{-1} for the flux-locked SQUID from an analysis similar to that in Sec. IV.C.6.

In summary, the procedure to obtain optimum performance from a tunnel junction SQUID is as follows. One first chooses a SQUID configuration, and thus one fixes L. The critical currents of the junctions are set by the constraint $\beta = 2\ LI_o/\phi_o \approx 1$. The shunt resistance, R, for each junction is chosen to satisfy $2\ \pi I_o R^2 C/\Phi_o \lesssim 1$, where C is determined by the area of the junction. Finally, the SQUID is operated with a bias current approximately equal to the total critical current in the absence of noise.

B. Ultimate Performance of the dc SQUID

The dependence of $S_\Phi^\circ/2L$ on L, C, and T for $\beta = 1$ can be approximated as follows. From Fig. 17 we find $\zeta_\Phi^{\frac{1}{2}}(\beta, \Gamma) \approx 1$ for $\beta = 1$. Hence, from Eq. (4.18), we find $S_\Phi^\circ/2L \approx 4\ k_B TL/R$ or

$$S_\Phi^\circ/2L \approx 4\ k_B T(\pi LC)^{\frac{1}{2}} \qquad (\beta = 1), \tag{5.1}$$

where we have used the constraint $R^2 = \Phi_o/2\pi I_o C = L/\pi C$. Thus, apart from numerical factors close to unity, the energy resolution for $\beta = 1$ is just $k_B T$ divided by the resonant frequency of the ring, $1/2\pi(LC/2)^{\frac{1}{2}}$. We expect Eq. (5.1) to remain valid provided the Johnson noise associated with the shunts is the dominant noise source. However, when $k_B T/eV \approx k_B T/eI_o R \ll 1$ (V is the bias voltage), the shot noise in the tunnel junctions will be the dominant noise source.[26] For junctions biased at a current of about $2I_o$, the shot noise voltage will have a low frequency spectral density of approximately $2e(2I_o)(R/2)^2 \approx eI_o R^2$ in the low temperature limit. If we replace $2k_B TR$ with $eI_o R^2$ in Eqs. (4.20) and

(4.21), we obtain

$$S_\Phi^\circ/2L \approx h\beta/4 \qquad (\beta \gg 1,\ eI_oR \gg k_BT)\ , \tag{5.2}$$

$$\text{and } S_\Phi^\circ/2L \approx h/8\beta \qquad (\beta \ll 1,\ eI_oR \gg k_BT)\ . \tag{5.3}$$

For the optimum value $\beta \approx 1$, Eq. (6.1) becomes

$$S_\Phi^\circ/2L \approx h/2 \qquad (\beta = 1,\ eI_oR \gg k_BT)\ . \tag{5.4}$$

For $\beta = 1$, Eqs. (5.1) and (5.4) imply that the inductance and capacitance must satisfy $8k_BT(\pi LC)^{\frac{1}{2}} \leq h$. For $T \approx 2K$ and $L \approx 0.35$ nH, this is $C \lesssim 10^{-2}$ pF, or a junction area $A \lesssim 0.5 \times 10^{-6}$ mm^2 for a Nb-NbO$_x$-Pb junction similar to that used in the SQUID of Clarke, Goubau and Ketchen[3] (see also Ref. 54). In principle junctions with these characteristics can be fabricated with electron beam milling techniques. For $\beta = 1$ and $L = 0.35$ nH, the required critical current, $I_o \approx 3$ μA, corresponds to a current density of about 0.6 KA cm^{-2}, a value that is readily achieved with junctions or larger area.[54] The shunt resistance is about 100 Ω for $\beta \sim 1$. These values of L and C correspond to a SQUID frequency, $1/2\pi(LC/2)^{\frac{1}{2}}$, of approximately 10^{11} Hz. Although this frequency is below the gap frequency ($\sim 3 \times 10^{11}$ Hz), other relaxation processes may limit the SQUID to a lower frequency of operation. In that case, it will not be possible to achieve the resolution given by Eq. (5.4) with a SQUID operated at 2 K.

One may also attempt to achieve the resolution suggested by Eq. (5.4) by operating the SQUID at a lower temperature: With L = 0.35 nH and C = 1 pF, the temperature must be below 0.2 K. The corresponding frequency at which the SQUID would operate is about 10^{10} Hz. A pre-amplifier with a noise temperature below 0.2 K would be required.

VI. APPLICATIONS

A. The Low Noise dc SQUID Preamplifier

In this section we develop a model for the dc SQUID preamplifier. First we adapt the basic circuit for a superconducting voltmeter developed by McWane, Neighbor, and Newbower[22] to the particular case of a dc SQUID magnetometer. Next we review the discussion of noise temperature, frequency response and bandwidth for the SQUID preamplifier characterized by a single voltage noise source and purely inductive input impedance. Finally, we develop a model for the dc SQUID preamplifier characterized by both current and voltage noise sources. We determine the dependence of the noise temperature on the input circuit parameters and the SQUID noise figures $S_v^o/2\Gamma$, $S_j^o/2\Gamma$ and $S_{vj}^o/2\Gamma$. We compute values of T_N for the particular case of a dc SQUID with $L \approx 10^{-9}$H, $R \approx 1\Omega$, $I_o \approx 1\mu$A operated at $T \approx 4.2$ K ($S_v^o/2\Gamma \approx 8$, $S_j^o/2\Gamma \approx 5.5$ and $S_{vj}^o/2\Gamma \approx 6$ at $\Phi_a = \Phi_o/4$).

1. *Basic Circuit*

The basic negative feedback circuit developed by McWane, Neighbor, and Newbower[22] is shown in Fig. 24. The input circuit consists of a voltage source $E_i(t)$ with impedance Z_i in series with a capacitance C_i, inductance L_i and feedback resistance R_F. The mutual inductance between L_i and the SQUID inductance L is $M_i = \alpha^2 L L_i$. The current $I_i(t)$ in the input circuit generates a flux $\Phi_a(t) = M_i I_i(t)$ through the SQUID. The resultant voltage across the SQUID, $V(t) = (\partial\bar{V}/\partial\Phi_a)\Phi_a(t)$, is usually amplified first by a cooled resonant circuit or transformer,[3] and then by a room temperature amplifier. The output voltage is then $V_o(t) = AV(t)$, where A is the gain of the amplifier chain. The output voltage

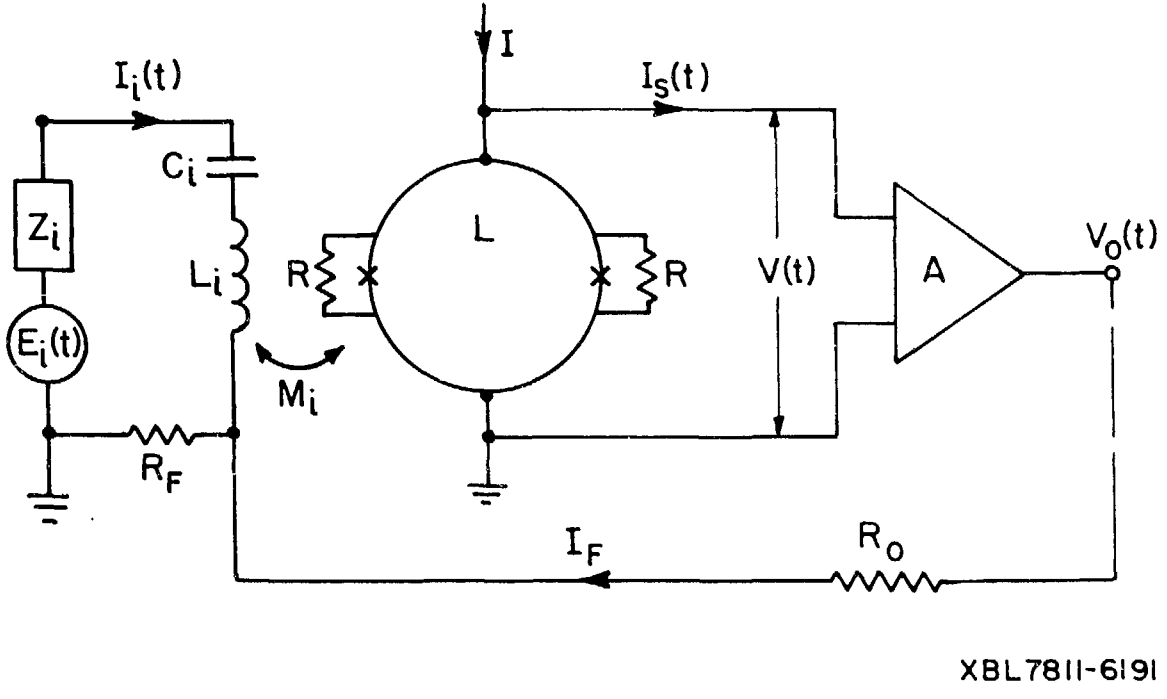

Fig. 24: Basic circuit for the dc SQUID preamplifier.

produces a feedback current $I_F = V_o/R_o$, which tends to null the input current $I_i(t)$.

The equivalent circuit for the dc SQUID magnetometer is shown in Fig. 25. The SQUID is modeled by a current-controlled voltage source with output voltage $Z_f I_i(t)$, where $Z_f = M_i(\partial\bar{V}/\partial\Phi_a)$. In the limit $\omega L \ll R_D$ $(\omega \ll \omega_J)$, the SQUID output impedance is approximated by the dynamic resistance $Z \approx R_D = (\partial\bar{V}/\partial I)_{\Phi a}$, and the SQUID input impedance is approximated by $Z_s \approx R_s = \omega^2 M_i^2/4R_D$. We will also use the approximation $(\partial\bar{V}/\partial\Phi_a) \approx R/L$.

2. *Model for the dc SQUID Preamplifier*

Davidson, Newbower, and Beasley[21] characterize the noise in the SQUID by the effective flux noise power spectral density $\langle \phi_n^2 \rangle = S_\phi^\circ$. This is equivalent to characterizing the SQUID noise by a voltage noise source at the output $(S_V^\circ = S_\phi^\circ\ (\partial\bar{V}/\partial\Phi_a)^2)$. Thus they take $E_i(t) = 0$ in Fig. 25. Now, the voltage noise at the SQUID output due to a source resistance R_i maintained at temperature T_i is

$$S_V^{source} = \frac{(4k_B T_i R_i)}{(R_T^2 + X_T^2)} M_i^2\ (\partial\bar{v}/\partial\Phi_a)^2 \quad , \tag{6.1}$$

where $Z_T = R_T + jX_T$ is the total input impedance. The noise temperature T_N^D, of the SQUID preamplifier is defined to be the value of the source temperature at which the source voltage noise equals the intrinsic SQUID voltage noise. Thus Davidson, et al[21] take

$$S_V^\circ = S_\phi^\circ(\partial\bar{V}/\partial\Phi_a)^2 = \frac{4k_B T_N^D R_i}{(R_T^2+X_T^2)} M_i^2\ (\partial\bar{V}/\partial\Phi_a)^2 \quad , \tag{6.2}$$

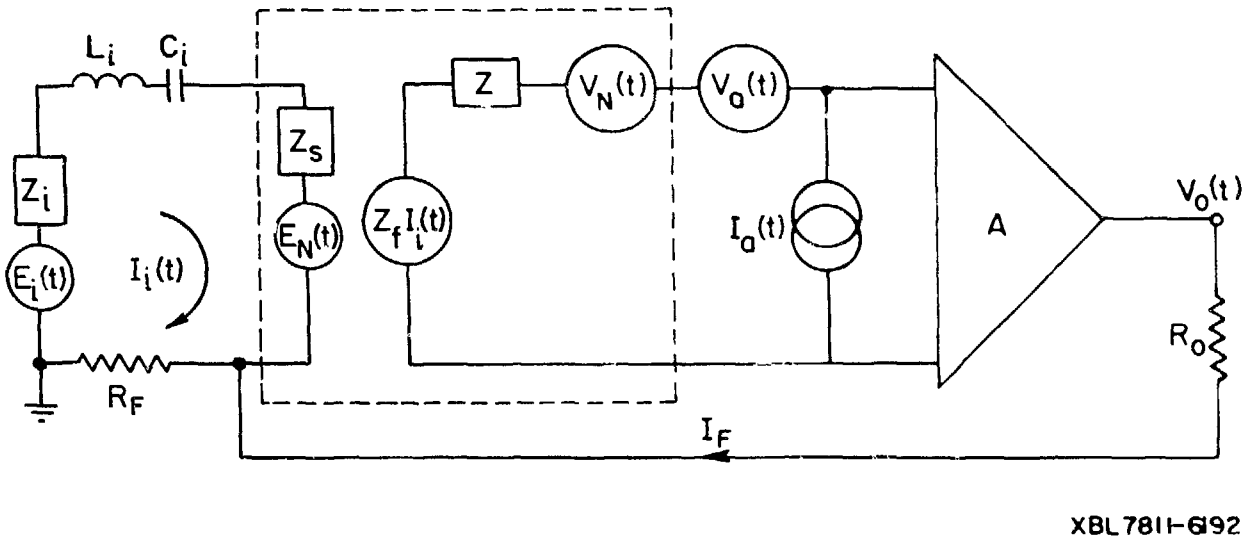

XBL7811-6192

Fig. 25: Equivalent circuit for the dc SQUID preamplifier.

and

$$T_N^D(\omega) = \left(\frac{S_\Phi^\circ}{2\alpha^2 L}\right) \frac{(R_T^2 + X_T^2)}{2k_B R_i L_i} \quad . \tag{6.3}$$

From Eq. (6.3) we see that the only figure of merit for the dc SQUID in this approximation is the energy spectral density, $S_E^\circ = S_\Phi^\circ/2\alpha^2 L$, determined by the isolated SQUID voltage noise S_v° and transfer function $(\partial\bar{v}/\partial\Phi_a)$. In the limit $R_T \approx R_i \gg X_T$, $T_N^D(\omega) \approx S_E^\circ/2k_B\tau_i$, where $\tau_i = L_i/R_i$. Note that S_E° is independent of the input circuit parameters R_T, X_T, R_i, and L_i. Note also that the authors take the SQUID impedance reflected into the input circuit to be purely inductive. (Their discussion was actually applied to the case of an rf SQUID magnetometer. The results mentioned here also hold for the preamplifier with a dc SQUID magnetometer under the same approximation scheme.)

In general, the voltage noise at the output of a preamplifier is not independent of the input circuit parameters. The dependence on the input circuit is often described by defining an amplifier voltage noise source, $E_N(t)$, in the input circuit (see Fig. 25). The resultant noise current in the input circuit, $E_N(t)/Z_T$, produces a voltage noise at the output of $E_N(t)Z_f/Z_T$. The total voltage noise at the SQUID output is

$$V_T(t) = V_N(t) + E_N(t)Z_f/Z_T \quad . \tag{6.4}$$

The actual total voltage noise at the output for the SQUID loaded down by the input circuit could in principle be calculated by including the input circuit into the basic SQUID equations, Eq. (2.24)-(2.27). However, it is impractical to apply the computor altorighm to solving the loaded equations for all cases of interest. A reasonable

approximation is the following. The SQUID is coupled to the input circuit through the mutual inductance M_i. The current circulating around the isolated SQUID loop, $J(t)$, induces a voltage across the coupling coil in the input circuit of $M_i dJ(t)/dt$. Thus, we take the voltage source in the input circuit to be proportional to the unloaded circulating current,

$$E_N(t) = M_i(dJ(t)/dt) \quad . \tag{6.5}$$

From Eqs. (6.4)-(6.5), the spectral density of the total voltage noise at the output in terms of the voltage noise spectral density, S_V°, the current noise spectral density, S_J°, and the imaginary part of the correlatron noise spectral density, S_{VJ}°, is

$$S_{VT}^\circ = S_V^\circ + S_{VJ}^\circ \; 2\omega M_i Z_f X_T/|Z_T|^2 + S_J^\circ \; \omega^2 M_i^2 \; Z_f^2/|Z_T|^2 \quad , \tag{6.6}$$

where we have taken the voltage source at the output to be $V_N(t)$ for the isolated SQUID. The noise temperature, T_N, is then

$$T_N(\omega) = \left(\frac{S^\circ{}_{VT}(\partial\bar{V}/\partial\Phi_a)^{-2}}{2\alpha^2 L}\right)\frac{(R_T^2 + X_T^2)}{2k_B R_i L_i} \quad . \tag{6.7}$$

In terms of the normalized dimensionless spectral densities computed in section IV,

$$T_N(\omega) = \frac{T}{2\alpha^2}\left(\frac{\omega}{R/L}\right)\left[\left(\frac{R_T^2 + X_T^2}{R_i\omega L_i}\right)\left(\frac{S_v^\circ}{2\Gamma}\right) + 2\alpha^2\left(\frac{X_T}{R_i}\right)\left(\frac{S_{vj}^\circ}{2\Gamma}\right) + \alpha^4\left(\frac{\omega L_i}{R_i}\right)\left(\frac{S_j}{2\Gamma}\right)\right] \quad , \tag{6.8}$$

where we have used $S_V^\circ = (S_v^\circ/2\Gamma)2k_B TR$, $S_J^\circ = (S_j^\circ/2\Gamma)2k_B T/R$, and

$S^{\circ}_{VJ} = (S^{\circ}_{VJ}/2\Gamma)2k_BT$, and the approximation $(\partial\bar{V}/\partial\Phi_a)$ for the loaded SQUID $\approx (\partial\bar{V}/\partial\Phi_a)$ for the isolated SQUID, where $(\partial\bar{V}/\partial\Phi_a) = (\partial\bar{V}/\partial\Phi_a)(\beta/2)(R/L) \approx (R/L)$.

3. *Optimal T_N for the Untuned Input Circuit*

From Eq. (6.8) we see that T_N is a function of the isolated SQUID parameters, the frequency, ω, and the input circuit parameters. The usual input circuit configuration is with $1/C_i = 0$. Then $X_T = \omega L_i$ and $R_T = R_i + R_F + R_S$, where R_i and R_F are the source and feedback resistances and $R_S = \omega^2 M_i/4R_D$ is the effective SQUID input resistance. We optimize $T_N(\omega)$ at a particular frequency ω_o by setting $(\partial T_N(\omega)/\partial R_i)_{\omega=\omega_o} = 0$. The optimal value of the source resistance is then a function of ω_o,

$$R_i^{Opt} = \omega_o L_i[1 + (R_F+R_S)^2/\omega_o^2 L_i^2 + 2\alpha^2 S^{\circ}_{VJ}/S^{\circ}_V + \alpha^4 S^{\circ}_J/S^{\circ}_V]^{1/2} , \qquad (6.9)$$

the optimized value of T_N at ω_o is

$$T_N^{Opt}(\omega_o) = \frac{T}{\alpha^2}\left(\frac{\omega_o}{R/L}\right)\left(\frac{S^{\circ}_V}{2\Gamma}\right)\left(\frac{R_i^{Opt}+R_f+R_S}{\omega_o L_i}\right) . \qquad (6.10)$$

and the noise temperature at arbitrary ω is

$$T_N^{Opt}(\omega) = T_N^{Opt}(\omega_o) + \frac{T(S^{\circ}_V/2\Gamma)(\omega^2/\omega_o^2-1)}{2\alpha^2(R/L)(L_i/R_i^{Opt})}\left[1 - \left(\frac{R_F+R_S}{R_i^{Opt}}\right)^2\right], \qquad (6.11)$$

Notice that both $T_N^{Opt}(\omega_o)$ and $T_N^{Opt}(\omega)$ depend on the SQUID parameters through R_i^{Opt} and through the usual figure of merit, $S^{\circ}_{\Phi}/2\alpha^2 L = (S^{\circ}_V/2\Gamma)k_BT/\alpha^2(R/L)$. Also note that the minimum in $T_N^{Opt}(\omega)$ occurs at $\omega = 0$ and not at ω_o. That is, $T_N^{Opt}(0) = T_N^{Opt}(\omega_o)(R_i^{Opt} + R_F + R_S)/2R_i^{Opt}$.

For the SQUID parameters given in section VI.A., in the limit

$\omega_o L_i \gg R_s + R_F$, $R_i^{Opt} \approx \omega_o L_i\ (1 + 3\alpha^2/2 + 11\alpha^4/16)^{\frac{1}{2}}$ and $T_N^{Opt}(\omega_o) \approx 8(\omega_o L/R)T(1 + 3\alpha^2/2 + 11\alpha^4/16)^{\frac{1}{2}}/\alpha^2$. Notice that the noise temperature is proportional to the SQUID temperature, T. This is as expected since for these values of the SQUID parameters, the dominant noise source is the thermal Johnson noise in the shunts. As the temperature is decreased, however, the Johnson noise will eventually be dominated by the shot noise in the junctions. We can compute $T_N^{Opt}(\omega_o)$ in this limit as follows. We assume that the ratios S_{vj}^o/S_v^o and S_j^o/S_v^o are not changed. Thus R_i^{Opt} is unchanged, and from Eq. (6.11), T_N^{Opt} is a function of the usual figure of merit, $S_v^o/2\Gamma$. From Eq. (5.4) we have $S_\phi^o/2L = (S_v^o/2\Gamma)k_BT/(R/L) \to h/2$ in the shot noise limit. Thus the noise temperature optimized at ω_o in the shot noise limit

is $T_N^{Opt}(\omega_o) \to \dfrac{\hbar\omega_o}{k_B}\ \dfrac{\pi(1+3\alpha^2/2+11\alpha^4/16)^{\frac{1}{2}}}{\alpha^2}$. As the coupling constant $\alpha^2 \to 0$, $T_N^{Opt}(\omega_o) \to \infty$. In the limit of perfect coupling between the input circuit and the SQUID, $T_N^{Opt}(\omega_o) \gtrsim 6\hbar\omega_o/k_B$. For the particular case of the dc SQUID with $\beta = 1$, $\Gamma = 0.5$, $\alpha^2 = 1/2$ and $(\partial\bar{V}/\partial\Phi_a) \approx R/L$, the shot noise limit is $T_N^{Opt}(\omega_o) \approx 17\hbar\omega_o/k_B$. Both the approximations for $T_N^{Opt}(\omega_o)$ are consistent with the relationship between noise temperature and operating frequency for a linear amplifier determined by Heffner.[7] He found that the uncertainty principle limits the optimal noise temperature to $T_N < \hbar\omega/k_B$ in the limit of large amplifier gain.

Notice that Eq. (6.9), $R_i \approx \omega_o L_i$, and Eq. (6.10), $T_N^{Opt}(\omega_o) \approx (\omega_o L/R)T/\alpha^2$ imply that the optimal noise temperatures are obtained for source resistances $R_i \lesssim 1\Omega$. For a SQUID inductance $L \sim 10^{-9}$H, reasonable

values of $\alpha^2 (\alpha^2 \approx 1/2)$ are obtainable for 10^{-6}H $\lesssim L_i \lesssim 10^{-9}$H. This implies for $\omega_o \sim 10^6$Hz, $1\Omega \lesssim R_i^{Opt} \lesssim 10^{-3}\Omega$, and $T_N^{Opt} \approx 10^{-3}$K for a SQUID operated at 1K with 1Ω shunt resistances. At $\omega_o \sim 1$Hz, the optimal resistance, R_i^{Opt}, falls to $10^{-6}\Omega$.

4. *Optimal T_N for the Tuned Input Circuit*

We assume that the input circuit is tuned with some capacitance C_i in series with the coupling coil L_i and the feedback and source resistances, R_F and R_i. Then $R_T \approx R_i + R_F + R_S$ and $X_T \approx \omega L_i - 1/\omega C_i$. We can optimize $T_N(\omega)$ at a particular frequency ω_o by setting $\partial T_N/\partial C_i = 0$. From Eq. (6.8), the optimal relationship between the inductance and capacitance is

$$1/\omega_o C_i^{Opt} = \omega_o L_i \; (1 + \alpha^2 \; S^o_{vj}/S^o_v) \; , \tag{6.12}$$

and the optimal noise temperature at ω_o is

$$T_N^{OptC_i}(\omega_o) = \frac{T}{2\alpha^2}\left(\frac{\omega_o}{R/L}\right)\left[\frac{R_T^2}{R_i \omega_o L_i}\left(\frac{S^o_v}{2\Gamma}\right) + \alpha^4\left(\frac{\omega_o L_i}{R_i}\right)\left(\frac{S^o_j}{2\Gamma} - \frac{S^o_{vj}}{S^o_v}\left(\frac{S^o_{vj}}{2\Gamma}\right)\right)\right] . \tag{6.13}$$

We now optimize $T_N^{OptC_i}(\omega_o)$ with respect to R_i by setting $\partial T_N^{OptC_i}(\omega_o)/\partial R_i = 0$ to obtain

$$R_i^{OptC_i} = \left[\alpha^4 \omega_o^2 L_i^2 (S^o_v S^o_j - S^{o\,2}_{vj})/S^{o\,2}_v + (R_S + R_F)^2\right]^{1/2} \tag{6.14}$$

and

$$T_N^{OptC_i R_i}(\omega_o) = \frac{T}{\alpha^2}\left(\frac{\omega_o}{R/L}\right)\left(\frac{S^o_v}{2\Gamma}\right)\left[\frac{R_i^{OptC_i} + R_F + R_S}{\omega_o L_i}\right] \tag{6.15}$$

The value of the optimized noise temperature at arbitrary ω is given by Eq. (6.8) with $1/\omega_o C_i$ replaced by $1/\omega_o C_i^{Opt}$ and R_i replaced by $R_i^{OptC_i}$. As an example, we plot the reduced noise temperature $T_N^{Red}(\omega) = T_N^{OptC_i}(\omega)(R/\omega_o L)/T$ versus the reduced frequency ω/ω_o in Fig. 26. Capacitance has been optimized according o Eq. (6.12). A range of input resistances R_i have been chosen. Notice that the parameter $Q_o = \omega_o L_i/R_i$ is not the "Q" of the input L-R-C circuit, since $\omega_o > 1/\sqrt{L_i C_i}$. The noise figures S_v^o, S_j^o and S_{vj}^o are those for the dc SQUID with the parameters given in section VI.A. The coupling constant $\alpha^2 = 1/2$.

For the SQUID parameters given in section VI.A., in the limit $\omega_o L_i \gg R_S + R_F$, $1/\omega_o C_i^{Opt} \approx (1 + 3\alpha^2/4)\omega_o L$ $R_i^{OptC_i} \approx 0.35\ \alpha^2\omega_o L_i$, and $T_N^{OptC_i,R_i}(\omega_o) \approx 2.8(\omega_o L/R)T$ independent o α^2. (Notice, however, that $R_i^{OptC_i} \to 0$ as $\alpha^2 \to 0$.) For $\omega_o/2\pi = 10^4$Hz, $L_i = 10^{-4}$H, T = 4.2, and $\alpha^2 = 0.5$, $C_i^{Opt} \approx 1.8\mu$F, $R_i^{OptC_i} \approx 1.1\Omega$ and $T_N^{OptC_i,R_i} \approx 0.74$mK. Notice that $R_i^{OptC_i}$ can be reduced to a more convenient value if necessary by reducing the coupling constant α^2. In the limit $\alpha^2 \ll 1/2$, C_i^{Opt} $1/\omega_o^2 L_i = 2.5\mu$F and $T_N^{OptC_i,R_i} \approx 0.74$ mK independent of α^2, while $R_i^{OptC_i} \approx 2.2\alpha^2\Omega$.

For the shot noise limited SQUID in the general case from Eq. (5.4), $T_N^{OptC_i,R_i}(\omega_o) \gtrsim \hbar\omega_0/k_B$, where we have assumed $(S_v^o S_j^o - S_{vj}^{o\,2})/S_v^{o\,2} \approx 0.125$ as given by the values of $(S_v^o/2\Gamma)$, $(S_j^o/2\Gamma)$ and $(S_{vj}^o/2\Gamma)$ for $\beta = 1$, $\Gamma = 0.05$. For the particular case of the SQUID with $\beta = 1$, $\Gamma = 0.05$, $T_N^{OptC_i,R_i}(\omega_o)$ $\approx 2.2\hbar\omega_o/k_B$ from Eq. (6.15). As for the case of the untuned magnetometer, both expressions are consistent with the restriction, $T_N(\omega_o) > \hbar\omega_o/k_B$, placed on the noise temperature by the uncertainty principle.

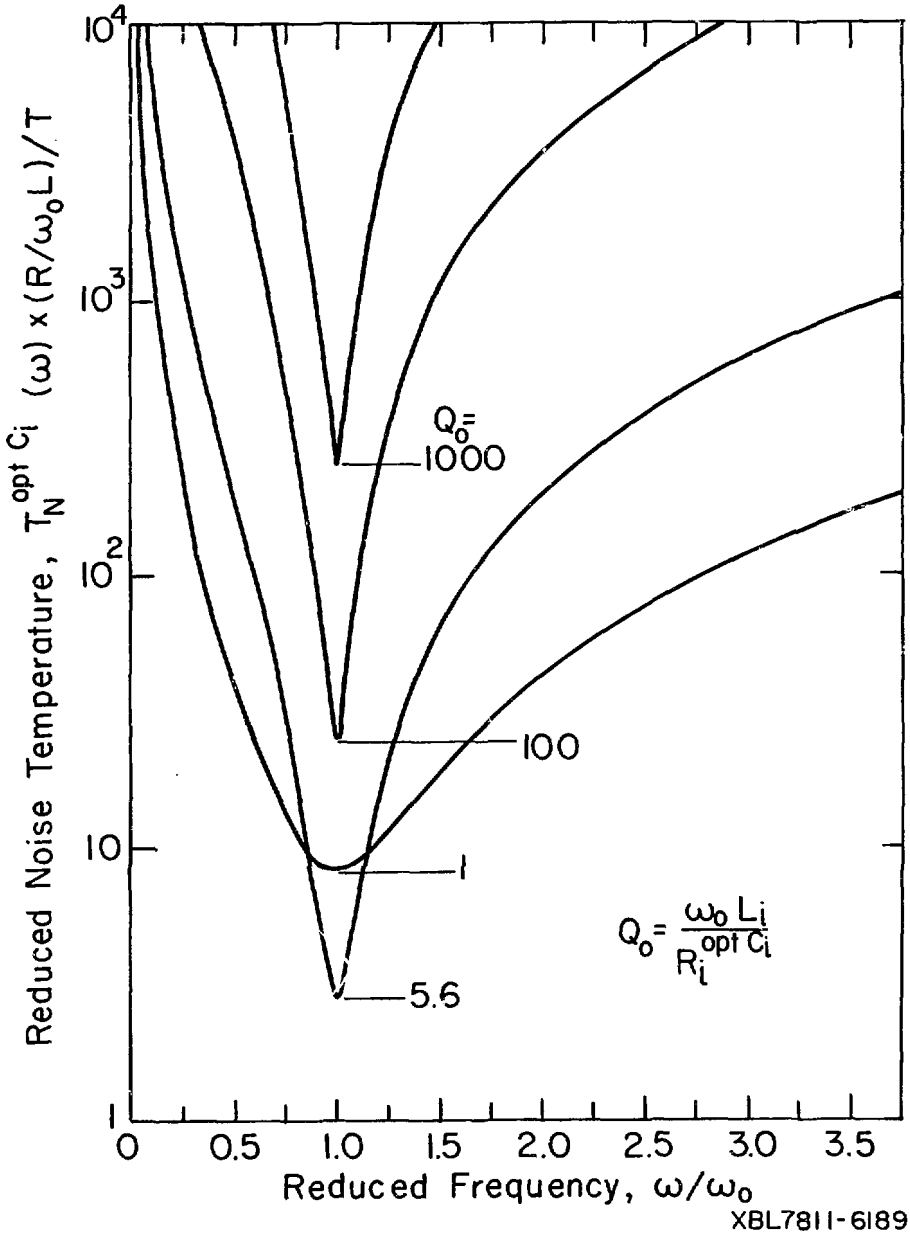

Fig. 26: Normalized optimal noise temperature $T_N^{optC_i}(\omega)(R/\omega_o L)/T$ vs. reduced frequency ω/ω_o as a function of $Q_0 = \omega_o L_i/R_i$.

B. Magnetometers

The basic circuit for a dc SQUID magnetometer is similar to the preamplifier shown in Fig. 24. The input voltage source consists of a single input coil or a system of coils threaded by a time dependent magnetic field. The input impedance is purely inductive. The feedback signal is often applied by coupling a feedback coil directly to the SQUID. The untuned magnetometer ($1/C_i = 0$) can thus be constructed with an extremely small input resistance, $R_T = R_S \approx \omega^2 M_i^2/4R_D$. For the tuned case, there will be some resistance R_i associated with the losses in the tuned circuit.

1. Untuned Magnetometer

We begin by considering the case of a single pick-up loop threaded by an axial magnetic field. For a long n-turn solenoid of length ℓ and radius r, the inductance is $L_p = \mu_o \pi r^2 n^2/\ell$. The mean square voltage induced by a magnetic field of magnitude B_o oscillating sinusoidally at frequency w is

$$\langle E_i^2 \rangle = \omega^2 B_o^2 \pi^2 r^4 n^2/2 = 2\omega^2 u_o L_p \tag{6.16}$$

where $u_o = B_o^2 \pi r^2 \ell/\mu_o$ is the mean signal energy in the volume of the coil. We take $R_F = R_i = 0$, $R_S = \omega^2 M_i^2/4R_D$, and $X_T = \omega L_i + \omega L_p$ for the untuned case ($1/\omega C_i = 0$). The mean square signal voltage at the SQUID output is

$$\langle V_S^2 \rangle = \frac{\langle E_i^2 \rangle M_i^2}{(R_S^2 + X_T^2)} \quad (\partial \bar{V}/\partial \Phi_a)^2 \quad , \tag{6.17}$$

and the mean square SQUID noise at the output in the bandwidth B from Sq. (6.6) is

$$\langle V_T^2 \rangle = S_{VT}^{\circ} B = [(R_S^2+X_T^2)S_V^{\circ} + 2\omega M_i Z_f X_T S_{VJ}^{\circ} + \omega^2 M_i^2 Z_f^2 S_J^{\circ}]B/(R_S^2+X_T^2) \quad . \tag{6.18}$$

We set $\langle V_s^2 \rangle = \langle V_T^2 \rangle$ and use the approximation $(\partial\bar{V}/\partial\Phi_a) \approx R/L$ to obtain

$$u_o = \frac{k_B TB\ L_i}{\alpha^2 (R/L) L_p} \left\{ (S_v^{\circ}/2\Gamma) \left[\left(\frac{\alpha^2 \omega L}{4R_D}\right)^2 + \left(1 + \frac{L_p}{L_i}\right)^2 \right] + 2\alpha^2 \ (S_{vj}^{\circ}/2\Gamma)\left(1 + \frac{L_p}{L_i}\right) + \alpha^4 (S_j^{\circ}/2\Gamma) \right\} \quad . \tag{6.19}$$

We now minimize u_o with respect to L_i for fixed input coil L_p, and obtain

$$L_i^{Opt} = L_p \ \{1 + 2\alpha^2 S_{vj}^{\circ}/S_v^{\circ} + \alpha^4 S_j^{\circ}/S_v^{\circ} + (\alpha^2 \omega L/4R_D)^2\}^{-\frac{1}{2}} \tag{6.20}$$

and

$$u_o^{Opt} = \frac{2k_B TB(S_v^{\circ}/2\Gamma)}{\alpha^2 (R/L)} \ (1 + L_p/L_i^{Opt} + \alpha^2 S_{vj}^{\circ}/S_v^{\circ}) \quad . \tag{6.21}$$

In the limit $\omega L_i \gg R_S$, for the dc SQUID with the parameters listed in section IV.A. with $\alpha^2 = 1/2$, $L_i^{Opt} \approx 0.72 L_p$ and $u_o^{Opt} \approx 9k_B T(B/f_J) \approx 5 \times 10^{-30}$ (B/1Hz)J. As in the case of the voltage preamplifier, previous calculations[6,19] of L_i^{Opt} and U_o^{Opt} have included only the voltage noise S_v°. In that case, $L_i^{Opt} \approx L_p$, and $U_o^{Opt} \approx 2k_B TB(S_v^{\circ}/2\Gamma)/\alpha^2(R/L) \approx 2(S_{\Phi}^{\circ}/2\alpha^2 L)B$.

In the shot noise limit for the SQUID parameter listed with $\alpha^2 = 1/2$, $u_o^{Opt} \approx 11hB$. From Eq. (5.4) $(S_{\Phi}^{\circ}/2L \to \frac{h}{2})$, $u_o^{Opt} \gtrsim 2hB/\alpha^2$ for $\alpha^2 \ll 1$. Notice that, although the minimum resolvable mean signal energy u_o is limited by the shot noise in the junctions, the minimum resolvable mean square field, $\tilde{B}^2$, is not. We have $u_o = \tilde{B}^2 V/4\mu_o$, where V is the volume of the pickup coil. Thus the optimal $B_0 \approx 7 \times 10^{-7} \ (k_B TB/V)^{\frac{1}{2}}$ where $L_i^{Opt} = 0.72\ L_p$ as before. Now one can in principle

make V arbitrarily large for fixed inductance L_p. Thus the ultimate resolution is limited only by the dewar size, provided that parasitic noise sources can be made negligible.

2. *Superconducting Input Circuit*

The untuned magnetometer input circuit with pick-up coil L_p and coupling coil L_i can also be made purely superconducting. This is not equivalent to the untuned magnetometer input circuit with $R_i \to 0$. The superconducting input circuit introduces the additional constraint that the flux must be quantized around the input loop. In this case, the basic equations which describe the SQUID plus input circuit can be reduced to the isolated SQUID equations. The SQUID loop inductance L is replaced by an effective inductance $L_{eff} = L(1 - \alpha^2 r)$, where $r = L_i/(L_i + L_p) \leq 1$. Thus, instead of approximating the total loaded voltage spectral density at the output, S^o_{VT} by Eq. (6.6), we can use the computer model results for S^o_V with $\beta_L = 2L_{eff}I_o/\Phi_o = \beta(1 - \alpha^2 r)$ and $\Gamma_L = 2\pi k_B T/I_o\Phi_o = \Gamma$. These two numbers are not equal in general. For $\beta = 1$, $\Gamma = 0.05$, $\alpha^2 = 1/2$ and $r = 0.5$ $(L_i = L_p)$, $S^o_{V\Gamma} \approx 23\ k_B TR$ and $S^o_V \approx 17\ k_B TR$.

For the superconducting transformer, the minimum energy that can be resolved in bandwidth B is

$$u_o = \frac{S^o_\Phi}{4\alpha^2 L} \frac{B}{r(1-r)^2}, \tag{6.22}$$

where S^o_Φ is the flux resolution of the isolated SQUID with parameters β_r and Γ. We use the approximate expressions for $S^o_\Phi/2L$ in the high β_r and low β_r limits [Eq. (4.18)-(4.19)] to optimize u_o with respect to

r. For $\beta_r \ll 1$ and $\alpha^2 = 1/2$, $r^{opt} = 0.42$ and $u_o^{opt} = 2B(S_\Phi^\circ/2\alpha^2 L)$. For $\beta_r \gg 1$ and arbitrary α^2, $r^{opt} = 0.5$ and $u_o^{opt} = 2B(S_\Phi^\circ/2\alpha^2 L)$. Thus for $\beta_r \sim 1$, we reproduce the standard result, $L_i \lesssim L_p$ and $u_o^{opt} \approx 16\, k_\beta TLB/\alpha^2 R$. Notice that, although the approximate value for S_{VT}° for the untuned magnetometer with $R_i \to 0$ is substantially larger than the value of S_v° for the superconductor input circuit magnetometer, the energy resolution and optimal coil ratios are essentially the same.

3. *Tuned Magnetometer*

In this case, the input circuit is tuned by a capacitance C_i in series with L_i and L_p. The resistance R_i in series with C_i accounts for the losses in the tuned circuit. The mean square voltage induced by the incident magnetic field is $\langle E_i^2 \rangle = 2\omega^2 u_o L_p$. This circuit is now identical to the tuned peramplifier circuit, with $X_T = \omega(L_i + L_p) - 1/\omega C_i$, and $R_T = R_i + R_s$. The voltage noise in the input circuit due to the resistance R_i is $4k_B T_i R_i B$, and the voltage noise of the SQUID preamplifier referred to the input circuit is $4k_B T_N R_i B$, where T_N is given by Eq. (6.8). Notice that the temperature in Eq. (6.8) is the SQUID shunt resistance temperature, T, and not the input resistance temperature, T_i. The two noise sources are incoherent. Thus we take

$$\langle E_i^2 \rangle = 2\omega^2 u_o L_p = 4k_B T_i R_i B + 4k_B T_N R_i B \quad . \tag{6.23}$$

The minimization of u_o with respect to C_i at some fixed frequency ω_o yields

$$1/\omega_o C_i^{opt} = \omega_o L_i \left(1 + L_p/L_i + \alpha^2 S_{vj}^\circ/S_v^\circ\right) \tag{6.24}$$

(compare with Eq. (6.12)), and

$$2\omega_o^2 L_p U_o^{optC_i} = 4k_B T_i R_i B + 4k_B T_N^{optC_i} R_i B, \tag{6.25}$$

where $T_N^{optC_i}$ is given by Eq. (6.13).

Minimizing $U_o^{optC_i}$ with respect to L_i for fixed L_p and R_i at the same frequency ω_o yields

$$\omega_o L_i^{opt} = R_i \left\{ (\alpha^2 \omega_o L/4R_D)^2 + \alpha^4 (S_j^\circ/S_v^\circ - S_{vj}^\circ/S_v^{\circ 2}) \right\}^{-\frac{1}{2}} \tag{6.26}$$

and

$$2\omega_o^2 L_p U_o^{optC_i, L_i} = 4k_B T_i R_i B + 4k_B T_N^* R_i B, \tag{6.27}$$

where T_N^* has the same form as $T_N^{optC_i, R_i}$ in Eq. (6.15) with $R_i^{opt} \to R_i$ and $L_i \to L_i^{opt}$ (also compare Eq. (6.27) to Eq. (6.14)). The optimal value for U_o is then

$$2\omega_o^2 L_p U_o^{optC_i, L_i} = 4k_B T_i R_i B + 4k_B T_N^* R_i B \ . \tag{6.28}$$

Using the SQUID parameters listed in section VI.A., for $\omega_o L_i \gg R_s$, we have $\omega_o L_i^{opt} \approx 2.8 R_i/\alpha^2$, $1/\omega_o C_i^{opt} \approx \omega_o L_i^{opt}(1+3\alpha^2/4) + \omega_o L_p$, and $2\omega_o^2 L_p U_o^{optC_i, L_i} \approx 4k_B T_i R_i B + 4k_B T_N^* R_i B$, where $T_N^* \approx 2.8(\omega_o L/R)T$. For most applications, $T \approx T_1 \approx 4.2K$, and $\omega_o \ll R/L \sim 10^9$ rad sec^{-1}. Thus for a wide range of the parameters ω_o, R_i, L_i, C_i and L_p, $T_N \ll T_i$, and $2\omega_o^2 L_p U_o \approx 4k_B T_i R_i B$. This is just the condition that the signal voltage should dominate the Johnson noise voltage of the resistance R_i in the input circuit.

In some applications (typically high Q input circuits operated at high frequency) $T_N^* \gtrsim T_i$. For a particular choice of operating frequency ω_o at which the noise temperature is to be optimized, we express $T_N^*(\omega)$

in terms of the following parameters, $r = L_i/L_T$, $\gamma_T = 1/\omega_o^2 L_T C_i$ and $Q_T = \omega_o L_T/R_i$ for $L_T = L_i + L_p$. Notice that Q_T is not necessarily the Q of the input circuit. From Eq. (6.8) with $X_T = \omega L_T - 1/\omega C_i$,

$$T^*_{red} = Q_T \left[\left(\frac{S^\circ_v}{2\Gamma}\right) \frac{1}{Q_T^2 r} - 2\left(\frac{S^\circ_v}{2\Gamma}\right)\frac{\gamma_T}{r} - \left(\frac{S^\circ_{vj}}{2\Gamma}\right)\gamma_T \right.$$

$$+ \left(\frac{\omega}{\omega_o}\right)^2 \left(\left(\frac{S^\circ_v}{2\Gamma}\right)\frac{1}{r} + \left(\frac{S^\circ_{vj}}{2\Gamma}\right) + \left(\frac{S^\circ_j}{2\Gamma}\right)\frac{r}{4} \right)$$

$$\left. + \left(\frac{\omega_o}{\omega}\right)^2 \left(\frac{S^\circ_v}{2\Gamma}\right)\frac{\gamma_T^2}{r} \right] . \qquad (6.29)$$

The optimal value of γ_T is $\gamma_T^{opt} = 1 + (S^\circ_{vj}/S^\circ_v)r/2 \to 1$ for $L_i \ll L_p$. In this case $\omega_o \approx 1/\sqrt{L_T C_i}$ and $Q_T \approx Q$ input. The optimal value of Q_T is $Q_T^{opt} = 2/r \left[S^\circ_j/S^\circ_v -)S^\circ_{vj}/S^\circ_v)^2\right]^{\frac{1}{2}}$. Thus $Q_T^{opt} \propto 1/r$. The value of T^*_{red} at optimal γ_T and Q_T is $T^{*opt}_{red} = \left[(S^\circ_v/2\Gamma)(S^\circ_j/2\Gamma) - (S^\circ_{vj}/2\Gamma)^2\right]^{\frac{1}{2}}$. This is identical to the result obtained for the tuned voltage preamplifier. For the dc SQUID mentioned in section VI.A, $\gamma_T^{opt} = 1 + 3r/8$, $Q_T = 5.6/r$ and $T^{*opt}_{red} = 2.8$. Thus for an input circuit with $L_p \gtrsim L_i$ $(r \lesssim 1)$, $\gamma_T \approx 1$ and $Q_T \approx Q = 1000$, the actual noise temperature is substantially larger than the optimal value. For example, for $r = 1$, $T^*_N \approx Q_T(\omega_o/(R/L))T$. Thus for $T = T_i = 4.2K$, $f_o = 2 \times 10^6$Hz, $R = 1\Omega$, $L = 10^{-9}$H and $Q_T = 1000$, $T^*_N = 4.2K$ at ω_o. For $\omega \neq \omega_o$, $T^*_N > 4.2K$. To illustrate the dependence of T^*_N on ω and r for the highly tuned input circuit, we plot the reduced noise temperature T^*_{red} versus (ω/ω_o) for $Q_T = 1000$ for various values of r in Fig. 27.

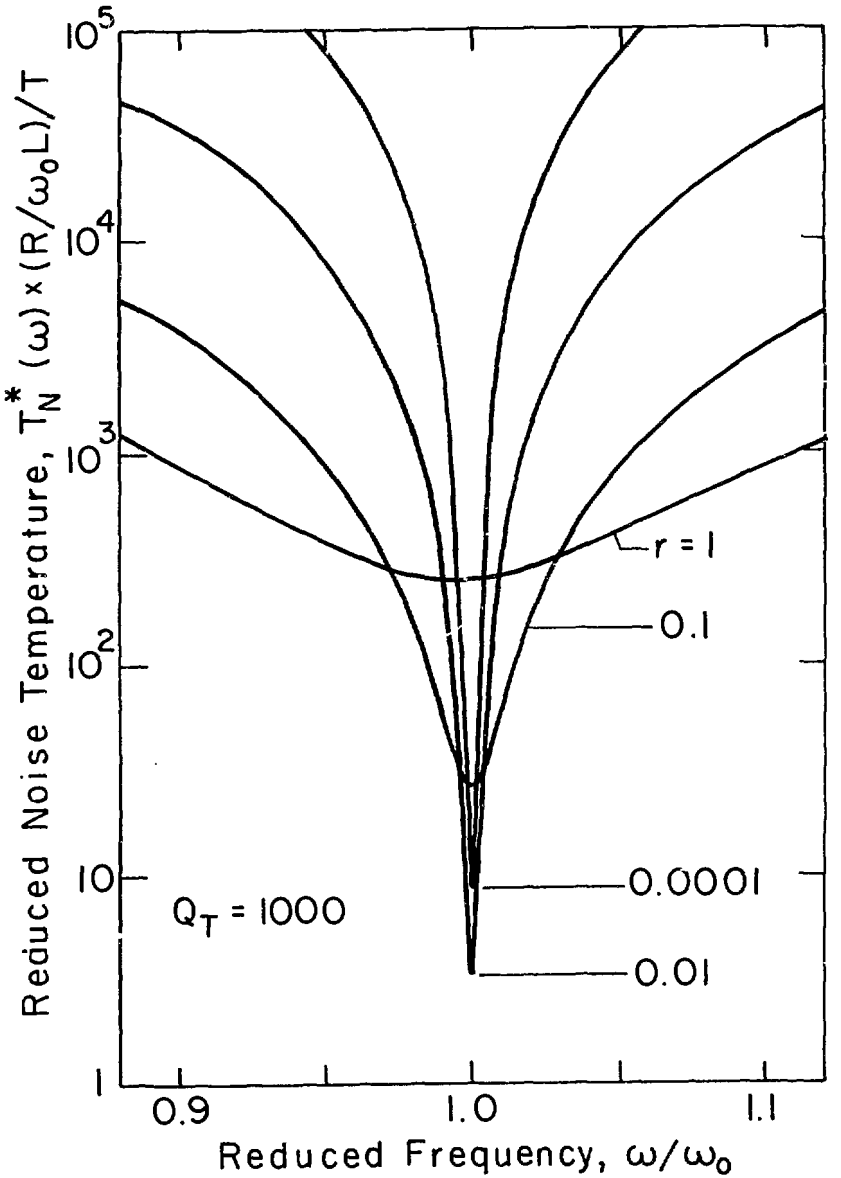

Fig. 27: Normalized noise temperature $T_N^*(\omega)(R/\omega_o L)/T$ vs. reduced frequency (ω/ω_o) as a function of $r = L_i/(L_i + L_p)$ for $Q_T = \omega_o(L_i + L_p)/R_i = 1000$.

At very low temperatures T and T_i, the energy resolution will be limited by the shot noise in the SQUID. In that case we have from section VI.A.3, $T_N^* \rightarrow \hbar\omega_o/k_B$, and $2\omega_o^2 L_p U_o^{opt} L_i C_i \approx 4k_B T_N^* R_i B \approx 4\hbar\omega_o R_i B$. This is the optimal energy resolution consistent with the uncertainty principle restriction on the noise temperature for the SQUID magnetometer in this configuration.

References

1. R.C. Jaklevic, J. Lambe, A.H. Silver, and J.E. Mercereau, Phys. Rev. Lett. 12, 159 (1964); Phys. Rev. Lett. 14, 887 (1965); Phys. Rev. 140, A1628 (1965).

2. B.D. Josephson, Phys. Lett. 1, 251 (1962); Adv. Phys. 14, 419 (1965).

3. J. Clarke, W.M. Goubau, and M.B. Ketchen, J. Low Temp. Phys. 25, 99 (1976).

4. M.B. Ketchen, W.M. Goubau, J. Clarke, and G.B. Donaldson, IEEE Trans. Magn. MAG-13, 372-374 (1977).

5. M. Tinkham, Introduction to Superconductivity (McGraw-Hill, 1975), p. 214.

6. J.H. Claassen, J. Appl. Phys. 46, 2268 (1975).

7. H. Heffner, Proc. IRE 50, 1604 (1962).

8. J.E. Zimmerman and A.H. Silver, Phys. Rev. 141, 367 (1966).

9. E.O. Schulz-DuBois, IBM Research RZ 564, April 13, 1973.

10. A. Th. A. M. De Waele and R. DeBruyn Ouboter, Physica 41, 225 (1969).

11. A. Th. A. M. De Waele and R. De Bruyn Ouboter, Physica 42, 626 (1969).

12. T.A. Fulton, Solid State Commun. 8, 1353 (1970).

13. J. Clarke and J.L. Paterson, Appl. Phys. Lett. 19, 469 (1971).

14. W.-T. Tsang and T. Van Duzer, J. Appl. Phys. 46, 4573 (1975).

15. T.A. Fulton, L.N. Dunkleberger, and R.C. Dynes, Phys. Rev. B6, 855 (1972).

16. W.-T. Tsang and T. Van Duzer, J. Appl. Phys. 47, 2656 (1976).

17. J. Clarke, W.E. Tennant, and D. Woody, J. Appl. Phys. 42, 3859 (1971).

18. J. Clarke, Rev. Phys. Appl. 5, 32 (1970).

19. J.E. Zimmerman, J. Appl. Phys. 42, 30 (1971).

20. V. Radhakrishnan and V.L. Newhouse, J. Appl. Phys. 42, 129 (1971).

21. A. Davidson, R.S. Newbower, and M.R. Beasley, Rev. Sci. Instrum. 45, 838 (1974).

22. J.W. McWane, J.E. Neighbor, and R.S. Newbower, Rev. Sci. Instrum. 37, 1602 (1966).

23. R.S. Newbower, Ph.D. thesis, Harvard University, 1971.

24. R.P. Giffard, R.A. Webb, and J.C. Wheatley, J. Low Temp. Phys. 6, 533 (1972).

25. R.P. Giffard, Phys. Rev. D, 14, 2478 (1976).

26. A.J. Dahm, A. Denenstein, D.N. Langenberg, W.H. Parker, D. Rogovin, and D.J. Scalapino, Phys. Rev. Lett. 22, 1416 (1969).

27. M.J. Stephen, Phys. Rev. Lett. 21, 1629 (1968).

28. J. Clarke and G.A. Hawkins. IEEE Trans. Magn. MAG-11, 724 (1975).

29. Gilbert A. Hawkins and John Clarke, J. Appl. Phys. 47, 1616 (1976).

30. W.C. Stewart, Appl. Phys. Lett. 12, 277 (1968).

31. D.E. McCumber, J. Appl. Phys. 39, 3113 (1968).

32. F. Auracher, Ph.D. thesis, University of California, Berkeley (1973).

33. V. Ambegaokar and B.I. Halperin, Phys. Rev. Lett. 22, 1364 (1969).

34. A.N. Vystavkin, V.N. Gubankov, L.S. Kuzmin, K.K. Likharev, V.V. Migulin, and V.K. Semenov, Rev. Phys. Appl. 9, 79 (1974).

35. J. Kurkijarvi, Phys. Rev. B6, 832 (1972).

36. J. Kurkijarvi and W.W. Webb, Proc. Appl. Superconductivity Conf. Annapolis (IEEE, NY) 581, (1972).

37. T.A. Fulton, IEEE Trans. Magn. MAG-11, 749 (1975).

38. C. Tesche and J. Clarke, IEEE Trans. Magn. MAG-13, 859 (1977).

39. Claudia D. Tesche and John Clarke, J. Low Temp. Phys. 29, 301 (1977).

40. Claudia D. Tesche and John Clarke, to be published in J. Low Temp. Phys.

41. J. Clarke, C.D. Tesche and R.P. Giffard, to be published.

42. J.R. Waldram, Rep. Prog. Phys. 39, 751 (1976).

43. L.G. Aslamazov and A.I. Larkin, Zh. Eksp. Teor. Phys. Pis. Red. 9, 150 (1968).

44. S. Chandrasekhar, Rev. Mod. Phys. 15, 1 (1943).

45. H.A. Kramers, Physica 7, 284 (1940).

46. Y.H. Ivanchenko and L.A. Zil'berman, Zh. Eksperim. I. Teor. Fiz. 55, 2395 (1968) (Sov. Phys. JETP 28, 1272 (1969).

47. V. Ambegaokar and B.I. Halperin, Phys. Rev. Lett. 22, 1364 (1969).

48. J. Clarke, Phil. Mag. 13, 115 (1966).

49. L. Solymar, Superconductive Tunneling and Applications (Chapman and Hall, London, 1972), p. 202.

50. J. Clarke and J.L. Paterson (unpublished).

51. A. Van der Ziel, Noise (Prentice-Hall, Inc., New York, 1954), p. 320.

52. J. Kadlec and K.H. Gundlach (preprint).

53. M. Ketchen, Ph.D. thesis, University of California, Berkeley (1977).

54. S. Basavaiah and J.H. Greiner, J. Appl. Phys. 47, 4201 (1976).

U.S.GPO:1979-689-058(F)19